

AD-A270 152

DOCUMENTATION PAGE

Form Approved
OMB No. 0704-0188

2



Information is estimated to average 1 hour per response, including the time for reviewing instructions, searching existing data sources, completing and reviewing the collection of information. Send comments regarding this burden estimate or any other aspect of this collection of information, including suggestions for reducing this burden, to Washington Headquarters Services, Directorate for Information Operations and Reports, 1215 Jefferson Avenue, Washington, DC 20503, and to the Office of Management and Budget, Paperwork Reduction Project (0704-0188) Washington, DC 20503.

2. REPORT DATE
9/15/933. REPORT TYPE AND DATES COVERED
Final Technical 8/1/91 - 7/31/93

4. TITLE AND SUBTITLE

Advances in Laser Cooling

5. FUNDING NUMBERS

AFOSR910305

6. AUTHOR(S)

Harold J. Metcalf

7. PERFORMING ORGANIZATION NAME(S) AND ADDRESS(ES)

Research Foundation
State University of New York at Stony Brook
Stony Brook, NY 117948. PERFORMING ORGANIZATION
REPORT NUMBER

AEOSR-TR- 93 0745

9. SPONSORING / MONITORING AGENCY NAME(S) AND ADDRESS(ES)

AFOSR NE
110 DUNCAN AVE SUITE B115
BOLLING AFB DC 20332-000110. SPONSORING / MONITORING
AGENCY REPORT NUMBER

2361 DS

11. SUPPLEMENTARY NOTES

DISTRIBUTION STATEMENT A

Approved for public release
Distribution is unlimited

12a. DISTRIBUTION - AVAILABILITY STATEMENT

Unlimited

12b. DISTRIBUTION CODE

13. ABSTRACT (Maximum 200 words)

We have made significant advances in the science of laser cooling on a number of topics.

DTIC
OCT 05 1993

93-23152

93 10 1 279

14. SUBJECT TERMS

15. NUMBER OF PAGES

16. PRICE CODE

17. SECURITY CLASSIFICATION
OF REPORT18. SECURITY CLASSIFICATION
OF THIS PAGE19. SECURITY CLASSIFICATION
OF ABSTRACT20. SECURITY CLASSIFICATION
OF ABSTRACT

FINAL TECHNICAL REPORT

HAROLD METCALF

STATE UNIVERSITY OF NEW YORK AT STONY BROOK

Submitted 15 September 1993

1

D

- ●

1

1

A-1

Longitudinal Magnetic Field Effects in Sub-Doppler Cooling

R. Gupta, S. Padua, C. Xie, H. Batelaan, and H. Metcalf

Physics Dept., S.U.N.Y., Stony Brook, NY, 11790

The experimental discovery of sub-Doppler laser cooling was soon followed by theoretical descriptions that depended on optical pumping processes among the sublevels of multiply degenerate atomic ground states. These theories were based on polarization gradients in counterpropagating light beams. Later it was found that sub-Doppler cooling could also be achieved in the absence of polarization gradients when a weak transverse magnetic field was used for mixing eigenstates of the light shift operator.

By contrast, Zeeman shifts from magnetic fields B_z along the quantization axis can add or subtract with the light shifts of those states. B_z thus provides an additional degree of freedom for studying magnetic effects in laser cooling since the set of sinusoidal potentials that derives from the spatially periodic light shifts in a standing wave can be manipulated with the field. For example, with circularly polarized light a finite B_z can switch the normal heating to cooling, and vice versa. We have done such experiments in the $F = 3 \rightarrow 4$ transition of ^{85}Rb at $\lambda = 780$ nm with diode laser light, and have shown that sub-Doppler heating and cooling can be interchanged with opposite longitudinal

field directions, in good agreement with this model. Such experiments may also allow us to characterize precisely the magnetic fields seen by the atoms along their trajectories in the beam.

The simplest angular momentum schemes that permit sub-Doppler cooling have 4 levels, and one example is an $F = 1 \rightarrow 0$ transition in either a linearly or circularly polarized standing wave with a weak transverse magnetic field. The 28% abundant ^{87}Rb isotope has an $F = 1 \rightarrow 0$ transition that is ideal for studying this simplest possible case. Magnetically induced laser cooling can reduce atomic kinetic energies to below the peaks of the spatially periodic potential seen by the atoms as a result of their light shifts, thus channeling them between the planes of the standing wave. Furthermore, their deBroglie wavelengths become comparable to the channel size so that their motion is quantized in these half-wavelength sized optical traps.

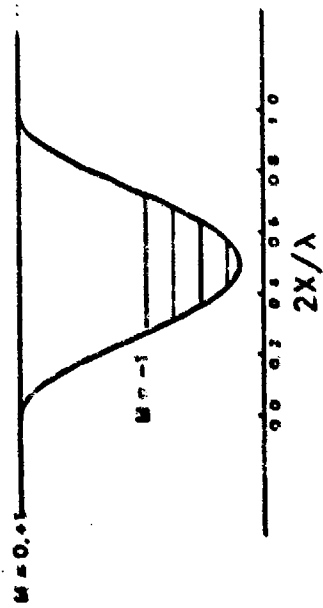
This $F = 1 \rightarrow 0$ transition produces only one light-shifted level, and thus only one ground state sublevel that can support bound quantized states. An rf-induced transition that would change the populations of the quantum vibrational states of this potential (see Fig. 1) would be particularly easy to interpret, and would be subject to easily understood Zeeman shifts in a longitudinal field. We are presently studying this problem.

Supported by NSF, ONR, AFOSR, and CAPES (Brazil)

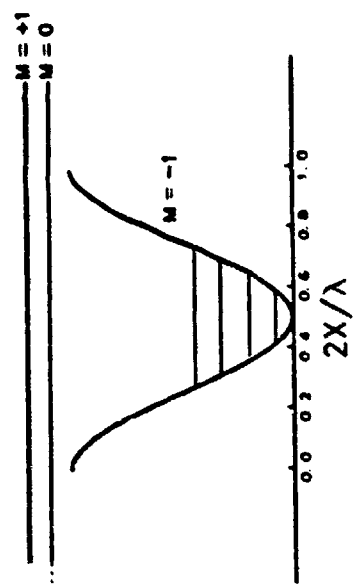
FIGURE CAPTION

Figure 1. Energies of quantized states in the optical light shift potential for an $F = 1 \rightarrow 0$ transition in circularly polarized light with no magnetic field (left) and positive longitudinal magnetic field (right).

Longitudinal $B=0$



Longitudinal $B=0.1$ Gauss



Abstract Submitted
for the May 1993 Meeting of the
Division of Atomic, Molecular and Optical Physics

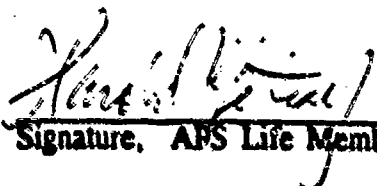
Physical Review
Analytic Subject Index
Number: 32.80.Pj

Bulletin Subject Heading
in which paper should be placed:
Laser Cooling

A Simplest Possible Scheme For Sub-Doppler Laser Cooling. R. GUPTA, S. PADUA, C. XIE, H. BATELAAN, and H. METCALF, SUNY Stony Brook -- The simplest angular momentum schemes that permit sub-Doppler cooling have 4 levels, and one example is an $F = 1 \rightarrow 0$ transition in either a linearly or circularly polarized standing wave with a weak transverse magnetic field. The 28% abundant ^{87}Rb isotope has an $F = 1 \rightarrow 0$ transition that is ideal for studying this case. Magnetically induced laser cooling can reduce atomic KE to below the peaks of the spatially periodic potential seen by the atoms as a result of their light shifts, thus channeling them between the planes of the standing wave. Furthermore, their deBroglie wavelengths become comparable to the channel size so that the motion is quantized in these half-wavelength sized optical traps. This $F = 1 \rightarrow 0$ transition produces only one light-shifted level, and thus only one ground state sublevel that can support bound quantized states. An rf-induced transition that would change the populations of the quantum vibrational states of this potential would be particularly easy to interpret, and would be subject to easily understood Zeeman shifts in a longitudinal field. We are presently studying this problem.

Supported by NSF, ONR, AFOSR, and CAPES (Brazil)

Submitted by Harold Metcalf


Signature, APS Life Member

- ☒ Prefer Poster Session
☐ Prefer Standard Session
☐ No Preference

Harold Metcalf
Physics Department
State University
Stony Brook, NY 11794

Abstract Submitted
for the May 1993 Meeting of the
Division of Atomic, Molecular and Optical Physics

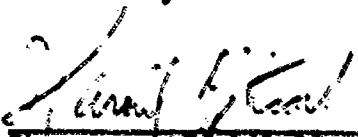
Physical Review
Analytic Subject Index
Number: 32.80.Pj

Bulletin Subject Heading
in which paper should be placed:
Laser Cooling

Raman Processes in Sub-Doppler Laser Cooling. C. XIE, S. PADUA, R. GUPTA, H. BATELAAN, and H. METCALF, SUNY Stony Brook - We have observed a new type of sub-Doppler laser cooling with neither polarization gradients nor magnetic fields. All known sub-Doppler laser cooling methods require one of these two to redistribute the atomic population among the energy levels. This allows the irreversible processes of optical pumping (OP) to manipulate the conservative force of light shifts (e.g. resonant exchange between the two beams comprising a standing wave) [1] into a damping force. Our scheme employs stimulated Raman transitions between ground state hyperfine levels of Rb with a bichromatic standing wave, accompanied by a momentum change of $\Delta p \approx 2\hbar k$. OP, with $\Delta p = 1\hbar k$, creates a population imbalance allowing repetition of the Raman process. When the detuning of the light from Raman resonance δ is properly chosen, the net momentum exchange damps the atomic motion. Changing δ by only $\pi/6$ (1 MHz) replaces cooling by heating. This process separates the velocity selective Raman resonance and OP processes differently from others, and helps clarify the role of these different mechanisms.

1. G. Nienhuis et al., Phys. Rev. **A44**, 462 (1991).
Supported by NSF, ONR, AFOSR, and CAPES (Brazil)

Submitted by Harold Metcalf


Signature, APS Life Member

- () Prefer Poster Session
(X) Prefer Standard Session
() No Preference

Harold Metcalf
Physics Department
State University
Stony Brook, NY 11794

Abstract Submitted
for the May 1993 Meeting of the
Division of Atomic, Molecular and Optical Physics

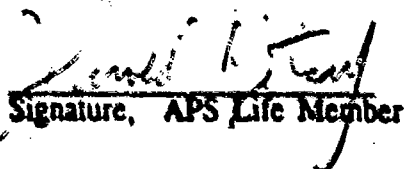
Physical Review
Analytic Subject Index
Number: 32.80.Pj

Bulletin Subject Heading
in which paper should be placed:
Laser Cooling

Transient Effects in Laser Cooling. S. PADUA, C. XIE, R. GUPTA, H. BATELAAN, T. BERGEMAN, and H. METCALF, SUNY Stony Brook -- Transient laser cooling (TLC) can produce cooling and heating, but often with the opposite detuning from that found in steady state. In TLC the time scale is set by the optical pumping (OP) rate to a state not coupled by the laser field. The combination of such OP processes and the conservative light shift potential $U_0 \sin^2 k z$ leads to TLC. The average PE of atoms entering a standing wave is $U_0/2$. They experience the optical force until undergoing OP to an uncoupled state, which is more likely to happen at high light intensity, near an antinode. For $\delta > 0$ this means higher PE and thus lower KE, and conversely for $\delta < 0$. In TLC there is no final "temperature" resulting from competition between a damping force and diffusive heating. Instead the changes in KE are bounded by U_0 so that the signal widths decrease with intensity. This can result in sub-Doppler widths. We have made two independent theoretical studies of these experiments. In a semiclassical calculation we evolve the motion for a calculated OP time and calculate the velocity distribution. We have also performed fully quantum mechanical calculations of the motion of atoms in the standing wave whose basis set consists of product states of internal and external atomic coordinates.

Supported by NSF, ONR, AFOSR, and CAPES (Brazil)

Submitted by Harold Metcalf


Signature, APS Life Member

- ☐ Prefer Poster Session
☐ Prefer Standard Session
☒ No Preference

Harold Metcalf
Physics Department
State University
Stony Brook, NY 11794

Abstract Submitted

for the May 1993 Meeting of the

Division of Atomic, Molecular and Optical Physics

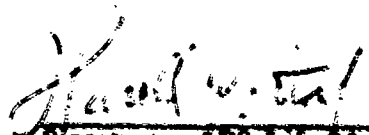
Physical Review
Analytic Subject Index
Number: 32.80.Pj

Bulletin Subject Heading
in which paper should be placed:
Laser Cooling

Longitudinal Magnetic Field Effects in SubDoppler Cooling. R. GUPTA, C. XIE, S. PADUA, H. BATELAAN, and H. METCALF, SUNY Stony Brook--Sub-Doppler laser cooling can be achieved in the absence of polarization gradients when a weak transverse magnetic field is used for mixing eigenstates of the light shift operator. By contrast, Zeeman shifts from magnetic fields B_z along the quantization axis can add or subtract with the light shifts of those states. B_z thus provides an additional degree of freedom for studying magnetic effects in laser cooling since the set of sinusoidal potentials that derives from the spatially periodic light shifts in a standing wave can be manipulated with the field. For example, with circularly polarized light, a finite B_z can switch the normal heating to cooling, and vice versa. We have done such experiments in the $F = 3 \rightarrow 4$ transition of ^{85}Rb at $\lambda = 780$ nm with diode laser light, and have shown that sub-Doppler heating and cooling can be interchanged with opposite longitudinal field directions, in good agreement with this model. One application of such experiments is to characterize precisely the magnetic fields seen by the atoms along their trajectories in the beam.

Supported by NSF, ONR, AFOSR, and CAPES (Brazil)

Submitted by Harold Metcalf


Signature, APS Life Member

- ☒ Prefer Poster Session
☐ Prefer Standard Session
☐ No Preference

Harold Metcalf
Physics Department
State University
Stony Brook, NY 11794

Abstract Submitted

for the May 1993 Meeting of the

Division of Atomic, Molecular and Optical Physics

Physical Review
Analytic Subject Index
Number: 32.80.Pj

Bulletin Subject Heading
in which paper should be placed:
Laser Cooling

Sub-Doppler Laser Cooling of Metastable He. M. WIDMER, M.J. BELLANCA, E. VREDENBREGT, T. BERGEMAN, and H. METCALF, SUNY Stony Brook -- We have observed magnetically induced laser cooling (MILC) on the $J = 1 \rightarrow 2$ component of the $2^3S \rightarrow 2^3P$ transition at $\lambda = 1.083 \mu\text{m}$ in metastable helium (He^*). At low magnetic field the measured widths of our atomic velocity distributions are as narrow as $2\hbar k$, corresponding to a temperature $\approx 3 \mu\text{K}$ (1-D Doppler limit $\approx 26 \text{ K}$). At higher fields ($\sim 150 \text{ mG}$) the velocity distribution splits into two peaks of sub-Doppler width whose separation is proportional to the Zeeman splitting. Our measurements are consistent with model calculations based on the time evolution of quantum density matrices. Our experiments explore the transition regime between the quantum mechanical and semiclassical models of momentum exchange in atom-light interactions because of the large ratio (0.4) of the recoil velocity $\hbar k/M$ to the rms of the Doppler-limited velocity distribution $\sqrt{\hbar\gamma/3M}$ for this transition. We use a supersonic LN_2 cooled nozzle source excited by a dc discharge for He^* , and we excite the 2^3P state with a home-built diode-laser-pumped LNA laser.

Supported by NSF, ONR, AFOSR, and Dept. Educ.

Submitted by Harold Metcalf


Signature, APS Life Member

- () Prefer Poster Session
- () Prefer Standard Session
- () No Preference

Harold Metcalf
Physics Department
State University
Stony Brook, NY 11794

Abstract Submitted
for the May 1993 Meeting of the
Division of Atomic, Molecular and Optical Physics

Physical Review
Analytic Subject Index
Number: 32.80.Pj

Bulletin Subject Heading
in which paper should be placed:
Laser Cooling


Quantum Calculations For One-Dimensional Cooling Of Helium. E. VREDENBREGT, M. DOERY, T. BERGEMAN and H. METCALF, SUNY Stony Brook -- We report theoretical velocity distributions for sub-Doppler laser cooling of metastable $\text{He}^*(2^3\text{S})$, calculated with the Density Matrix ¹⁾ and Monte Carlo Wavefunction ^{2,3)} approaches. For low-field ($B = 50$ mG) magnetic-field induced laser cooling on the $2^3\text{S} \rightarrow (2^3\text{P}, J = 2)$ transition ($\lambda = 1083$ nm), we get a narrow, sub-Doppler structure, consisting of three, ~ 1 photon recoil wide peaks, spaced ~ 1 recoil apart. With increasing field, this three-peak structure develops into two velocity-selective resonance (VSR) peaks, each ~ 2 recoils wide. For the $2^3\text{S} \rightarrow (3^3\text{P}, J = 2)$ transition ($\lambda = 389$ nm), VSR peaks are predicted to appear at low field without the third, central peak, which only develops at higher field ($B = 200$ mG). Additional computations deal with polarization-gradient cooling. In general, we find that for one-dimensional cooling calculations, the Density Matrix method is more efficient than the Monte Carlo Wavefunction approach. Experiments are currently under way to test the results. Supported by NSF, ONR, AFOSR and CNSF.

1) Y. Castin, J. Dalibard and C. Cohen-Tannoudji, Proceedings LIKE, Eds. L. Moi et al. (ETS Editrice, Pisa, 1990) pg. 5

2) J. Dalibard, et al., Phys. Rev. Lett. 68 (1992) 580

3) R. Dum, P. Zoller and H. Ritsch, Phys. Rev. A45 (1992) 4879

Submitted by Harold Metcalf


Signature, APS Life Member

- () Prefer Poster Session
- () Prefer Standard Session
- () No Preference

Harold Metcalf
Physics Department
State University
Stony Brook, NY 11794

ABSTRACT CONTRIBUTED TO WORKSHOP ON QUANTUM OPTICS

JILA, UNIV COLORADO, BOULDER, CO 30 JUNE - 2 JULY 1993

DARK STATES AND LASER COOLING

R. Gupta, S. Padua, C. Xie, M. Widmer, M-J. Bellanca,
H. Batelaan, E. Vredenburg, and H. Metcalf

PHYSICS DEPT. STATE UNIVERSITY OF NEW YORK, STONY BROOK, NY 11790

I. Introduction. We present the results of a series of one-dimensional laser cooling experiments where atomic dark states play an important role. In some cases the atoms are removed from the dark states, and this process is vital to the cooling mechanism. In other cases the dark states are velocity dependent, and thus atoms in such states are "cold" by virtue of their narrow velocity distribution. All the experiments are done in a one-dimensional standing wave at sufficiently low intensity and large detuning that the excited state population is small. The laser beams are crossed by an atomic beam that is cooled in its transverse direction by its interaction with the light field.

We define a generic dark state as a stationary state of the Hamiltonian \mathcal{H} that can not be excited by the light field. \mathcal{H} must include the atom-light interaction as well as the kinetic energy of the atomic motion. In principle, atoms in a dark state could be detected by magnetic deflection or by excitation from a probe laser beam not included in \mathcal{H} .

II.1. Transient Laser Cooling. In the first of the four studies reported here, we consider cooling in the non-steady state case. The optical Bloch equations cannot be solved by setting $dp/dt = 0$ as is usually done, because now atoms are quickly pumped into uncoupled ground states (e.g. alkali hfs) at a rate γ_p . Even in the short optical pumping time $1/\gamma_p$, atoms are subject to the conservative force from the light shift potential (calculated by adiabatically eliminating the excited state). Its sinusoidal spatial dependence, together with optical pumping to the dark state, can be exploited to reduce the average KE of the atoms.

We consider the case of a blue-tuned laser field whose light shift is positive. Atoms that enter in the antinodes are quickly pumped to the dark state by the high intensity light before there is enough time for their KE to change significantly. By contrast, atoms that enter in the nodes must travel to a higher intensity region before they can be pumped, and in doing so must work against the positive light shift and therefore be slowed. Thus on the average atoms are slowed, and cooled. For red tuned light the atoms are heated. Once pumped to the dark state, the cooled atoms are unperturbed by either the conservative force or momentum diffusion because they no longer interact with the light.

II.2. Velocity Selective Coherent Population Trapping (VSCPT) In some arrangements of polarization and atomic angular momentum, atoms irradiated by light beams of different polarizations may be optically pumped to a coherent dark state. This occurs if the light beams are resonant with a Raman transition to provide coherence. For a degenerate pair of ground state sublevels, the two light beams must have the same frequency in the atomic

frame. When they also have the same frequency in the lab frame, then only atoms with $\langle v \rangle = 0$ in a coherent superposition states of $v = \pm \hbar k$ can populate the dark state. Moving atoms will see opposite Doppler shifts of the two laser beams so the Raman resonance condition is not fulfilled unless the atomic energies (including KE) are appropriately split. For cases studied up to now, the dark state can only be reached by a random walk in momentum space (associated with spontaneous emission) with steps of size $\hbar k$. Thus the rate of populating the dark state is quite small.

Recently two groups have suggested that the polarization scheme $\text{lin} \angle \text{lin}$ at 45° can both produce dark states and provide polarization gradient cooling into them. We have observed the dramatically increased rate of populating these states in the $J = 1 \rightarrow 1$ transition of metastable He. This has enormous promise for production of diffraction limited atomic beams (limited only by their deBroglie wavelength). We are now studying this effect for quantitative comparison with theory.

II.3. The Simplest Angular Momentum Scheme for Sub-Doppler Laser Cooling (SDLC) All the polarization gradient and magnetic mixing schemes of SDLC require multiple ground state sublevels and optical pumping among them. The natural question to ask is "What is the simplest possible level structure that permits all types of SDLC?" For realistic situations, this "hydrogen atom of SDLC" is an $F_g = 1 \rightarrow F_e = 0$ transition. Such a system always has dark states in 1-D, although the choice of basis determines their composition from the M_F states. In a pure standing wave there are always two dark states, but in a polarization gradient there is only one. Atoms pumped into these may be released from them by an appropriate \vec{B} field.

We have demonstrated all the different types of SDLC in this system using ^{87}Rb . These include $\text{lin} \perp \text{lin}$ and $\sigma^+ - \sigma^-$ polarization gradients in a \vec{B} field to empty the dark states. The \vec{B} field must not be parallel to any polarization axes, and must be strong enough to define the quantization axis. All these experiments can be described by a Sisyphus picture of cooling to $v = 0$. Furthermore, we have observed several examples of SDLC to a non-zero velocity proportional to $|\vec{B}|$ using velocity selective Raman resonances (VSR). All our $F = 1 \rightarrow 0$ experiments can be described in the momentum exchange picture of VSR.

II.4. Two Frequency SDLC. Selection rules for the $F = 1 \rightarrow 0$ excitation do not allow decay to a dark hfs state, so re-pumping is not necessary, but this is not so for all excitations. In ^{85}Rb we used two frequencies of light generated by an EOM and tuned to couple the hfs ground states via Raman resonance. When the nodes of the two standing waves coincide, there is only Doppler cooling. However, when the nodes are separated by $\lambda/4$ there is another type of Sisyphus cooling with both lasers tuned blue of resonance, or heating with red tuning. We have measured the dependence of the cooling efficiency on this spatial phase shift and found it sinusoidal, as expected. Furthermore, we also observed VSR peaks that shift linearly with the detuning from Raman resonance in this configuration.

When the two lasers have opposite detuning, one red and one blue, a deflection force appears that does not change sign with velocity. We measured the velocity dependence and capture range of this optical rectification force and found it to be consistent with a simple model.

III. Conclusion. In sections II.1 and II.2 we described experiments where atoms are pumped into dark states, and in II.3 and II.4 we described experiments where dark states were emptied by a \vec{B} field or by light of a different frequency. In each example atoms were cooled below the Doppler temperature (to the recoil limit in VSCPT). In all cases there is a conservative force from the spatially varying light shift potential, and this is manipulated into a dissipative force by the irreversible process of spontaneous decay.

Supported by N.S.F., O.N.R., and A.F.O.S.R.

Beam profile flattener for Gaussian beams

C. Xie, R. Gupta, and H. Metcalf

Department of Physics, State University of New York at Stony Brook, Stony Brook, New York 11790

Received September 8, 1992

We describe a novel technique to make a Gaussian laser beam profile spatially flat. We exploit the angular dependence of the transmission of an étalon to tailor the spatial profile to the desired form. A simple analysis shows why our method works so well and how an étalon could be tuned to give the optimum results at all wavelengths. This technique has enormous advantages over other methods.

The output beams of most lasers are not spatially uniform because the resonant modes of their optical cavities have Gaussian profiles. The output beams of single-mode lasers are usually in the fundamental TEM₀₀ mode that has a Gaussian spatial profile. Since a number of experiments require a flat spatial beam profile, it is important to be able to transform to this kind of laser beam, and several techniques for converting these Gaussian beams to others that have flatter profiles have been developed. We demonstrate a new but relatively simple approach that has the advantages of being highly efficient, quite flexible, and low cost.

There are at least two obvious ways to perform this task. One is to block all but the central region of the laser beam with a small aperture. The resulting beam intensity has a central maximum and decreases toward the edge, but the decrease is not significant if the aperture size is small compared with the Gaussian beam half-width. The advantages of this method are its low cost and ease of implementation. The principal disadvantage of this method is the loss of light. In order to have the intensity difference between the center and the edge be less than 5%, the aperture can only transmit less than 5% of the total beam power. Another disadvantage arises from diffraction by the aperture's edges; the experimental region must not be separated from the aperture by too many times its diameter, or imaging optics must be employed.

Another way is to use a filter whose transmission is not spatially uniform. Consider a nonuniform filter whose transmission $T(r)$ increases from some value $\beta < 1$ at the center ($r = 0$) to unity at some distance r_c from the center. We define $G(r)$ as a Gaussian profile of characteristic width w_r and let the transmission vary as $T(r) = \beta/G(r)$ for $r < r_c$, where $G(r_c) = \beta$, and $T(r) = 1$ for $r > r_c$. The profile of a Gaussian laser beam of waist $w_l = w_r$ transmitted by such a filter is uniform over the region from $r = 0$ to r_c . For $\beta = 1$, $r_c = 0$, and the power of such a beam is zero, but for $\beta = 1/e^2$, this area extends until $r_c = w_l$. The intensity in the uniform part of the beam profile is β times smaller than the peak intensity of the original Gaussian beam, and the total power transmitted in the flat profile region is $-\beta \ln(\beta)$ times the laser beam power.

Such a filter overcomes the great loss of laser power that occurs when one uses an aperture as described above, but there are at least three severe disadvantages to this method of beam profile flattening. First, although such filters are commercially available, they are expensive and usually custom made. Second, it is necessary to choose a filter for a particular value of β and w_r and then match the laser beam waist to the filter. Any flexibility would demand an assortment of such filters. Third, mounting and alignment of the filter is quite critical; it must be centered precisely on the laser beam.

We have developed a beam profile flattening scheme that has many of the advantages of both of these methods without their disadvantages. We exploit the angular dependence of the transmission characteristic of a thin Fabry-Perot étalon to tailor the spatial profile of the beam as desired. Transmission of a nonparallel beam through an étalon gives the familiar bull's-eye pattern similar to Newton's rings. With the proper choice of various parameters, the central region can have transmission $\beta < 1$ at $r = 0$, and its increase toward the first bright ring at $r = r_c$ can vary nearly as $\beta/G(r)$.

For a parallel beam of light whose wavelength is λ in air incident at angle θ , the transmission in air of a solid étalon of thickness d , reflectivity R , and refractive index n' is¹

$$T(\theta') = \frac{1}{1 + F \sin^2(\alpha/2)}, \quad (1)$$

where $\alpha = 4\pi n'd \cos \theta'/\lambda = \alpha \cos \theta'$, $F = 4R/(1 - R)^2$, and $n' \sin \theta' = \sin \theta$. This function is plotted in Fig. 1. At the center, where $\theta' = \theta = 0$, the transmission β is given by $1/\beta = 1 + F \sin^2(\alpha/2)$, and $\beta < 1$ as expected.

For a tunable laser in an application where the laser frequency is not crucial, the frequency can be adjusted for selection of any chosen value of β . For an étalon ~1 mm thick, $\alpha = 4\pi n'd/\lambda \sim 10^4$, so a shift of only a few gigahertz can vary $(1 - \beta)$ by a factor of 3 or more. In a spectroscopy experiment where the laser frequency is constrained by atomic resonances, the value of β can instead be adjusted by varying d or n' . It is particularly convenient to use an air-spaced étalon that can be tuned by varying d with piezoelectric elements. On the other hand, a

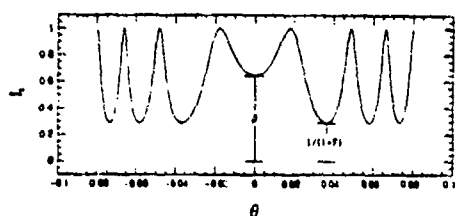


Fig. 1. Angular dependence of the transmission of a Fabry-Perot étalon.

solid étalon can be tuned by varying its temperature, which changes α through both n' and d .^{2,3} For an étalon of modest reflectivity ($F \sim 3$), β can be varied by 0.5 by a change of just a few degrees Celsius.

To calculate the effect of the filter function $T(\theta')$ on a diverging or converging Gaussian laser beam, we note that because α is so large, the lowest-order region requires only a small divergence angle. Thus we can restrict our attention to $\theta' \ll 1$, expand $\cos \theta'$, and keep only the first two terms. We write

$$\begin{aligned} 2 \sin^2(\alpha/2) &= 1 - \cos(\alpha \cos \theta') \\ &= 1 - \cos[\alpha(1 - \theta'^2/2 + \dots)] \\ &= 1 - \cos(\alpha) \cos(\alpha\theta'^2/2) \\ &\quad - \sin(\alpha) \sin(\alpha\theta'^2/2) + \dots \end{aligned} \quad (2)$$

Even though $\alpha \sim 10^4$, $\alpha\theta'^2$ varies between 0 and 2π , so the approximation $\alpha\theta'^2/24 \ll 1$ in Eq. (2) is very well satisfied.

To see that such a filter function will efficiently flatten the profile of a Gaussian beam we note that for a diverging or converging laser beam, θ is proportional to the distance r from the center in a plane perpendicular to the beam axis. We write $r = \theta L$, where $L \gg d$ is the distance from the beam waist to the étalon, and $\theta = n'\theta'$ because $\theta \ll 1$. We write the beam profile as $G_i(r) = G_i(n'L\theta') = \exp[-2(n'L\theta'/w_i)^2]$, set $T(\theta')G_i(\theta') = \beta$, and expand both $T(\theta')$ and $G_i(\theta')$ about $\theta' = 0$. We find that

$$\begin{aligned} 1 - 2(p\theta')^2 + 2(p\theta')^4 + \dots \\ = \beta[1 + (F/2)[1 - \cos(\alpha) \cos(\alpha\theta'^2/2) \\ - \sin(\alpha) \sin(\alpha\theta'^2/2)] \end{aligned} \quad (3)$$

where $p = n'L/w_i$ and typically $p \gg 1$.

Equating the θ' -independent terms gives β as discussed above, and choosing a particular spacing or temperature sets both α and β for a given étalon (fixed F). Comparing the next-order terms in θ' , we find that the condition for cancellation of the θ'^2 term is $\beta\alpha F \sin(\alpha) = 8p^2$, and it can be satisfied by varying L (and thus p) with a small telescope. Similarly, the condition for cancellation of the θ'^4 term is $\beta\alpha^2 F \cos(\alpha) = 32p^4$. This last condition can be met by selecting F and modifying the étalon spacing or temperature accordingly to maintain the desired α . The two conditions together require that $\cos(\alpha) = F/(F+2)$. Keeping terms in θ'^4 in Eq. (2) does not change these conclusions but only causes small changes in the numerical factors. Figure 2 shows plots of the function $T(r)G_i(r)$ for a range of

β 's. Of course, the choice of which parameter (T , p , or F) to cancel which term in θ' can be made in any order, and F could be used, for example, to choose β .

This system has several obvious advantages over previously used beam-flattening methods. First, it allows maximum flexibility for the use of the available power and still achieves extraordinary uniformity across the beam profile, as shown in Fig. 2. Second, it is easily adjustable for beams of different sizes. The angular divergence is simply adjusted with a small Galilean telescope. No centering of the beam or the étalon is needed. Third, its cost is much lower than that of most available Gaussian filters, and suitable étalons are widely available. By contrast, it has two notable disadvantages. First, β is frequency dependent, and in a scanned frequency spectroscopy experiment, the étalon spacing or temperature would have to be tuned with the laser. In addition, there might be some problems with multi-mode lasers, but since typical mode separations are a few hundred megahertz, the effect on β should be small. Second, light that is not transmitted by the étalon is reflected back to the laser, where such feedback may cause stability problems.

In our experiments, we use diode-laser light to excite atoms in an atomic beam. We need a rectangular beam of light that is uniform only along the atomic beam direction. Furthermore, we can afford to have absolutely no reflection back to the laser because diode lasers are extremely sensitive to tiny amounts of feedback. Fortunately the étalon filter described above offers solutions to both of these problems by using higher orders of the étalon for beam profile flattening. In this case, the beam is diverging in only one dimension, and the étalon is tilted to some few-degree angle θ_0 with respect to the laser beam. Thus the transmission pattern is a series of unequally spaced parallel stripes instead of rings, and we work in one of the outer stripes. Of course, the range of angles θ' about θ_0 is still restricted to allow $\sin(\alpha/2)$ to range over less than one cycle.

This scheme offers two additional advantages over the zero-order method described above. First, the choice of θ_0 offers yet another free parameter to help flatten the beam profile. For example, θ_0 can be varied to maintain β in a frequency-swept spectroscopy experiment. Second, light not transmitted by the

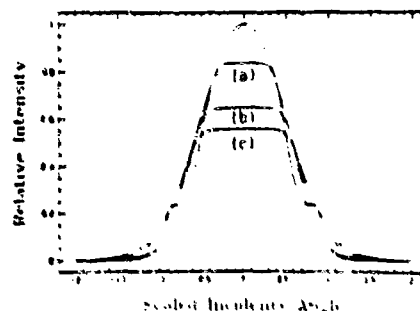


Fig. 2. Calculated transmitted profile of a Gaussian beam by a solid étalon for several different values of β . Here β is varied by choosing R to be 10% [curve (a)], 30% [curve (b)], and 50% [curve (c)].

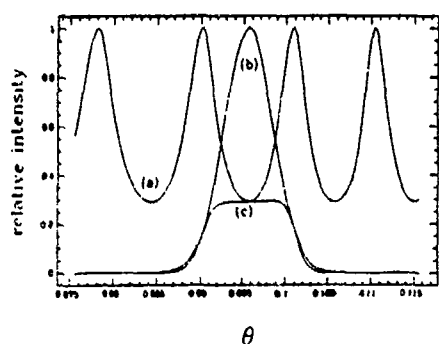


Fig. 3. Calculated transmitted profile of a Gaussian beam in one dimension by a solid étalon in third order (third ring). Curve (a) shows the transmission function, curve (b) shows the Gaussian profile, and curve (c) is their product.

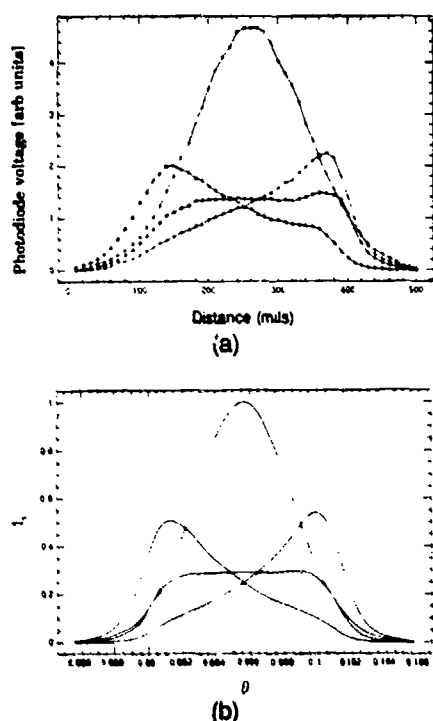


Fig. 4. (a) Measured and (b) calculated spatial profiles of a diode-laser beam using our solid étalon.

étalon is reflected, and the spatial profile of the light beam reflected out at angle 2θ , has a strong central intensity maximum that can be easily injected into a fiber and/or used for laser diagnostics such as saturated absorption for laser frequency locking. Note that this scheme flattens the beam profile in only one dimension instead of two, but that is precisely what is needed for exciting atoms in a beam that crosses the laser beam.

The few center stripes of the transmission pattern are rather asymmetrical about their minima (Fig. 1), but the next few are quite satisfactory, both because their asymmetry is relatively small and because they are not so tiny that they are difficult to use. Expansion about $\theta' = \theta_0/n'$ instead of $\theta' = 0$ is straightforward, but in that case β is determined by F instead of being a free parameter. The expansion

is not discussed here, but the results of numerical calculations are presented in Fig. 3.

We have measured the flattened beam profiles produced this way for several different laser and étalon parameters and present the results in Fig. 4. In all cases, the experimental curves in Fig. 4(a) are in excellent agreement with the calculated curves in Fig. 4(b). The most striking aspect of Fig. 4 is not the good agreement between the measured and calculated beam profiles but just how flat the profiles can be made with this simple device. By changing the angle of the étalon, one can tailor a profile that is very flat from one end to the other. The slight asymmetry introduced by the asymmetry of the transmission curve can be partially compensated by a slight additional tilt and can be minimized by using a higher-order transmission curve. We found that, over a wide range of values of β , typically 40% of the laser beam power could be in the top-hat-shaped profile this way.

All the measurements were done with a Sharp LT021 5-mW semiconductor laser operating at 780 nm at room temperature. The solid étalon was ≈ 0.6 mm thick and coated for $R \approx 30\%$ at $\lambda = 800$ nm. The spatial profile was scanned with a photodiode by using a 100- μ m slit mounted in front of it.

In summary, we have demonstrated an extremely flexible, efficient, and low-cost technique to make a Gaussian laser beam profile spatially flat by exploiting the angular dependence of the transmission of an étalon. The method can be easily scaled up to high-power lasers for industrial cutting and welding and scaled down to miniature devices for printers, communications, and medical diagnostics and treatment. It can be used in the UV for curing, photolithography, and semiconductor processing and in the IR for heating. It is applicable to any Gaussian beam but may be especially useful with diode lasers that have different angular divergences in two dimensions. One could also imagine using the spatially dependent light shift of atoms traveling through the ring pattern as a Fresnel lens for focusing the atoms. One future topic for study is the long-distance propagation of the sub-Gaussian transmitted beam and the super-Gaussian reflected beam. We have calculated that the phase fronts of the flat profile region are quite uniform and thus expect this portion of the beam to propagate as a plane wave over a long distance.

This research was supported by the National Science Foundation, the U.S. Office of Naval Research, and the U.S. Air Force Office of Scientific Research.

References

1. M. Born and E. Wolf, *Principles of Optics* (Pergamon, New York, 1975), p. 327.
2. For a temperature τ we have $da/d\tau = a[(1/n')(dn'/d\tau) + (1/d)(dd/d\tau)]$. For a quartz étalon, the first term in brackets is $6.5 \times 10^{-6}/^\circ\text{C}$ and the second term is $0.55 \times 10^{-6}/^\circ\text{C}$, so for $a = 10^4$, $da/d\tau \sim 0.07 \text{ rad}/^\circ\text{C}$.
3. W. Koechner, *Solid-State Laser Engineering*, 2nd ed. (Springer-Verlag, New York, 1988), pp. 217-218.

Transient Laser Cooling

S. Padua, C. Xie, R. Gupta, H. Batelaan, T. Bergeman, and H. Metcalf

Physics Department, State University of New York, Stony Brook, New York 11790

(Received 17 February 1993)

We observed a new type of sub-Doppler cooling that employs neither polarization gradients nor magnetic fields, and involves neither a damping force nor significant diffusive heating. Instead, light shifts combined with optical pumping (OP) to levels not coupled by the laser field gives transient cooling, and steady state is not achieved. The time scale is set by the OP rate. We observe both cooling and heating, but often with the opposite detuning from that of steady state. A semiclassical and a fully quantum mechanical calculation of transient cooling agree very well with one another and with our data.

PACS numbers: 32.80.Pj

Laser cooling of neutral atoms requires velocity-dependent optical forces that arise from the motion of an atom in a nearly resonant light field. If the selection rules require that excited atoms spontaneously decay to only the initial state, the velocity-dependent interaction arises from the Doppler shift of the laser-driven transition. In this case one readily calculates a minimum achievable temperature called the Doppler limit, $T_D = \hbar\gamma/2k_B$, where $\tau \equiv 1/\gamma$ is the excited-state lifetime [1]. By contrast, if the ground state has multiple sublevels accessible from the excited state, much lower temperatures are achievable [2-4]. The transitions from these sublevels may be driven by different polarizations, and thus sub-Doppler temperatures are often associated with polarization gradients. The cooling force derives from the failure of the internal state of moving atoms to follow adiabatically the changing optical environment of a spatially inhomogeneous optical field, such as that produced by light beams of different polarizations.

For slow enough atomic velocities, however, this non-adiabatic part of the force is small compared with the velocity-independent force that derives from the spatially varying light shifts of the atoms. In a standing wave, this conservative force produces channels that can strongly influence atomic motion or even confine atoms in $\lambda/2$ size regions [5,6]. Furthermore, spontaneous decay in a standing wave can provide the irreversible process needed to produce a dissipative force that cools atoms [7].

We report here a theoretical and experimental study of sub-Doppler atom cooling achieved by transient effects of laser excitation. We have found that cooling and heating can occur when the atom goes through only a few optical pumping (OP) cycles, but often with opposite detuning from that of steady-state situations. In most other types of sub-Doppler laser cooling, a damping force $F = -\tau(\rho \nabla H)$ can be computed from the steady-state solution of the optical Bloch equations for the density matrix ρ . This is appropriate because the laser cooling processes generally continue for times long compared with OP transients. In transient laser cooling, the time scale is set by the OP rate to a ground state that is not coupled to an excited state by the laser field ("dark state") so steady-state solutions are inappropriate and a damping

force cannot be defined [8].

For an intuitive understanding of how transient cooling works, consider the conservative motion of atoms that enter a standing-wave field nearly transverse to its \mathbf{k} vectors, but with a small velocity component v_z of a few cm/s parallel to $\mathbf{k} = k\hat{z}$. Such atoms experience a spatially varying light shift potential $U(z) = U_0 \sin^2(kz)$ that produces a sinusoidal force. (U_0 takes the sign of the detuning $\delta \equiv \omega_{\text{laser}} - \omega_{\text{atom}}$ and is proportional to the intensity at low intensity.)

The atoms experience this force until they are optically pumped to a dark state. Since the OP rate $\gamma_p(z) \equiv \tilde{\gamma}_p \times \sin^2(kz)$ vanishes at the nodes, OP is slower for atoms that enter the standing wave near a node, and thus the average kinetic energy (KE) change is greater for such atoms. For $\delta > 0$, more KE is lost by atoms moving away from a node than gained by atoms moving away from an antinode, so on average atoms lose KE [Fig. 1(a)] and conversely for $\delta < 0$ [Fig. 1(b)]. This contrasts with other types of cooling where the optical force may either heat or cool the atoms depending on both the angular momentum scheme ($F_g - F_e$) and the detuning: Here $\delta > 0$ always gives cooling.

We have performed classical trajectory calculations based on the above model by integrating the equation $m\ddot{z} = kU_0 \sin(2kz)$. For initial conditions we choose v_0 and z_0 distributed uniformly in the intervals $[-30, 30]$ cm/s and $[0, \lambda/2]$, respectively. In the weak excitation approximation, the upper state can be neglected, and the ground-state potential amplitude $U_0 = 2\hbar s C \delta / L$, where $s = I/I_{\text{sat}}$ is the laser saturation parameter, C is the strength of a particular transition, and $L = 1 + (2\delta/\gamma)^2$. The saturation intensity for the strongest component of this transition ($C=1$) is $I_{\text{sat}} = \hbar c / \lambda^3 \tau \approx 1.6$ mW/cm² in Rb, where $\tau = 1/\gamma \approx 27$ ns.

From the solution $z(t)$ to these equations of motion we find the OP rate $\gamma_p(t) = \tilde{\gamma}_p \sin^2[kz(t)]$, where $\tilde{\gamma}_p = 2sC \times B\gamma/(L + sC)$ and B is the branching ratio to the dark states. Then the probability of OP between t and $t+dt$ is $P(t)dt = \gamma_p(t) \exp[-\int_0^t \gamma_p(t')dt']dt$. The primitive of $P(t)$ is then inverted to find a distribution of pumping times. A Monte Carlo approach uses these pumping times to terminate the classical motion, and the resulting

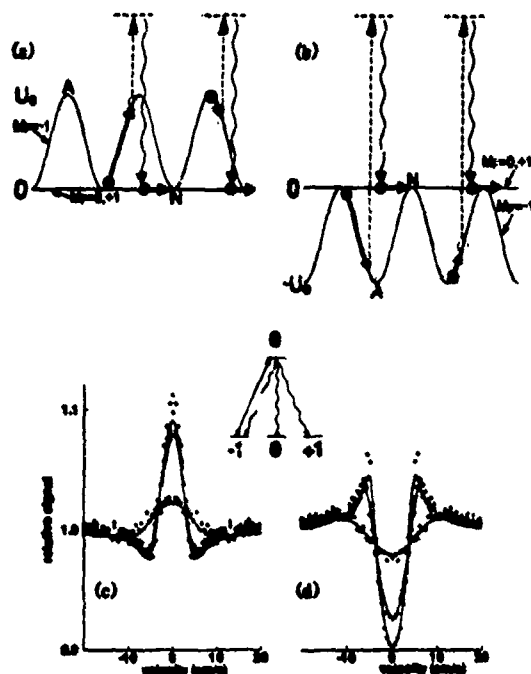


FIG. 1. (a) The light shift potential and optical pumping scheme for $\delta > 0$. Atoms entering near a node travel further before OP, and therefore lose more KE than atoms entering near an antinode, which travel a shorter distance before OP. (b) Similar to (a), but for $\delta < 0$ atoms gain more KE than they lose. (c) Velocity distributions found from the semiclassical calculation (dots) for the transition shown in the inset. Here $s=0.66$ and $\delta=+12$ MHz (as in Fig. 3). "Snapshots" of the velocity distribution are made at times 3, 6, and 9 μ s. The solid lines show the results of quantum mechanical calculations for the same conditions. (d) Similar to (c) but for $\delta=-12$ MHz. Inset: One of the simplest level schemes for transient cooling, $F_g=1 \rightarrow F_e=0$ with σ^+ excitation.

velocity distribution is calculated.

We have applied this approach to the simplest atomic scheme of the classical scheme above, an $F=1 \rightarrow 0$ transition with σ^+ excitation, shown in Fig. 1 (inset). Results of these calculations are shown in Figs. 1(c) and 1(d) (dots). The sharp features in Fig. 1(d) for $\delta < 0$ occur at stationary points where $E_{\text{kin}}=U_0$. It is clear that this simple model of transient laser interactions gives cooling for blue detuning and heating for red detuning for this $F=1 \rightarrow 0$ transition.

Figures 1(c) and 1(d) also show remarkable agreement between the classical results and results of a fully quantum mechanical calculation including the excited state explicitly (solid lines). The sharp cooling and heating features in the classical results are smoothed in the quantum results. We attribute this to neglect of the uncertainty in position and of recoil in the classical calculation.

We can estimate the velocity capture range of transient blue cooling for atoms that move freely without being channeled between the planes of the standing waves. The probability of OP in time t_1 is $P(t_1)=\int_0^{t_1} \gamma_p(z) dt$ for $P(t_1) \ll 1$. To find the mean distance z_1 from a node

where OP occurs, we use $dt=dz/v_z$ and set

$$\int_0^{t_1} [\gamma_p(z)/v_z] dz = \int_{z_1}^{z_1+2\lambda} [\gamma_p(z)/v_z] dz.$$

For $E > 2U_0$, the variation of v_z with z has little effect on z_1 so it comes out of the integrals, and we find $\sin^2(kz_1)=0.83$. Thus atoms undergo OP from a position where their average light shift (potential energy) is $\sim \frac{1}{2} U_0$, and since their initial spatial distribution was uniform so their average initial potential energy was $U_0/2$, the average total energy change is $\Delta E \sim -U_0/3$. This is a mechanical energy loss for $U_0 > 0$ ($\delta > 0$) and a gain for $U_0 < 0$ ($\delta < 0$). This process does not make a very large change in the velocity distribution for atoms with E more than a few times U_0 because $\Delta v_z/v_z = \Delta E/2E \sim -U_0/6E$. This estimate of the capture velocity is consistent with the detailed computational results of Fig. 1 and with the data.

In this transient cooling process, the final velocity distribution does not result from competition between a steady-state damping force and diffusive heating. Instead we find the changes in KE are bounded by U_0 . The widths of the cooling peaks (and heating dips) in the measured velocity distributions decrease with intensity so that widths substantially below the Doppler limit are attainable, as shown by our measurements.

The experiments use a thermal beam of natural Rb produced by an oven at $T \sim 150^\circ\text{C}$ with horizontal slit aperture 0.06 mm high by 2 mm wide, and a vertical beam defining slit 2 mm high by 0.06 mm wide about 35 cm away [9]. The atoms emerge from the vertical slit in a fan-shaped beam and then interact with a pair of counterpropagating laser beams transverse to the atomic beam axis. The nearly flat atomic beam profile is measured with a scanning hot platinum-tungsten wire, 25 μ m in diameter, 1.3 m away from the region of interaction with the laser beam. Three square Helmholtz coil pairs cancel the Earth's field.

A 35 mW Sharp LT025 diode laser is locked at the $5S \rightarrow 5P$ transition of Rb near $\lambda=780$ nm by saturated absorption in a vapor cell at room temperature. The spatial intensity profile of the 23 mm long \times 5 mm high laser beam is flattened to a few percent by a tilted etalon [10]. For thermal velocity atoms ($\bar{v} \sim 350$ m/s) the average interaction time is 63 μ s. The turn-on and turn-off edges of the light field are sharpened by an aperture and diffraction limited to about 0.3 mm, corresponding to an entrance and exit time of < 1 μ s for atoms at thermal velocity. For most experimental conditions, the OP time is longer than 1 μ s.

In order to explore the phenomena sketched above, we have measured the transverse velocity distribution of our atomic beam after it passes through the circularly polarized standing wave in zero magnetic field. For the $F_g=1 \rightarrow F_e=2$ transition of ^{87}Rb (dashed line in Fig. 2), OP to the dark state $F_g=2$ is allowed. Figure 3(a) shows clear evidence of cooling for light detuned blue by

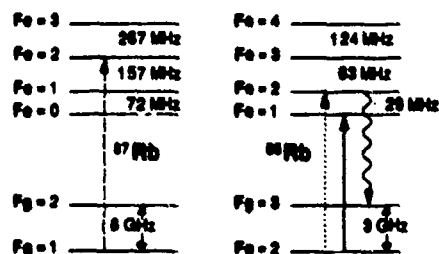


FIG. 2. The hyperfine energy level scheme of the Rb isotopes showing transitions of interest in this paper.

$\delta = +12$ MHz ($\approx 2\gamma$) from this transition, and Fig. 3(b) shows heating for $\delta = -12$ MHz. This demonstration of blue cooling (sub-Doppler) and red heating appears in all our data for all the allowed transitions of Fig. 2.

Figure 3(a) shows significant blue cooling even with s lowered to ~ 0.066 by a neutral density (ND=2) filter. At this intensity, the average OP time $\bar{\tau}_p = 1/\bar{\gamma}_p$, found by averaging γ_p over a wavelength and over the various transitions, is 64 μ s. (Typically, $\bar{\gamma}_p/\bar{\gamma}$ ranges from 2 to 4.) This is fortuitously close to the average 63 μ s interaction time for atoms in our thermal beam. When the interaction region is shortened from the 23 mm of Fig. 3(a) to only 1.4 mm, corresponding to an average interaction time of only 4 μ s, there is still clear evidence of cooling on the blue side for $s \approx 6.6$.

Excitation of ^{85}Rb on the $F_g=2 \rightarrow F_e=1$ transition (solid line of Fig. 2) presents a close analog to the $F_g=1 \rightarrow F_e=0$ model discussed above, because the $F_e=1$ state cannot decay to $F_g=3$. However, OP can occur to the $F_g=2$, $M_F=+1$ and $+2$ magnetic sublevels, which are "dark" in our σ^+ light. The low intensity data near the top of Fig. 4(a) clearly show cooling signals with σ^+ light detuned +6 MHz blue of this $F_g=2 \rightarrow F_e=1$ transition. At the lowest intensity of Fig. 4(a) (top trace), U_0/\hbar is only 11 kHz so the expected change in the velocity of an atom is less than the recoil velocity $\hbar k/M$, the transient cooling effects are washed out by the momentum changes from the random direction of spontaneous emission.

At higher intensity, a second phenomenon appears. Light tuned 6 MHz blue of this $F_g=2 \rightarrow F_e=1$ transition of ^{85}Rb is also 23 MHz red of the $F_g=2 \rightarrow F_e=2$ transition (dotted line of Fig. 2). Although atoms optically pumped to the $(F_g, M_F)=(2,1)$ sublevel cannot be excited to $F_e=1$ with σ^+ light, there is an allowed transition to the $(F_e, M_F)=(2,2)$ sublevel. Since this state can decay to the $F_g=3$ dark state (wiggly line in Fig. 2), transient effects can occur. Using $\bar{\tau}_p$ calculated as before, we find the rate for this further off-resonant transition to be significant only at high enough intensity. This slower process involves light tuned red of resonance, so it heats instead of cools the atoms as shown in the high intensity traces of Fig. 4(a). The data of Fig. 4(a) clearly show a change from cooling to heating as s increases

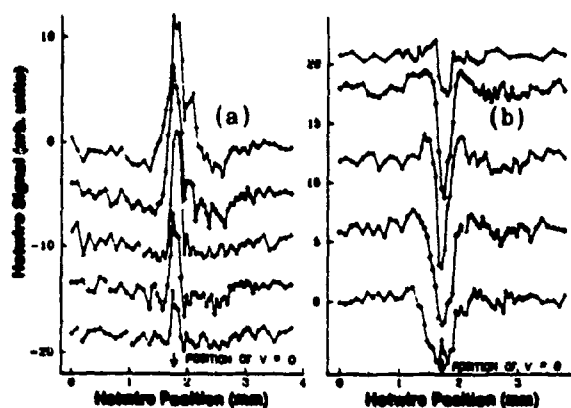


FIG. 3. (a) Measured atomic beam profiles for circularly polarized light tuned 12 MHz blue of the $F_g=1 \rightarrow F_e=2$ transition of ^{87}Rb . The intensities are 0.1, 0.3, 1.0, 3.0, and 10 mW/cm^2 (bottom to top), and the saturation intensities for the three magnetic components are 19.2, 6.4, and 3.2 mW/cm^2 (3.2 for $M_F=1 \rightarrow 2$). The vertical scale's arbitrary units are $\sim 1\%$ of the atomic beam intensity. For the mean longitudinal velocity of 350 m/s, a 37 μm displacement represents 1 cm/s, so the width of the third peak (saturation ≈ 1 for $M=1 \rightarrow 2$) is 6 cm/s, corresponding to about $\frac{1}{2}$ of the Doppler limit. (b) Similar results for light tuned 12 MHz red of the same transition.

from 0.3 to 1.0 for our 63 μ s interaction time, corresponding to $\bar{\tau}_p$ going from 80 to 24 μ s.

We can also observe this phenomenon by varying the interaction time at fixed s . Figure 4(b) shows transient cooling on this $F_g=2 \rightarrow F_e=1$ transition at short times,

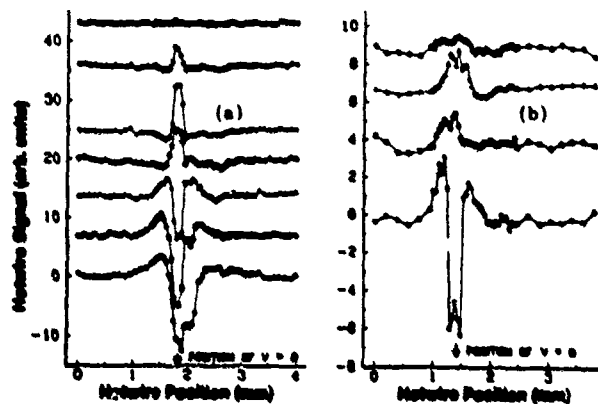


FIG. 4. (a) Measured atomic beam profiles for circularly polarized light tuned 6 MHz blue of the $F_g=2 \rightarrow F_e=1$ transition of ^{85}Rb . The intensities are 10, 3.0, 1.0, 0.3, 0.16, 0.03, and 0.01 mW/cm^2 (bottom to top), and the saturation intensities for the three components are 16, 5.3, and 2.7 mW/cm^2 (16 for $M_F=0 \rightarrow 1$). For the mean longitudinal velocity of 350 m/s, a 37 μm displacement represents 1 cm/s, so the width of the fourth peak is 4 cm/s, corresponding to about $\frac{1}{2}$ of the Doppler limit. (b) Similar data for interaction times of 32, 16, 8, and 4 μ s (bottom to top). Cooling becomes heating at higher intensity or longer interaction time.

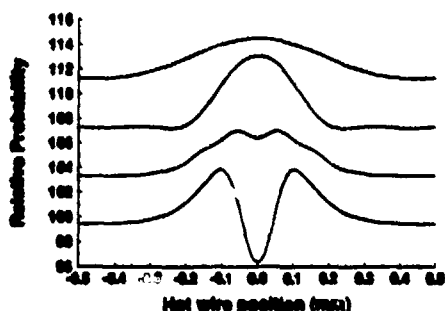


FIG. 5. Velocity distributions found from the fully quantum calculation with $F_g=2$, $F_g=3$, $F_e=1$, and $F_e=2$ internal states included, using appropriate excitation and decay matrix elements. The saturation parameter is taken to be 0.4 and the detuning is 6 MHz above the $F_e=1$ state, as for the experimental data in Fig. 4(b). The successive curves correspond to interaction times of 4, 8, 16, and 32 μ s for the most probable longitudinal velocity in the beam.

but heating as the interaction time increases from 16 to 32 μ s at $s=0.35$. In this case atoms in $(F_g, M_F)=(2,1)$ are given enough time for excitation to $F_e=2$. There is also a small but persistent and repeatable upward peak from the bottom of the heating dip in the high intensity data of Fig. 4(a) and in the long time data of Fig. 4(b). It may come from the $(F_g, M_F)=(2,2)$ atoms that are not heated by excitation to $F_e=2$. All the features of Fig. 4 have also been observed on the $F_g=1 \rightarrow F_e=0$ transition of ^{87}Rb .

As a further illustration of this transient cooling model, we have added a small magnetic field transverse to the axis defined by the circularly polarized standing wave ($B \perp k$). When the Larmor frequency is large enough to precess atoms in the $(F_g, M_F)=(2,1)$ or $(2,2)$ dark states back to the coupled $(2,0)$ state faster than they can be optically pumped to the $F_g=3$ dark state (via $F_e=2$, wiggle line in Fig. 2), the cooling persists to the higher intensities shown in Fig. 3(a).

Multistate processes are difficult to model accurately with classical trajectory calculations, but we have developed a fully quantum mechanical model [11]. The change from cooling to heating shown in Fig. 4 provides an opportunity for sensitive tests of such quantum mechanical calculations. The basis set consists of product states of internal and external atomic coordinates [12]. The set of internal states includes typically two ground and two excited levels so the calculation is not restricted to low excitation rates. The external, center-of-mass motion states are free particle wave functions, allowing inclusion of the recoil effect in every optical transition. The density matrix calculated in this basis includes optical coherence (off-diagonal elements) to sufficiently high order so that the calculated velocity distribution con-

verges. Equations for the temporal evolution of the density matrix are obtained from the optical Bloch equations.

Figure 5 shows the results from these quantum calculations for parameters corresponding to Fig. 4(b). The experimental conditions, including the longitudinal velocity distribution and instrumental resolution, have been carefully modeled. The transverse velocity distribution flips from cooling to heating as in the experiments, but there is an unexplained discrepancy of about a factor of 2 in the width of the final heating dip.

There are various repumping methods that might allow recycling of atoms for further cooling by this technique [7]. Furthermore, it can readily be extended to 2D or maybe even 3D. Also, this technique might be applied to atoms with a first transition in the deep ultraviolet and a metastable state where traditional cooling techniques are difficult to implement. For example, atomic hydrogen in its 2S state could be cooled this way on the easily produced Balmer- α line at 656 nm. Similar possibilities exist in singlet He, rare gases, and alkaline earth D states.

In summary, our experiments with a Rb atomic beam and a transverse standing-wave laser field have demonstrated a new mechanism for sub-Doppler laser cooling. This mechanism requires no polarization gradients or magnetic fields. It operates on a short time scale, determined by the OP times. We have developed a theoretical model with classical trajectories and have also applied a fully quantum mechanical treatment. These models give results close to each other and to the measurements.

This work was supported by NSF, ONR, AFOSR, and CAPES (Brazil). The quantum calculations were performed at the Cornell National Supercomputer Facility, funded by NSF and IBM.

- [1] D. Wineland and W. Itano, *Phys. Rev. A* **20**, 1521-1540 (1979).
- [2] P. Lett *et al.*, *Phys. Rev. Lett.* **61**, 169 (1988).
- [3] *J. Opt. Soc. Am.* **5**, 1961-2288 (1989) (special issue).
- [4] B. Shochy *et al.*, *Phys. Rev. Lett.* **64**, 858 (1990).
- [5] C. Saloman *et al.*, *Phys. Rev. Lett.* **59**, 1659 (1987).
- [6] C. Westbrook *et al.*, *Phys. Rev. Lett.* **65**, 33 (1990).
- [7] A. Aspect *et al.*, *Phys. Rev. Lett.* **57**, 1688 (1986).
- [8] O. Emile, R. Kaiser, C. Gerz, H. Wallis, A. Aspect, and C. Cohen-Tannoudji (to be published).
- [9] S.-Q. Shang *et al.*, *Phys. Rev. Lett.* **65**, 317 (1990); S.-Q. Shang *et al.*, in *Atomic Physics 12*, edited by J. Zorn and R. Lewis (World Scientific, Singapore, 1991), p. 105.
- [10] C. Xie *et al.*, *Opt. Lett.* **18**, 173 (1993).
- [11] T. H. Bergeman (to be published).
- [12] Y. Castin *et al.*, in *Light Induced Kinetic Effects on Atoms*, edited by L. Moi *et al.* (ETS Editrice, Pisa, Italy, 1991).

Quantum calculations for 1D laser cooling:
temporal evolution

T. Bergeman

Department of Physics, State University of New York

Stony Brook, NY 11794-3800

Temporal integration of density matrix equations with quantized translational motion gives new results for laser cooling of atoms. For polarization gradient cooling, the average kinetic energy in the cold atom peak after 1,000 radiative lifetimes decreases with increasing F_0 , and is <1 recoil energy at low laser intensity. With magnetically induced laser cooling (MILC) and low optical pumping rates, atoms cool slowly within the potential wells, giving minima in the velocity distribution at $v=0$. MILC is seen as a cyclic process; optical pumping cools and B field mixing slightly heats.

In view of many recent advances in techniques for cooling atoms by laser light, there is interest in theoretical methods that can address diverse experimental situations. Most of the theoretical results presented to date have been for the steady-state limit of the cooling process. For example, semiclassical theories[1, 2] for atom cooling employ a force versus velocity function and a diffusion parameter based on the steady-state solution of the density matrix equations. The first examples of density matrix calculations with a basis of quantized translational states [3, 4] also presented

steady-state solutions, obtained by inverting the evolution matrix. Exceptions to the steady-state limit are offered by quantum Monte Carlo methods, which have successfully reproduced laser heterodyne results [5]. However, these methods have not been extensively used for multi-level atomic transitions because of the large number of replications needed.

In many 1D atom cooling experiments where an atomic beam traverses counterpropagating laser beams, steady-state solutions are not suitable for comparisons with experiment. For atoms that have been precooled in a 3D magneto-optic trap, the interaction times in a 1D standing wave may indeed be adequate to achieve steady state [6]. However, in experiments with a thermal atomic beam, the interaction time is typically no more than 1,000 to 2,000 τ , where τ is the excited state radiative lifetime. The steady state limit may not be attained, particularly when the initial velocity distribution is appreciably wider than the so-called capture velocity, v_c . The range of atom velocities that are effectively slowed depends on the interaction time. Clearly a theory is needed for finite interaction times.

It will be demonstrated in this report that density matrix methods over a basis of free particle states or of eigenfunctions of the light shift potential are capable of significant extension beyond their use as previously reported [3, 4]. By efficient programming and the use of supercomputer technology, results have been obtained for the temporal evolution and for higher angular momentum. The computational techniques will be illustrated by both lin \perp lin polarization gradient cooling and magnetically induced laser cooling (MILC). Results will be shown for cases in which the incremental velocity change (the recoil velocity) is not small compared with the width of the velocity distribution, thus where semiclassical Fokker-Planck approaches would not be valid. Quantum methods will also be applied to atoms whose kinetic energy is less than the amplitude of the periodic light shift potential.

In this regime, the use of a constant velocity parameter in the computation of the semiclassical force function is inappropriate.

Calculations with a free particle basis here include the excited state explicitly [3]. The basis states, $|F, m_F, n\rangle = |F, m_F\rangle \exp(inkz/\hbar)$, where $2\pi/k$ is the laser wavelength, are products of internal atomic sublevels and free-particle momentum eigenfunctions. In the evolution equation for the density matrix, $\dot{\sigma} = -(i/\hbar)[H, \sigma] + \dot{\sigma}_{rel}$, the Hamiltonian, H , includes the laser-atom interactions (H_L) and possibly magnetic field effects, while $\dot{\sigma}_{rel}$ expresses the effects of spontaneous decay and repopulation, including an average over the spatial distribution of emitted light. Elements of H_L include photon recoil explicitly. Elements of σ are placed in a column vector, x , and the coupled equations $\dot{x} = Wx$ are integrated numerically. These computer programs have been modified to deal with transitions with $\Delta F = -1$ and 0, more than one ground and excited state hyperfine level, and spatially nonuniform laser intensity. In this report, however, only $F \rightarrow F + 1$ transitions are considered and the laser intensity is constant over the interaction region.

A full density matrix for up to ± 50 recoil momenta, even for a mesh spacing of one recoil and a $J = 1/2 \rightarrow 3/2$ transition, would have more than 3×10^4 elements and the evolution matrix would then have 10^9 elements. However, off-diagonal elements with $\Delta n > n_{max}$ are found not to affect the computed velocity distribution. n_{max} varies with laser intensity and detuning but is typically 6 to 12. Effectively, σ becomes a band matrix of order n . In the present calculations, there were up to 100,000 density matrix elements. The evolution matrix, W , can be simplified by neglecting elements less than 10^{-12} in magnitude, for example. No more than 20 to 50 elements are needed in each row for the free particle basis approach. By such means, it is possible to compute the temporal evolution to 1,000 radiative lifetimes with a basis of 65 momentum values for each F, m_F sublevel in

an $F = 3 \rightarrow 4$ transition with about 2 hours of equivalent Cray XMP CPU time.

When the atoms are weakly excited, excited state elements may be eliminated from the density matrix equations to obtain a periodic light shift potential for the ground state [4]. This approach gives a useful physical picture, and for certain applications, uses less computer time. The energy spectrum exhibits a band structure resembling that obtained for electron waves in a 1D crystal lattice. Optical pumping, magnetic field mixing, and spontaneous emission rates are computed for density matrix elements over the basis set of Bloch states.

Results obtained for the lin \perp lin laser configuration, in which two counterpropagating laser beams have orthogonal linear polarization, show that the steady-state limit may not reliably represent cooling processes occurring over shorter interaction times. Fig. 1 shows typical time evolution plots obtained with the free particle basis. Here, $\epsilon = E_R/\hbar\Gamma = 6.4 \times 10^{-4}$, as for Rb, where $E_R = \hbar^2 k^2/2M$ is the recoil energy and Γ is the radiative decay rate. The laser field is characterized by the light shift well depth, $U_0 = -fSh\delta/L$. For lin \perp lin cooling on an $F \rightarrow F+1$ transition, $f = [(2F+1)(F+1)-1]/[(2F+1)(F+1)]$, $S = 2\Omega^2/\Gamma^2$ where Ω is the single beam Rabi frequency, $\delta = \omega_{\text{laser}} - \omega_{\text{atom}}$ is the detuning, and $L = 1 + 4\delta^2/\Gamma^2$. ($S = 1$ for laser intensity $I = \hbar c/\lambda^3\tau$). The calculations shown in Fig. 1a, for $F = 1/2 \rightarrow 3/2$, are carried to 100 $\mu\text{sec.}$, or 3770 τ , where $\tau = 1/\Gamma$. Ultimately, the velocity distribution, $P(v)$, does evolve into the typical form for the asymptotic limit, namely a narrow Gaussian on top of a broad Gaussian [3]. However, up to 40 $\mu\text{s.}$ the narrow Gaussian is flanked by two dips at the capture velocity, v_c (about $16 v_R$ here). The time required to attain the steady state distribution depends on the width of the initial distribution (here assumed flat up to $v_R = 60$) as well as on the intensity and detuning.

With lower laser intensity or wider initial distribution over v , the dips at $v =$

$\pm v_C$ persist for longer times. The generic behavior is shown in Fig. 1b, for $F = 3 \rightarrow 4$. To extract an average kinetic energy for atoms in the central peak, two procedures have been used. The first assumes that the distribution for $|v| < v_C$ is Gaussian. The velocity $v_{1/e}$ at $1/e$ of the maximum height difference then yields a Gaussian average energy, $KE_G = Mv_{1/e}^2/2$. In the second method, one computes the average kinetic energy, KE_A , of atoms in the range $|v| < v_C$. When the distribution in the central peak is truly Gaussian, $KE_A = KE_G$, but typically, $KE_A \sim 0.7KE_G$.

The variation of KE_G with laser parameters after $30 \mu s$ ($1,130 \tau$ for Rb) is shown in Figs. 2a and 2b. For the calculations shown in Fig. 2, $\epsilon = 6.4 \times 10^{-4}$, $\delta = -5\Gamma$, and again the free particle basis was used. To emphasize the role of the well depth, in Fig. 2a KE_G/U_0 is plotted vs. U_0/E_R . For $F_g = 3$, the average kinetic energy in the cold atom peak is significantly less than for $F_g = 1/2$. Since this trend seems to persist to longer interaction times, this may in part explain the experimental observation that the fraction of atoms in the lowest quantum state in experiments on ^{85}Rb , with $F_g = 3$, was larger than computed for $F_g = 1/2$ [6]. One possible explanation for the lower kinetic energies with high F_g is the greater importance of $\Delta m_F = \pm 2$ coherences induced by the laser field, which produce progressively larger off-diagonal elements in the light-shift potential matrix. For high F , energy bands within the potential well are broadened, making the motion for $KE < U_0$ more nearly like that of free particles.

For finite interaction times and $U_0/E_R < 100$, the average kinetic energy for atoms in the central peak is significantly below that indicated in steady-state results, which gave a minimum of $KE \sim 5E_R$ [4]. Here, there appears to be no minimum, and at low intensity (Fig. 2b) $KE_A < E_R$. Because the amplitude of the cooling peak is only 5 - 10% of the initial amplitude at $v=0$ for this regime of low U_0/E_R , such extremely cold atom distributions may be difficult to observe.

For MILC [7, 8], the light shift potential matrix is diagonal and sinusoidal, so the wave equation for each m_F is simply a Mathieu equation. The periodic potential basis approach is appropriate for $S/L \ll 1$. To model experiments in which atoms move freely outside the interaction region, an initially flat distribution over free particle states is projected onto the periodic state basis. After computing the evolution to times t_i , the distribution over the periodic state basis is projected back onto the free particle basis. $Tr(\sigma)$ decreases by a few percent over typical interaction times because the total optical pumping rate out of any quantum basis state is greater than the repopulation terms from this level summed over any finite set of basis states. Results from the periodic potential basis states and free particle basis states are very similar for weak excitation.

The temporal behavior computed for MILC exhibits a new feature associated with the localization of atoms in the standing wave. In MILC, the counterpropagating laser beams have identical circular polarization and the light shift potential maxima and minima for different m_F sublevels are spatially in phase. A transverse magnetic field mixes different m_F sublevels. Zeeman mixing occurs most effectively at the nodes of the laser standing wave, where the potentials are degenerate. (Magnetic field mixing serves the same function as the polarization gradient in lin \perp lin cooling.) With red detuning, when the final kinetic energy is less than the depth of the light shift potential wells in MILC, atoms in the ground state cannot traverse the potential peaks at the nodes, the magnetic field mixing is suppressed, and the cooling rate slows. Although the asymptotic velocity distribution may still be nearly Gaussian, over very extended times there is a deficiency of the coldest atoms. The velocity distribution exhibits a flattened top, or even a minimum at $v = 0$. Fig. 3 shows this effect in the velocity distribution for $F_2 = 1/2$ (in Fig. 3a-c) and for $F_2 = 3$ (in Fig. 3d). In MILC, the effective optical pumping rate, $\Gamma_p = 2S\Gamma/L$.

and $U_0 = -2S\hbar\delta/L$. In Fig. 3a and 3c, $\hbar\Gamma_p = U_0$. When $\hbar\Gamma_p$ is small compared with U_0 , as in Fig. 3b and 3d for which $\hbar\Gamma_p = U_0/20$, the minimum in $P(v)$ at $v = 0$ is more persistent. Fig 4a and 4b show distributions over the states in the periodic potential corresponding to the $P(v)$ distributions shown in Figs. 3a and 3b. The energies of these states are shown at the top of Fig. 4. Below the potential maxima, $U_0/h = 1$ MHz here, there are quasi-discrete states, while for $E > U_0$, the gaps between the bands are narrow. Although cooling increases the population of the states lying below U_0 , the population of the lowest states increases very slowly, particularly when $\hbar\Gamma_p < U_0$.

For stationary states in the light shift potential, the explanations for sub-Doppler laser cooling derived from semiclassical models [2] do not apply. A damping force does not explicitly enter the present calculations. In the quantum representation, cooling occurs because of preferential optical pumping out of higher-lying states into lower-lying states. The way this works in MILC is shown in very schematically in Fig. 5 for states in the light shift potential. Energy bands are shown in columns for $m_F = -1/2$ (left of each transition pair) and for $m_F = 1/2$ (right of each pair). The magnetic field and the laser interactions redistribute the populations over this basis set. The widths of the arrows indicate the relative optical pumping rates or B-field mixing coefficients from various initial states. Not shown is the much slower process of diffusive heating in $\Delta m_F = 0$ excitation and decay. In the optical pumping process, on average the emitted photon takes away more energy than is added by the absorbed laser photon. This is due in part to the difference in the $m_F = \pm 1/2$ potential minima. In addition, optical pumping favors final states localized at the antinodes, namely the lower-lying states for red detuning. On the other hand, the magnetic field does not vary spatially over the interaction region, so the redistribution by the magnetic field is not so sharply peaked at $\Delta n = 0$. These

processes constitute a cooling cycle. The reduction of energy in the $\Delta m_F = 1$ optical pumping part of the cycle is greater than the increase of energy that occurs in $\Delta m_F = -1$ magnetic field mixing and in $\Delta m_F = 0$ diffusive heating.

Comparisons of the results present above with experiment are obviously of great interest. From preliminary results [9], it appears that the $\text{lin} \perp \text{lin}$ results are in good agreement with experiment on Rb and also that results for MILC agree well with experiments on $\text{He } 2^3S$ [10]. However, experimental cooling peaks observed for certain MILC experiments with Rb [9] are narrower, without the dip at $v=0$ found above. One possible explanation is that the optical wavefronts in the apparatus used for Rb are not ideal, and trapping in the light shift wells occurs less than in the calculations. These comparisons and comparisons with semiclassical calculations will be discussed in future publications.

This work was supported by NSF, ONR, and AFOSR. I am indebted to H. Metcalf J. Dalibard, R. Gupta, E. Vredenburg, M. Doery, and other colleagues for valuable discussions. Computing time was provided by the Cornell National Supercomputing Facility, which is funded by NSF and IBM.

REFERENCES

- [1] V. Minogin and V. Letokhov, *Laser Light Pressure on Atoms*, Gordon and Breach, New York, (1986).
- [2] G. Nienhuis, P. van der Straten, and S.-Q. Shang, *Phys. Rev. A* **44**, 462 (1991).
- [3] Y. Castin, J. Dalibard, and C. Cohen-Tannoudji in L. Moi *et al.*, Eds., *Light Induced Kinetic Effects on Atoms, Ions and Molecules*, ETS Editrice, Pisa (1991).
- [4] Y. Castin and J. Dalibard, *Europhys. Lett.* **14**, 761 (1991).
- [5] P. Marte, R. Dum, R. Taieb, and P. Zoller, *Phys. Rev. A* **47**, 1378 (1993).
- [6] P. Jessen, C. Gerz, P. Lett, W. Phillips, S. Rolston, R. Spreuw, and C. Westbrook, *Phys. Rev. Lett.* **69**, 49 (1992).
- [7] P. J. Ungar, D. S. Weiss, E. Riis, S. Chu, *J. Opt. Soc. Am. B*, **6**, 2072 (1989).
- [8] B. Sheehy, S.-Q. Shang, P. van der Straten, S. Hatamian, and H. Metcalf, *Phys. Rev. Lett.* **64**, 858 (1990).
- [9] S. Padua *et al.*, (private communication).
- [10] E. Vredenburg *et al.*, (private communication).

FIGURES

FIG. 1. Time evolution of lin \perp lin laser cooling with Rb atoms ($\tau = 26.5$ ns). (Top) Detuning = $-\Gamma$, time interval between traces = $10 \mu\text{s}$. (Bottom) Detuning = -5Γ , time interval = $3 \mu\text{s}$.

FIG. 2. Average kinetic energies after lin \perp lin cooling of Rb atoms for $30 \mu\text{s}$. (1130 τ). See text for definition of KE_G , KE_A , and U_0 .

FIG. 3. Calculated free particle velocity distributions with MILC for atoms with recoil energy 3.85 kHz, $\tau = 26.5$ ns (as for Rb) for interaction time intervals of $5 \mu\text{s}$ (solid lines) and $50 \mu\text{s}$ (dashed lines) for a) $B = 5 \mu\text{T}$, $S = 0.42$, $\delta = -\Gamma$, b) $B = 5 \mu\text{T}$, $S = 6.67$, $\delta = -20\Gamma$, c) $B = 2 \mu\text{T}$, $S = 0.083$, and $\delta = -\Gamma$, and d) $B = 7.5 \mu\text{T}$, $S = 6.86$, $\delta = -20\Gamma$. The initial velocity distribution is flat to $\pm 50V_R$.

FIG. 4. Calculated populations of the eigenstates of the periodic light shift potential for cases shown in Fig. 2a (top) and 2b (bottom). The well depth $U_0/h = 1$ MHz in each case. The time intervals are $0.3 \mu\text{s}$ (short dashed lines), $5 \mu\text{s}$ (solid lines), and $50 \mu\text{s}$ (long dashes). All levels initially have a population of 1 on this scale, and subsequently $m_F = 1/2$ levels become more populated, while $m_F = -1/2$ levels fall below 1. Band energies are displayed at the top. The distribution is non-Maxwellian for an extended time.

FIG. 5. B field mixing coefficients and $\Delta m_F = 1$ optical pumping rates between

quantum levels in the periodic light shift potential, for an $F = 1/2 \rightarrow F = 3/2$ σ^+ optical transition. Energy levels below the potential maxima (at 1 MHz in this case) and bands are shown for $m_F = -1/2$ (left in each transition pair) and for $m_F = 1/2$ (to the right in each pair). The width of each arrow is proportional to the magnitude of the mixing coefficient or the optical pumping rate.

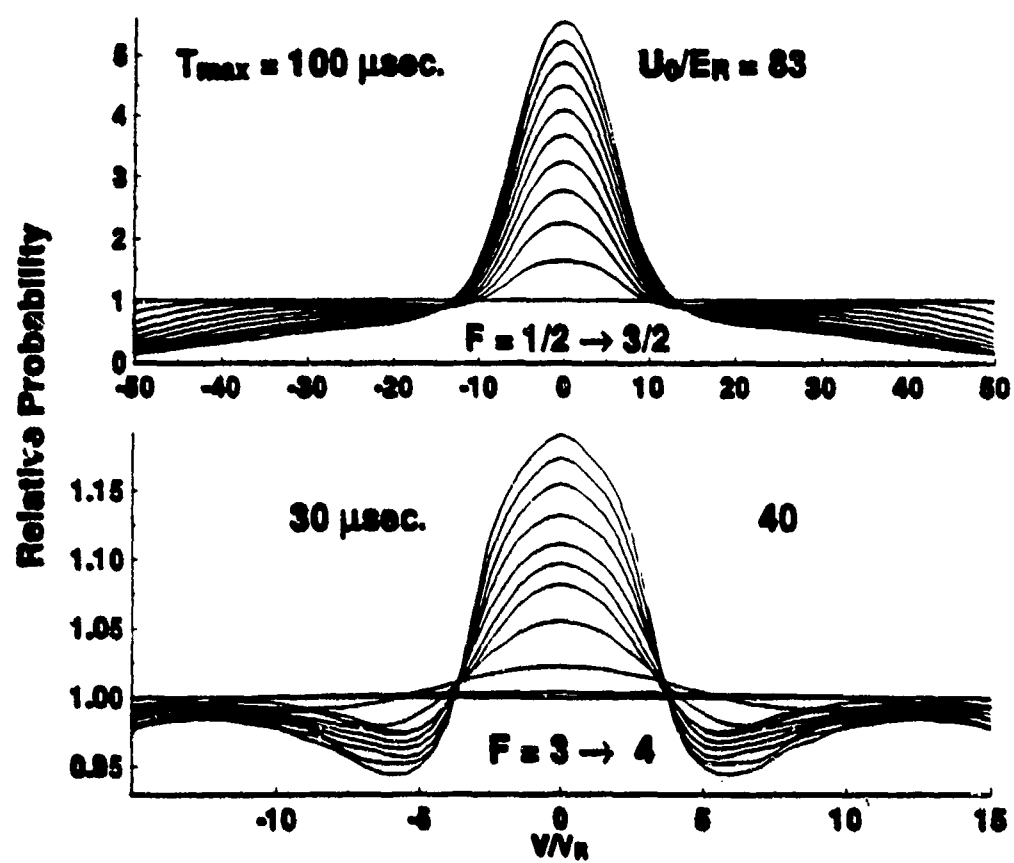


Fig. 1

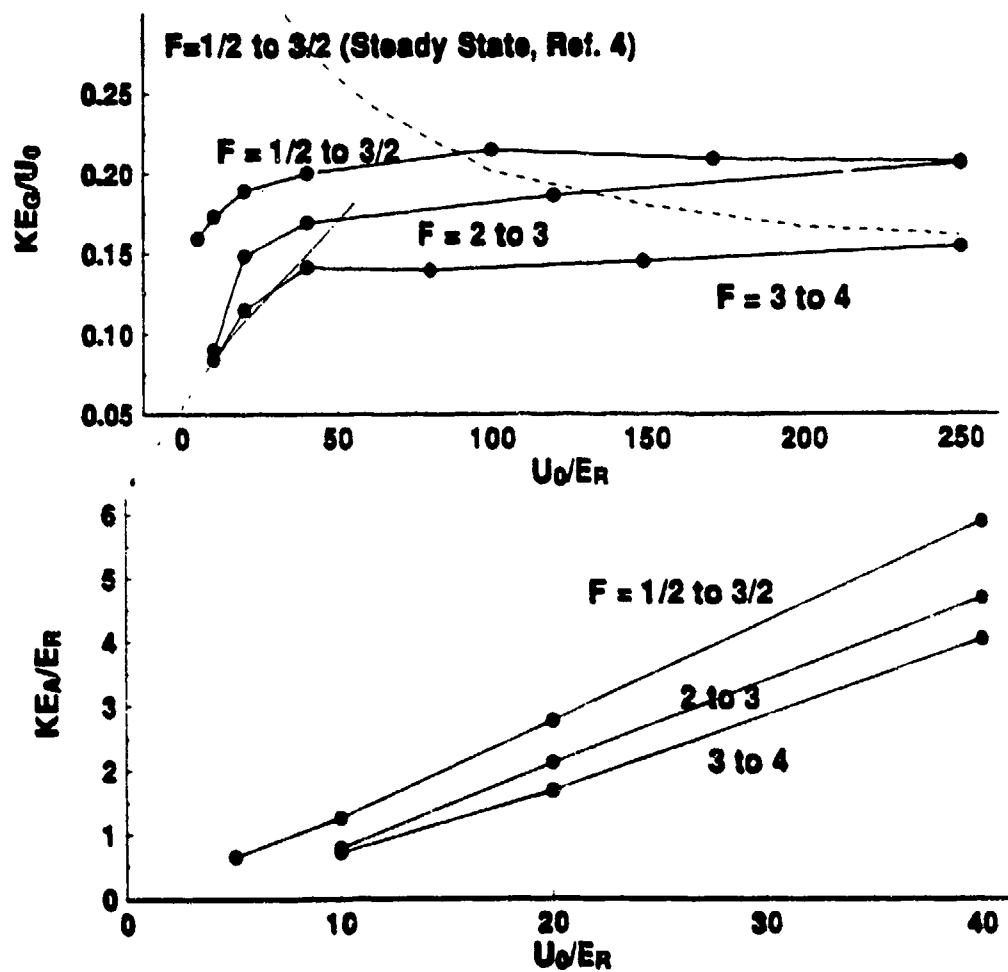


Fig 2

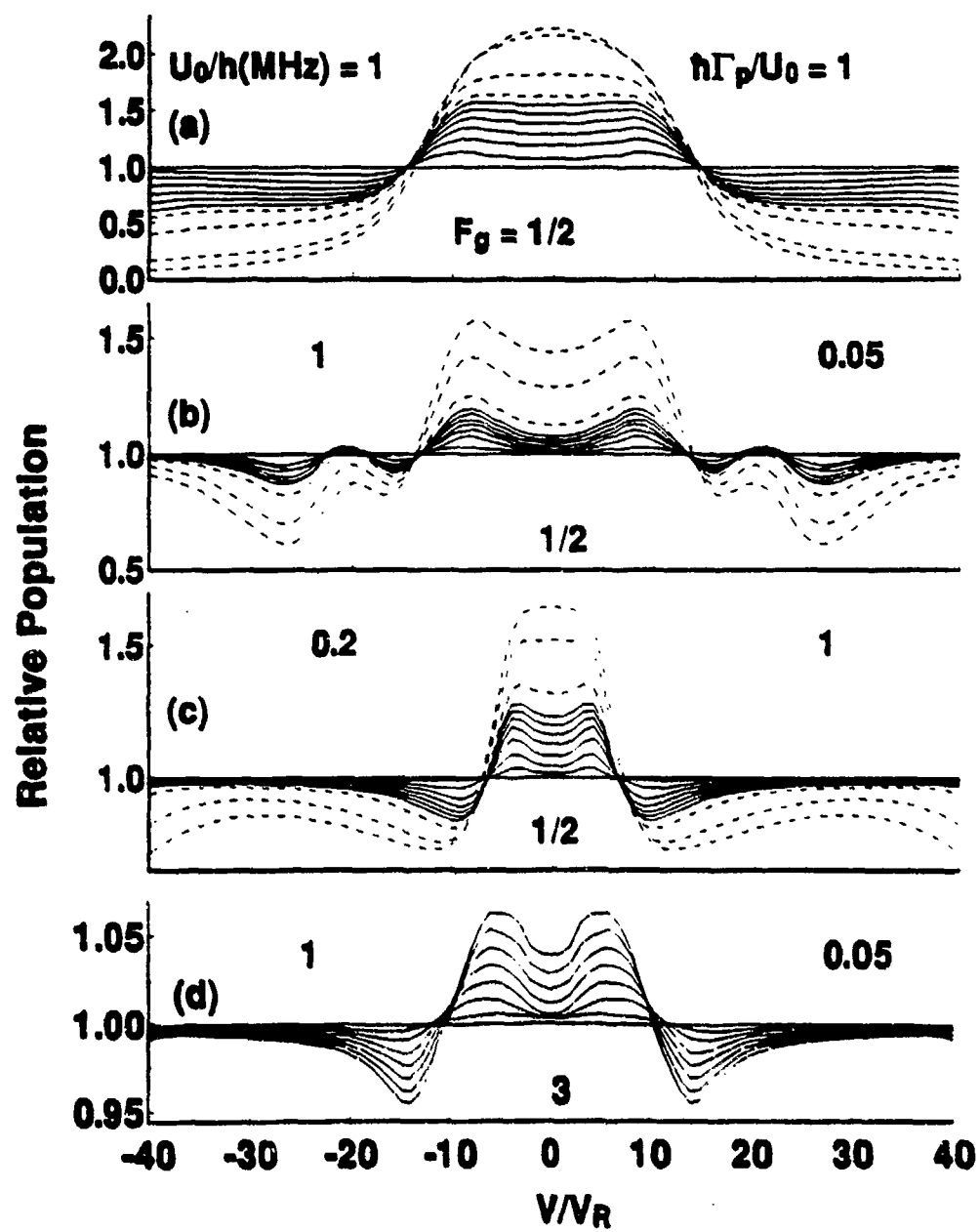


Fig 2

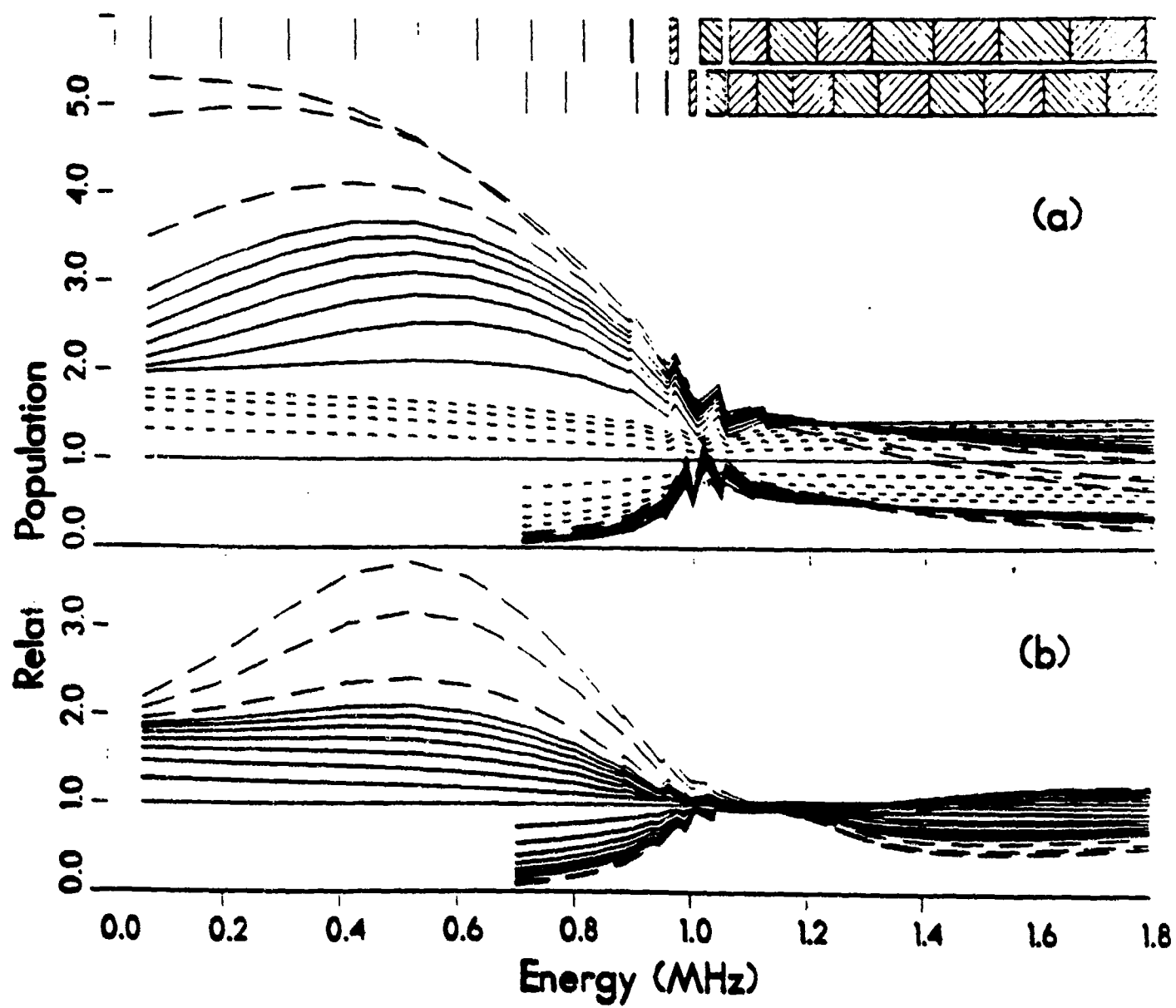


FIG. 4

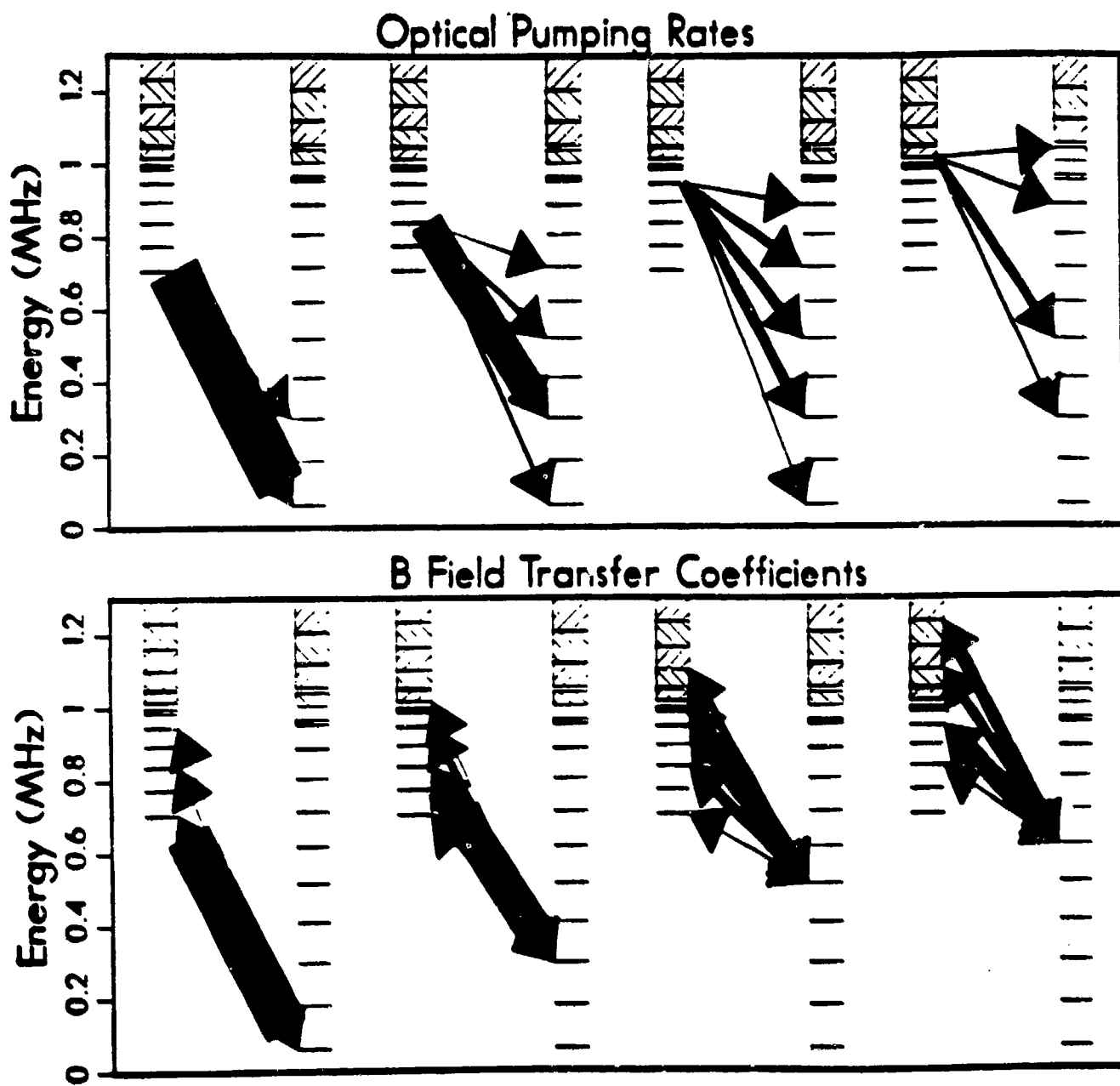


FIG 5

Submitted to JOSA.
8/18/93

THE SIMPLEST ATOMIC SYSTEM FOR SUB-DOPPLER LASER COOLING*

R. Gupta, S. Padua, C. Xie, H. Batelaan, and H. Metcalf

Physics Dept., SUNY Stony Brook, NY 11790

ABSTRACT

Sub-Doppler laser cooling requires optical pumping among differently light shifted ground state sublevels. In this paper we describe a study of the simplest possible angular momentum configuration that allow all sub-Doppler cooling phenomena. The $J_g = 1 \rightarrow J_e = 0$ angular momentum configuration shows recoil-limited cooling in the two most well-known types of polarization gradients, magnetically induced laser cooling, velocity selective resonances, transient cooling, and velocity selective population trapping.

PACS Numbers: 32.80.Pj, 42.50.Vk

I. Introduction

In all cases of sub-Doppler laser cooling (SDLC) the role of multiple ground state sublevels, including coherences between them established by either Raman or Zeeman processes, is of paramount importance. The next natural question is what is the simplest possible atomic level system that would permit SDLC. Since multiple ground state sublevels are required for SDLC, a four level $0 \rightarrow 1$ ($J_g \rightarrow J_e$) transition will not work, but $J = 1 \rightarrow 0$ or $1/2 \rightarrow 1/2$ transitions will both work. However, the $1/2 \rightarrow 1/2$ scheme will not permit $\sigma^+ - \sigma^-$ polarization gradient cooling because this requires atomic alignment [1], so $1 \rightarrow 0$ is the simplest possible general scheme for SDLC.

We have studied SDLC in the $F = 1 \rightarrow 0$ transition of the 28% abundant ^{87}Rb isotope in a 1-D optical molasses, with and without polarization gradients, and in weak and strong magnetic fields (strong means Zeeman splitting larger than the optical pumping rates). The single most important characteristic of this transition in light of either linear or circular polarization is the presence of two unexcitable ground state sublevels (dark states) as shown in Fig. 1. Effective laser cooling depends on very many scattering events because the momentum exchange from light scattering is typically much smaller than the momentum of thermal atoms. In the usual $J \rightarrow J + 1$ transition schemes, atoms are optically pumped into a cyclic transition that allows this required

multiple scattering, rather than into a dark state that precludes it. Thus laser cooling on the $F = 1 \rightarrow 0$ transition is quite different from the more common experiments because transient processes preclude steady state cooling forces [2,3] and there is no Doppler cooling. On the other hand, there is both transient laser cooling and Velocity Selective Population Trapping (VSPT).

For the $F = 1 \rightarrow 0$ transition in a one-dimensional field with no polarization gradients there are two dark states that are independent of atomic velocity. However, with counterpropagating beams of different polarizations \vec{e}_1 and \vec{e}_2 , for example circular and linear, there is only one velocity-independent dark state. The other two atomic ground state sublevels combine to form a second state that is dark only at $v = 0$ in a semiclassical picture, and a third one that is readily excited. This $v = 0$ dark state in a 1-D light field with polarization gradient is a new discovery, and will be discussed below. VSPT in this dark state of the 1-D optical field can only be eliminated with a strong \vec{B} field that is not parallel to either \vec{e} for linear polarization or to \vec{k} for circular polarization. The necessity of such a \vec{B} field is easily understood by considering that the \vec{e} 's have no components parallel to \vec{k} , and if \vec{k} were chosen as the z -axis, there would be no optical pumping from the $M_F = 0$ sublevel in the absence of a \vec{B} field to mix the states.

We note three special features of the $F = 1 \rightarrow 0$ transition. First, steady state processes are easier to study since non-steady state effects may be present for a much longer time for larger F_g values. For example, optical pumping in circularly polarized light to the steady state population distribution among the M_F sublevels occurs before steady state cooling on a cyclic transition begins [3]. Second, calculations of the damping force or the velocity distribution are simplified because of the relatively small Hamiltonian matrix. Third, $F_g = 0$ requires that the ground states can be optically coupled to only one excited state so that ground state coherences are not diluted by multiple excited states.

In section II below we present a detailed discussion of several special phenomena of laser cooling in the $F = 1 \rightarrow 0$ transition. In section III we describe our apparatus and present the experimental results, including observation of VSPT. In section IV we summarize our findings.

II. Sub-Doppler Cooling on an $F = 1 \rightarrow 0$ Transition.

The special characteristics of laser cooling on an $F = 1 \rightarrow 0$ transition can be used to elucidate many features of SDLC. We first consider laser cooling in either the $\sigma^+ - \sigma^-$ or the lin + lin configurations [4] with a strong \vec{B} field applied perpendicu-

lar to the optical \vec{k} vectors (for the lin \perp lin case, \vec{E} must not be parallel to either of the polarizations \vec{e}). In these cases each traveling wave laser beam can induce both π and σ transitions in the frame with quantization axis chosen along the strong magnetic field. Then both polarization schemes permit an energy-exchange-based description of laser cooling toward $v = 0$ (Sisyphus cooling).

To understand this description we view the optical field in either polarization scheme (with \vec{E} at $\pm 45^\circ$ to the \vec{e} 's of lin \perp lin) as two orthogonal, linearly polarized standing waves with nodes spatially displaced from one another as shown in Fig. 2a. Such a field is symmetric for rotation about \vec{k} , so we choose one of the \vec{e} 's along \vec{E} . Thus one standing wave field induces π transitions and the other one induces σ transitions.

We consider light of sufficiently low intensity and large detuning so that the excited state population is small. Atoms are then subject to the conservative force from the light shift potential (calculated by adiabatically eliminating the excited state). We consider the conservative motion of the atoms in the sinusoidal light shift potentials, coupled with the optical pumping that provides the required irreversibility to produce damping forces on the atomic motion, as shown schematically in Fig. 2b. Note that the strengths of the σ transitions are smaller than those of π transitions for the same linear polarization amplitude

$|\bar{\epsilon}|$, so the potential hills are correspondingly smaller. Since the potential hills associated with the light shift for the standing wave of one polarization are displaced from those of the other, optical pumping can switch the atomic populations among the ground state sublevels so that moving atoms always climb the potential hills [5].

This is indeed what happens when the detuning from atomic resonance, $\delta = \omega_{\text{laser}} - \omega_{\text{atom}} > 0$. Atoms that enter the light field near antinode of standing wave $\bar{\epsilon}_1$ are quickly optically pumped out of the sublevel excited by $\bar{\epsilon}_1$. Such atoms can not be excited by $\bar{\epsilon}_2$ because they are at the node for this polarization where the excitation rate is zero (as is the light shift). Their transverse velocity carries them towards the antinode of $\bar{\epsilon}_2$, and in the process they increase their internal energy because of positive light shift, and correspondingly decrease their kinetic energy and slow down. Near the antinode of $\bar{\epsilon}_2$ where the light intensity and light shift are largest, the slowed atoms are optically pumped into the state excited by $\bar{\epsilon}_1$, but they are now at the node of this standing wave. The energy loss process repeats, and the atomic sample is cooled.

In contrast to the energy based Sisyphus picture described above, laser cooling in these polarization configurations can also be viewed in the momentum-based, Velocity Selective Resonance (VSR) picture. In this case we necessarily choose a des-

cription of the light field as counterpropagating travelling waves instead of standing waves. When \bar{B} is strong enough for the Zeeman splitting to be larger than the optical pumping rate γ_p , and thereby make \bar{B} a suitable choice for the quantization axis, each light beam (not each standing wave) in either the $\sigma^+ - \sigma^-$ or the lin \perp lin configuration can induce both π and σ transitions. Thus there can be VSR, comprising excitation by one beam followed by stimulated emission by the other, back to the original ground state sublevel as shown by the dashed arrows in Fig. 3. Such a sequence can produce strong velocity damping toward the resonance velocity, which is $v = 0$ in this case, because the initial and final states have the same energy (same state) [6,7].

This VSR picture provides insight beyond the Sisyphus picture because there are also VSR's between pairs of sublevels of different energy. These are levels that are Zeeman split by $\omega_z = g_F \mu_B B$ [6,7], and Raman transitions between them are shown by the solid arrows in Fig. 3. Such Raman transitions are resonant when $2\bar{k} \cdot \bar{v} = \pm \omega_z$, and are resolvable when $\gamma_p < \omega_z$. Our data presented below show strong sub-Doppler cooling to both $v = 0$ and $v = \pm \omega_z / 2k$.

III.A. Experimental Apparatus

Most of our experimental setup has been described in previous work [6,8] and is only briefly described here. Rb atoms emerge from a 150 °C oven with a horizontal slit aperture 0.06 mm high by 2 mm wide (see Fig. 4). A horizontal atomic beam is formed by a vertical slit 2 mm high by 0.06 mm wide, 35 cm away from the oven. The atomic beam is crossed at 90° by a pair of counterpropagating, horizontal laser beams just beyond the vertical slit, and the polarization of the retroreflected beam can be modified by a quarter wave plate in front of the mirror. Three pairs of square Helmholtz coils are used for controlling the \vec{B} field in the interaction region. The atomic beam profile parallel to the direction of the optical \vec{k} vectors is measured with a scanning hot platinum-tungsten wire, 25 μm in diameter, 1.3 m away from the interaction region.

A 20 mW Sharp model LTO24 diode laser is side-locked to a Doppler-broadened signal from a Rb cell at room temperature. Light from this laser is used to optically pump the ^{87}Rb atoms from the $5S_{1/2}(F=2)$ to the $5S_{1/2}(F=1)$ ground hfs state before they reach the interaction region.

Light from a second diode laser, a 35 mW Sharp model LTO25, is split into two beams, and the weaker one passes through an 80 MHz AOM and then to another Rb vapor cell. A cross-over reso-

nance in its saturated absorption signal is used to lock the laser near the $F = 1 \rightarrow 0$ transition in ^{87}Rb near $\lambda = 780$ nm, and facilitates tuning on either side of the atomic resonance. About 10^{-5} of the laser light is fed back to the laser by a blazed grating (see Fig. 4) to reduce the spectral width to ~ 1 MHz [9]. The laser beam has its spatial intensity profile flattened to a few percent by a tilted etalon [10], and is then expanded to 23 mm wide by 5 mm high. A mechanical shutter interrupts this beam, and many systematic effects have been eliminated by subtracting data from measurements with the laser beam off from those with the beam on.

III.B. Experimental Results

Figure 5 shows the measured atomic beam profiles with \vec{B} perpendicular to the \vec{k} vectors for (a), the case of $\sigma^+ - \sigma^-$ and (b) lin + lin with \vec{B} at 45° to the polarization vectors. In each case \vec{B} is perpendicular to the horizontal atomic and laser beams. The top trace in each figure shows strong sub-Doppler cooling to $v = 0$, and a velocity width of only ~ 5.5 cm/s (Doppler limit ~ 13 cm/s in 1-D optical molasses). Both the top traces were taken with large \vec{B} ($\vec{B} > 1$ G), and both also show the VSR peaks at $v = 0$. As \vec{B} is reduced (lower traces), these VSR peaks move to lower velocities, and Fig. 6 shows the separation of these peaks vs. $|\vec{B}|$ for each case.

In the semiclassical approximation the "velocity capture range" of this cooling process is determined by the lifetime of the ground state populations and/or coherences produced by the VSR's. Atoms are optically excited out of these coherences at a rate $\gamma_p = \bar{\gamma}_p \cos^2(kx)$ where $\bar{\gamma}_p = 2s(\gamma/2)/(3L + s)$, $\tau = 1/\gamma$ is the excited state lifetime (27 ns for this Rb transition), $L = 1 + (2\delta/\gamma)^2$, and the saturation parameter for a single light beam is $s = I/I_{\text{sat}}$, where $I_{\text{sat}} = \pi\hbar c/3\lambda^3\tau$ (≈ 1.6 mW/cm² for the $\lambda = 780$ nm transition in Rb). The factor of 3 in the denominator of $\bar{\gamma}_p$ comes from the Clebsch-Gordan coefficient for the $1 \rightarrow 0$ transition for each value of M_F , and the factor of 2 in the numerator comes from the superposition of two orthogonal light beams. For Fig. 5a, $s \approx 1.33$ and $\delta \approx 2\pi \times 12$ MHz whence $\bar{\gamma}_p/2\pi \approx 150$ kHz and the average value over a wavelength $\bar{\gamma}_p$ is half of that.

Under optimum cooling conditions, the expected width of the velocity distribution is $\sim \bar{\gamma}_p/k \approx 6$ cm/s, about equal to the value observed for the $v = 0$ peak. The widths of the $v \neq 0$ peaks, Δv , are limited by the width of the longitudinal velocity distribution Δv_l through $\Delta v/v \sim (\Delta v_l/v_l) \sim 1/2$ for a thermal beam, and their widths are indeed about half their distances from the $v = 0$ peak. They begin to merge into it when their velocity is ~ 10 cm/s, corresponding to $|\bar{B}| \approx 0.3$ G for $g_F = 1/2$. Similar conclusions can be drawn from the data of Fig. 5b. Furthermore, at low \bar{B} fields some states are only weakly excited and transient cooling effects begin to appear [2].

The two bottom traces in Fig. 5, where $|\vec{B}| = 0$, reveal the velocity selective population trapping (VSPT) discussed above. Atoms travelling in either light field of Fig. 5 with nearly zero transverse velocities spend all their time in light of one particular polarization as they ride along a particular phase of the standing wave. For example, in $\text{lin} \perp \text{lin}$ this may be circular along one path across the standing wave, or linear along another path that is $\lambda/8$ away. In the absence of a \vec{B} field the quantization axis is chosen along the local polarization. Atoms are then optically pumped to a dark state of this basis (Fig. 1) and remain uncoupled to the excited state by the light. These slow atoms are subject to VSPT and thus do not experience momentum diffusion. They could therefore display an arbitrarily narrow velocity distribution with a long enough interaction time. (Note that this is not the same as the "coherent" population trapping of Ref. 11 which depends on the quantized center-of-mass motion of the atoms.) Atoms are cooled to the low velocities appropriate for VSPT by transient polarization gradient cooling, and these form the sub-Doppler peaks at the bottom of Fig. 5 with $\vec{B} = 0$. When atoms traverse either light field of Fig. 5 with a higher velocity, they experience a constantly changing polarization, and could thus be pumped out of the velocity selective "dark" states of Fig. 1.

We have tested this hypothesis of VSPT at $|\vec{B}| = 0$ several ways. First, we found that the cold atom peaks occur over a wide

range of detuning, both blue and red, although they are stronger in the blue case because there is residual polarization gradient cooling to feed the dark state. Second, we used an aperture on the laser beam to shorten the interaction time, and found that the cold atom peaks require a few optical pumping times $1/\bar{\gamma}_p$ to appear. Third, we note that $\bar{\gamma}_p = \gamma/80$ for the conditions of Fig. 5, so that optical pumping occurs in about $2.5 \mu\text{s}$. VSPT atoms that move less than $\lambda/4$ in this time will have to wait longer than this time to be pumped out of the dark state because they will not be subject to a different polarization. Thus there is also a cold peak even in the absence of a \bar{B} field with a velocity distribution of width $\sim 9 \text{ cm/s}$, about 50% larger than the large \bar{B} field peaks, just as shown at the bottom of Fig. 5.

In addition to all the experiments described above with the two types of polarization gradients, we have also studied SDLC in this $F = 1 \rightarrow 0$ transition in a standing wave of purely circularly polarized light. The presence of a weak transverse \bar{B} field then produces magnetically induced laser cooling [8]. At low \bar{B} field we observed a very narrow peak near $v = 0$, and at higher fields we saw this split into two peaks with sub-Doppler widths centered at $v_r = \pm\omega_z/2k$ just as in previous experiments using more complicated transitions [6]. We have also observed higher order VSR's where the resonance velocity satisfies $v_r' = \pm\omega_z/4k$, corresponding to redistribution of two photons between the two laser beams that form the optical molasses.

IV. Conclusions.

We have performed several other experiments on this simplest possible SDLC scheme to assure that it displays all the features we expect. For example, in the $\text{lin} \perp \text{lin}$ case with \vec{B} along one of the polarization vectors, we find that both the cold peaks of atoms indeed move at the resonance velocity $v_r = \pm \omega_z / 2k$ [12].

Thus we conclude that the $F = 1 \rightarrow 0$ transition is the paradigm of SDLC, displaying many of its special features in addition to μK temperatures, and holding claim to being the simplest possible angular momentum configuration with this capability. In the future we plan more extensive studies of VSPT, the higher order resonances, and other aspects of this extraordinary laser cooling system.

*Supported by N.S.F., O.N.R., A.F.O.S.R., and C.A.P.E.S. (Brazil).

REFERENCES

1. G. Nienhuis et al., Phys. Rev. A44, 462 (1991).
2. S. Padua et al., Phys. Rev. Lett. 70, 3217 (1993).
3. C. Valentin et al., Europhys. Lett. 17, 133 (1992).
4. J. Dalibard and C. Cohen-Tannoudji, J. Opt. Soc. Am. B6, 2023 (1989).

5. This presents no conflict with the usual view of $\sigma^+ - \sigma^-$ laser cooling (Ref's. 1 and 4) because of the strong \vec{B} field (see Ref. 7). In the usual views where $\vec{B} = 0$, the damping force can not be viewed as derived from a Sisyphus mechanism, but rather as a scattering force or radiation pressure derived from a population imbalance. Here, however, the strong \vec{B} field perpendicular to \vec{k} precludes the Larmor transformation responsible for the usual viewpoint (Ref. 4).

6. S-Q. Shang et al., Phys. Rev. Lett. 65, 317 (1990).
7. P. van der Straten et. al., Phys. Rev. A47, 4160 (1993).
8. B. Sheehy et al., Phys. Rev. Lett. 64, 858 (1990).
9. R. Ryan et al., J. Opt. Soc. Am. B10, 1643 (1993).
10. C. Xie et al., Opt. Lett. 18, 173 (1993).
11. A. Aspect et al., Phys. Rev. Lett. 61, 826 (1988).
12. S-Q. Shang et al., Phys. Rev. Lett. 67, 1094 (1991).

FIGURE CAPTIONS

Fig. 1. The energy level scheme for an $F = 1 \rightarrow 0$ transition showing allowed excitation for blue tuned σ^+ light (a) and π light (b). In (a) the $M_F = 0$ and 1 states are dark, whereas in (b) the $M_F = \pm 1$ states are dark. Linearly polarized light perpendicular to \bar{z} would excite both the $M_F = +1$ and -1 sublevels leaving $M_F = 0$ as one dark state, while an uncoupled superposition of the $M_F = \pm 1$ states would be the other.

Fig. 2a. The standing wave fields of either $\sigma^+ - \sigma^-$ or lin \perp lin polarization configurations. Both optical fields have the same $\pi/2$ spatial phase shift. The only difference between the two polarization schemes is the relative temporal phase of the linearly polarized standing waves. This phase difference is zero for $\sigma^+ - \sigma^-$ and $\pi/2$ (i.e., time lag of $\pi/2\omega_{\text{laser}}$) for lin \perp lin. The selection rules are the same. If \bar{B} is along one of the \bar{e} 's in the lin \perp lin case, one standing wave is parallel to the quantization axis along \bar{B} so it induces π transitions, and the other one is perpendicular to \bar{B} so it induces both σ^+ and σ^- transitions. In the $\sigma^+ - \sigma^-$ case, choosing \bar{z} along \bar{B} yields the same selection rules as the lin \perp lin case (see Ref. 7). 2b shows the spatial dependence of the light shift for the field of 2a when the quantization axis is chosen perpendicular to \bar{k} (at $\pm 45^\circ$ to the \bar{e} fields for lin \perp lin). Since the strength of the π transition is larger, the light shift is larger for the same $|\bar{e}|$.

Fig. 3. Raman transitions among the M_F sublevels of the $F = 1 \rightarrow 0$ transition in a magnetic field. VSR at $v = 0$ are induced in atoms that return to their original sublevel (dashed arrows), and at finite velocity $v_T = \omega_Z/2k$ for atoms that are transferred between states of different M_F (solid arrows).

Fig. 4. Schematic diagram of the apparatus.

Fig. 5. Measured atomic beam profiles for $\delta/2\pi = +12$ MHz ($\approx 2\gamma$) for the case of (a) $\sigma^+ - \sigma^-$ with $s = 1.33$, and (b) $\text{lin} \perp \text{lin}$ with $s = 0.66$. The highest \bar{B} values are at the top, decreasing to $\bar{B} = 0$ at the bottom. Note that the VSR signals on each side of the central peak are broadened by the longitudinal velocity distribution.

Fig. 6. Velocity of the VSR peaks in Fig. 5 vs \bar{B} . The solid dots are for σ^+ (Fig. 5a) and the open squares are for $\text{lin} \perp \text{lin}$ (Fig. 5b). The straight lines represent the resonance case, $v = \omega_Z/2k$ appropriate in each case because the light induces both π and σ transitions in the strong transverse \bar{B} field.

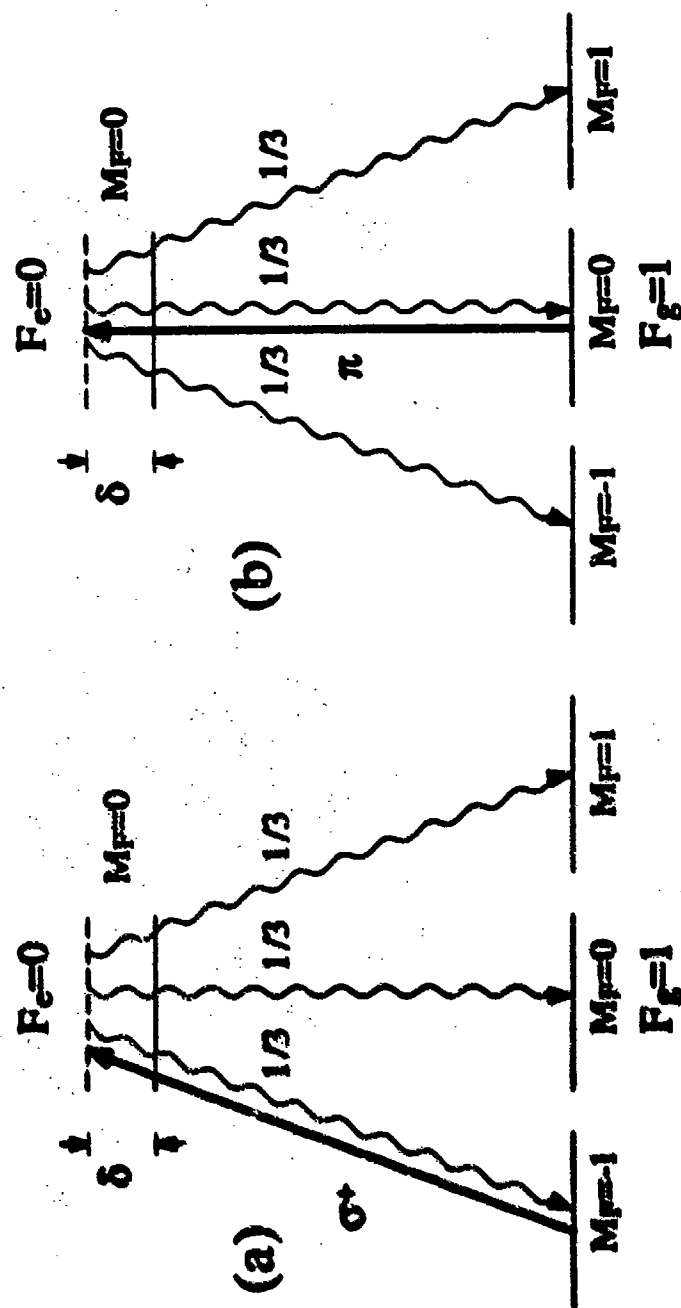


Fig 1

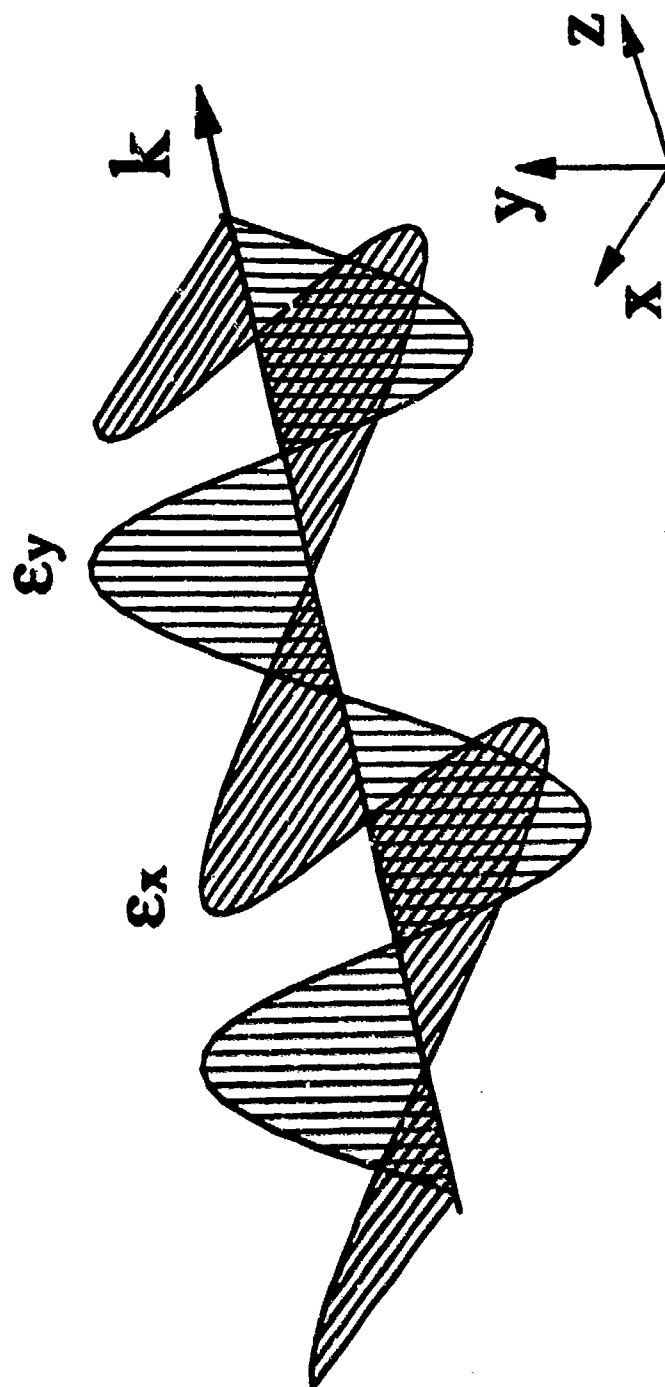


Fig 2a

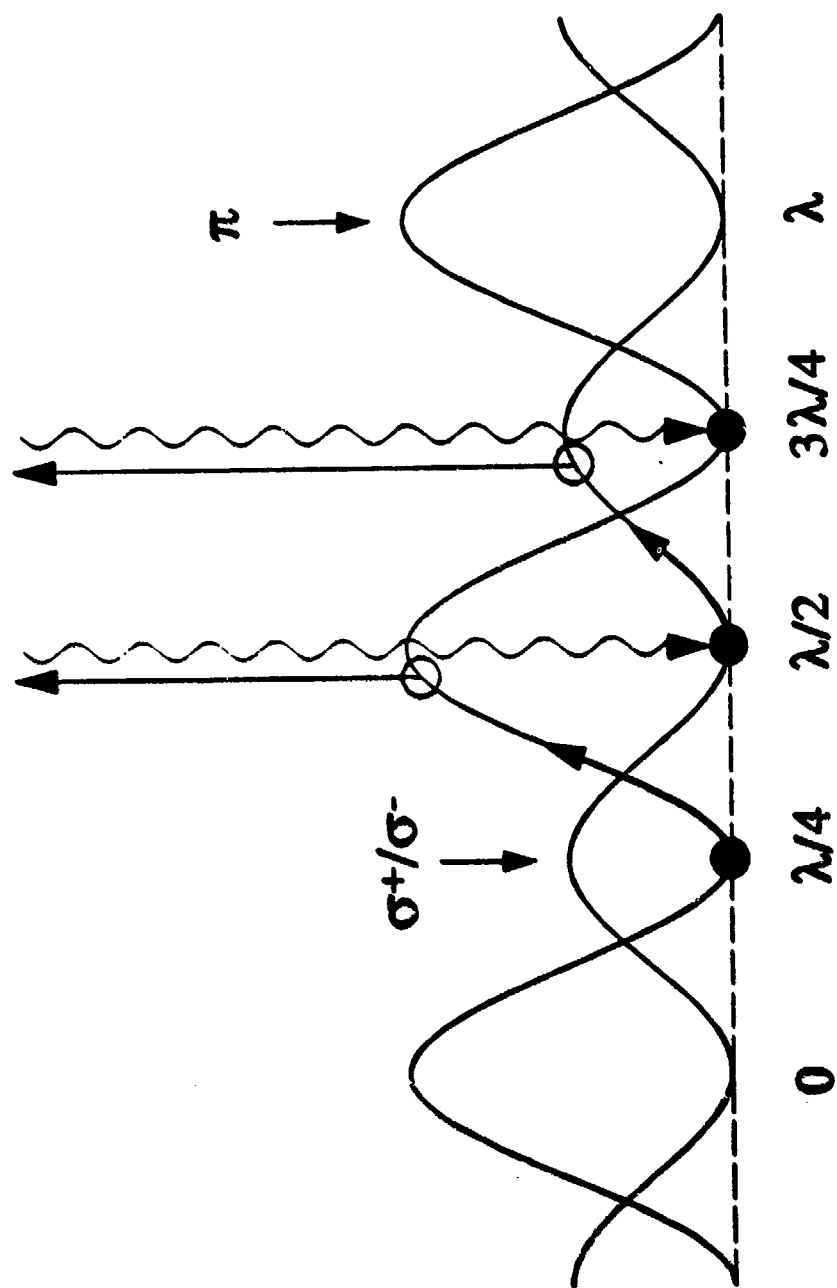


Fig 26

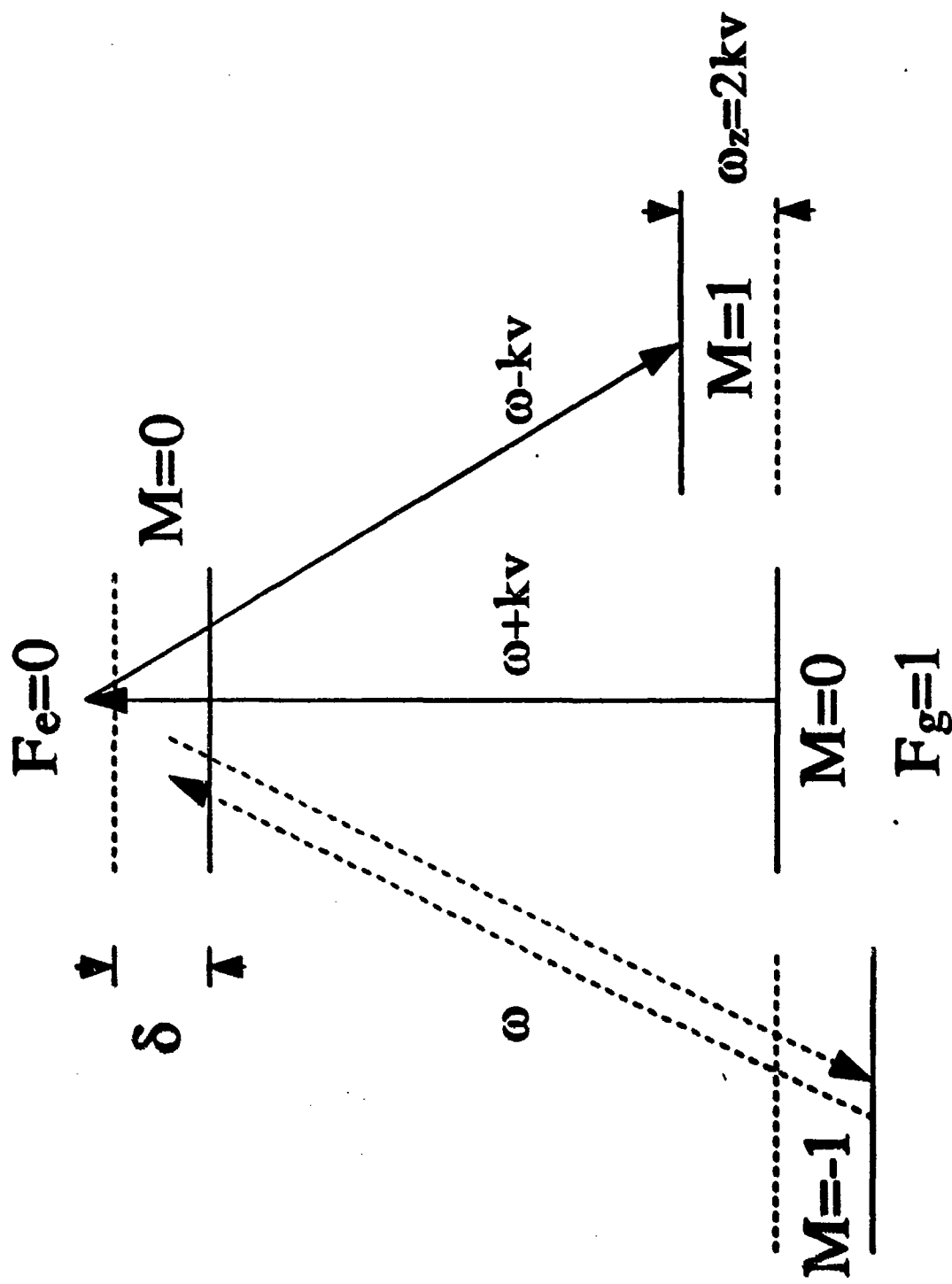


Fig 3

Fig 4.

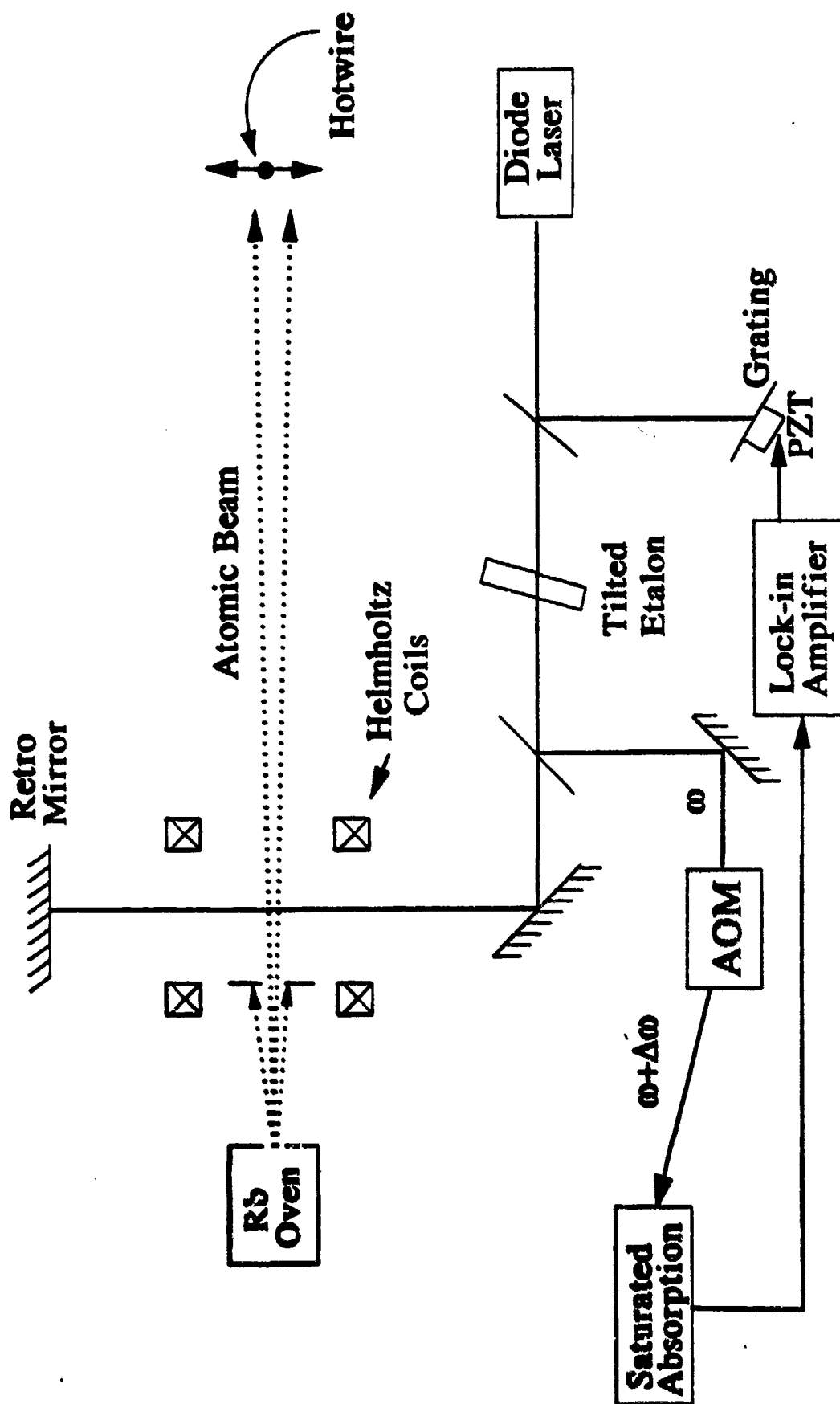
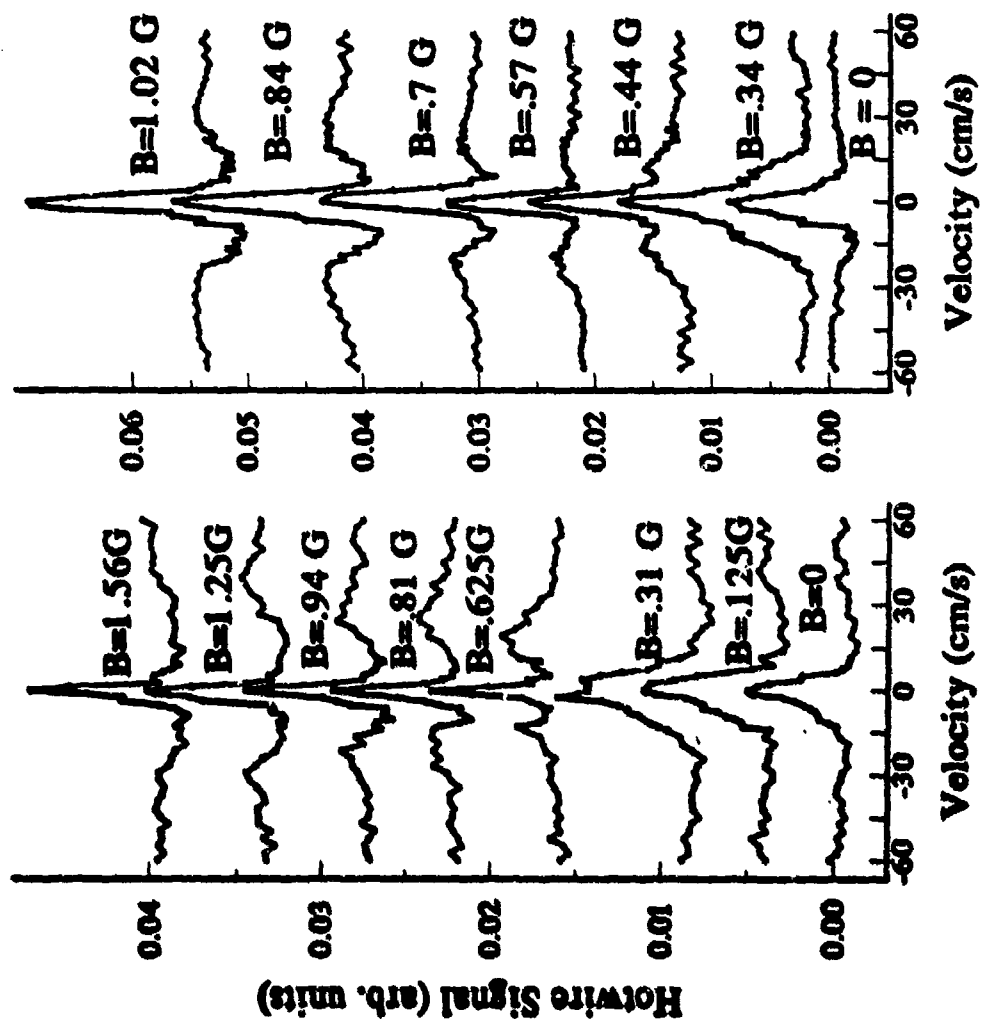


Fig 5



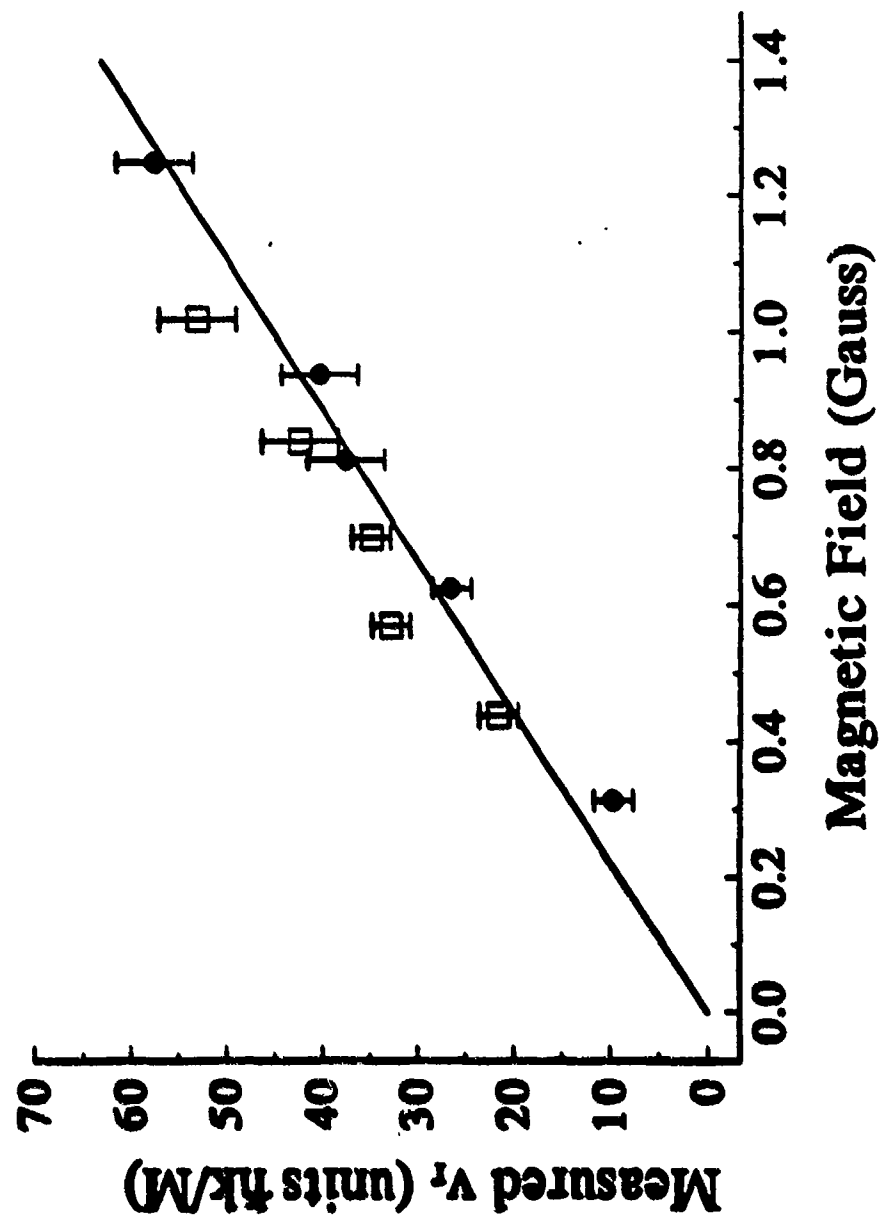


Fig 6

Submitted to Phys Rev
Lett 6/17/93

Bichromatic Laser Cooling in a Three Level System

R. Gupta, C. Xie, S. Padua, H. Batelaan, and H. Metcalf

Physics Department, SUNY, Stony Brook, NY 11790

ABSTRACT

We report a new type of sub-Doppler laser cooling in 1-D using neither polarization gradients nor magnetic fields. Two laser frequencies couple each of the two ground state hfs sub-levels to a common excited state of ^{85}Rb , thus forming a Λ system. We observe sub-Doppler cooling when the light is tuned blue of resonance, efficient heating with red detuning, deflection from a rectified dipole force, and velocity selective resonances associated with Raman transitions. A simplified semiclassical calculation agrees qualitatively with our measurements.

PACS numbers 32.80.Pj, 42.50.Vk

All sub-Doppler laser cooling (SDLC) methods can be characterized by a damping force derived from a spatially varying light field (e.g., from superposition of two counterpropagating laser beams) [1,2]. In all cases studied to date, motion of the atoms prevents their internal state distribution from reaching steady state. Deviation from the steady state is countered by the irreversible process of optical pumping (spontaneous emission) that tends to restore the steady state distribution. The time lag of this process leads to non-adiabatic response of moving atoms to the standing wave field, and under suitable conditions, a velocity dependent damping force. In the past polarization gradients [1,2] or magnetic fields [3] were used to create the spatial dependence of the atomic steady state. In this letter we report a new SDLC scheme that requires neither polarization gradients nor magnetic fields.

Our new scheme employs two standing waves with the same linear polarization but different laser frequencies, ω_1 and ω_2 , corresponding to excitation of the two ground state hyperfine levels of ^{85}Rb (separated by $\omega_{\text{hfs}} \approx 2\pi \times 3.036 \text{ GHz}$). When ω_1 , ω_2 , and $\delta \equiv (\omega_2 - \omega_1) - \omega_{\text{hfs}}$ are properly chosen, the time lag described above can also damp the motion of moving atoms because of the non-adiabatic response of the populations of levels $|1\rangle$ and $|2\rangle$. Recently there has been considerable theoretical interest in the optical forces on three level atoms with such a Λ configuration of levels [4-12] but only a few experiments [13-15].

SDLC is often described in a picture called Sisyphus cooling (because of the close analogy with a Greek myth [16]) where atoms lose kinetic energy when they move in the potentials caused by the light shifts of the laser field. Such descriptions exist at low intensity for the steady state processes of polarization gradient [1,16,17] and magnetically induced cooling [3], as well as transient laser cooling processes [18]. With two frequencies

present, a similar energy loss or Sisyphus picture is appropriate when the relative spatial phase of the standing waves is considered.

Consider the case where the intensity maxima of the standing wave at ω_1 correspond to the minima of ω_2 as shown in Fig. 1a, and both ω_i 's are larger than the corresponding atomic resonance frequencies as shown in Fig. 1b. The light shift of each ground state sublevel $|i\rangle$ is dominated by the nearly resonant frequency ω_i , and hence is positive. Atoms moving through the node of ω_1 are optically pumped to $|1\rangle$ and must increase their potential energy to move further as shown in Fig. 1a. This comes at the expense of their kinetic energy, and they slow down as they approach the top of the potential hill at the antinode of ω_1 . However, they are most likely to be optically pumped to $|2\rangle$ at a point where the intensity of light at ω_1 is high, and then they begin climbing another hill. Repetition of this process rapidly converts kinetic energy into potential energy which is then dissipated into the fluorescent light of the spontaneous decays, and atoms are cooled. This process obviously produces heating if the two frequencies are red of resonance thereby producing negative light shifts, and its effectiveness is compromised when the standing wave phase difference is different from π .

Most of our experimental setup has been described in previous work [3,17,18] and is only briefly described here. Rb atoms emerge from a 150 °C oven with a horizontal slit aperture 0.06 mm high by 2 mm wide. A horizontal atomic beam is formed by a vertical slit 2 mm high by 0.06 mm wide, 35 cm away from the oven. The atomic beam is crossed at 90° just after the second slit by a laser beam containing two frequencies that is retroreflected by a movable mirror to form two horizontal standing waves with the same polarization but different frequencies. The transit time of atoms with the average velocity 350 m/s in the 23 mm long by 5 mm

high laser beam is about 65 μ s. The Earth's magnetic field is carefully cancelled to less than 10 mG by square Helmholtz coils. We measure the atomic beam profile parallel to the direction of the optical \vec{k} vectors with a scanning hot platinum-tungsten wire, 25 μ m in diameter, 1.3 m away from the interaction region.

Linearly polarized light from a 35 mW Sharp model LTO25 diode laser is split into two beams, and the weaker one passes through a 80 MHz AOM and then to a Rb vapor cell. A crossover resonance in the saturated absorption signal is used to lock the laser near the $F = 3 \rightarrow 3$ transition in ^{85}Rb near $\lambda = 780$ nm, and facilitates tuning on either side of the atomic resonance. About 10^{-5} of the stronger beam is fed back to the laser by a blazed grating to reduce the spectral width to ~ 1 MHz. The two frequencies are generated by passing the light through an EOM [19]. A mechanical shutter interrupts this beam, and many systematic effects have been eliminated by subtracting laser beam off from laser on measurements.

The spatial phase difference between the two light shift potentials is of paramount importance in this experiment. The standing waves of the two frequencies have nodes at the surface of the retroreflecting mirror, but their relative phase $\phi = 2z(\omega_1 - \omega_2)/c$ varies with distance z from the mirror because of their frequency difference; for $\omega_1 - \omega_2 \approx 2\pi \times 3$ GHz the spatial period of this variation is ≈ 5 cm. Since this is much larger than the 0.06 mm atomic beam diameter, atoms see a fixed value of the phase between the standing waves. This can be varied by translation of the retroreflecting mirror.

Figure 2a shows the results of our measurements of SDLC using two optical frequency standing waves for the case of $\phi = \pi$ (optimum cooling) and $\phi = 0$ obtained by moving the retroreflecting mirror about 2.5 cm. Even at $\phi = 0$ there is a significant

signal of cooled atoms, but this arises from two additional cooling mechanisms operating in this experiment. First, the atomic coherences produced by stimulated Raman transitions between the states $|1\rangle$ and $|2\rangle$ for $\delta = 0$, neglected in this Sisyphus description, produce velocity selective resonances (VSR) at $v = 0$ as described below. Second, for the $F = 3 \rightarrow 3$ transition driven by linearly polarized light, the excitation of the $M_F = 0$ sublevel is forbidden, and transient cooling into this dark state contributes to this residual cooling [18].

We have tested that this residual peak of cold atoms is mostly the result of transient cooling by varying the interaction time with an aperture on the laser beams. We found that it is produced in a time comparable to the optical pumping time $1/\gamma_p$. For this test we used a large enough value of δ so that the VSR peaks are well resolved from the $v = 0$ signal, (see below), and the remaining signal at $\phi = 0$ is only from transient cooling. Figure 2b shows the ϕ dependence of the height of the cooled atom peak at $v = 0$ with large δ .

The Sisyphus description of these experiments given above is limited because it is based only on the populations of states, and neglects coherences that are associated with Raman processes between the two long lived ground states. It is well known that these coherences have important effects on the damping forces, and in previous experiments we have shown that damping to $v = 0$ [20] and to finite velocities [20,21] depends on Raman resonances between Zeeman shifted states that redistribute light between counterpropagating beams. These VSR are always present in all known cases of steady state SDLC [22,23].

The direct analog of the magnetic VSR can be seen with two laser frequencies when $\delta = (\omega_2 - \omega_1) - \omega_{hfs} = 0$ [20]. Then the condition for VSR is satisfied at the resonance velocity $v_r =$

$\pm \delta/2k$. Figure 3a shows the measured atomic beam profiles for different values of δ and Fig. 3b shows the velocity associated with the side peaks of Fig. 3a vs δ . Two side peaks appear for each value of δ because atoms at the resonance velocity v_r can absorb either ω_1 or ω_2 from either direction of the laser beam, depending on the sign of their velocity. Of course, stimulated emission into the other beam completes the Raman transition.

The widths of the $v \neq 0$ peaks, Δv , are limited by the width of the longitudinal velocity distribution Δv_l through $\Delta v/v \sim (\Delta v_l/v_l) \sim 1/2$ for a thermal beam, and their widths are indeed about half their distances from the $v = 0$ peak. They begin to merge into it when their velocity is ~ 20 cm/s, corresponding to $\delta \approx 0.25$ MHz. It must be emphasized that the widths of these peaks are all below the Doppler limit (10 cm/s): atoms undergo SDLC to the velocity v_r .

Up to this point we have considered only the special cases $\phi = 0$ or π , and the same sign for the detuning $\delta_i = \omega_i - \omega_{\text{atom}(i)}$ of the two individual laser frequencies (see Fig. 1). We now consider cases where these conditions are relaxed. In addition to SDLC, we show that various values of δ_1 and δ_2 can produce qualitatively new effects. In particular, when δ_1 and δ_2 have opposite signs, the light shifts for the two ground states $|1\rangle$ and $|2\rangle$ are opposite. For $\phi = 0$ or π , partial cancellation of the kinetic energy change when the atoms move on these oppositely light shifted potentials severely reduces the heating or cooling forces, but for other values of ϕ this cancellation is less complete, and there remains a "rectified" dipole force [11,13,15].

Figure 4 shows schematically how this works if we choose for simplicity equal probability for the optical pumping processes $|1\rangle \leftrightarrow |2\rangle$ and $|2\rangle \leftrightarrow |1\rangle$. Atoms are then optically pumped to the state with the lowest standing wave intensity as shown by the

arrows in Fig. 4. For velocity v small enough so that the average optical pumping time $1/\gamma_p$ is less than $\Delta z/v$, where Δz is the standing wave displacement, then the optical force (slope of the potential curve to which atoms are optically pumped) has a fixed direction independent of velocity when averaged over a wavelength. We therefore expect a maximum force near $v = 0$, with the same sign for $v < 0$ or $v > 0$. The force should decrease with a velocity width $\sim \gamma_p \Delta z \approx \gamma_p/k$.

In our experiment the atoms emerge from the second slit in a velocity range of $\sim \pm 1$ m/s, much larger than the "capture range" γ_p/k of ~ 10 cm/s. Atoms with a large transverse velocity are thus unaffected by the deflection force, while slower atoms undergo a deflection to the right or left depending on the sign of Δz . Changing the sign of Δz can be accomplished either by exchanging the signs of the δ_i 's or by moving the retroreflection mirror, and we have done both. The data of Fig. 5a and 5b clearly show such deflections of the atoms for opposite signs of Δz , and also provide a measure of the effective velocity range for this rectified force.

We have done semiclassical calculations of the force on moving atoms, starting with the optical Bloch equations to find the density matrix. Using only the transfer of population between states $|1\rangle$ and $|2\rangle$, and neglecting any coherences that may be produced in the optical excitation, we have calculated the force for the many experiments described above. For the data of Fig. 2 we find the usual dispersion-shaped velocity dependence with strength and capture range that correspond well with our measurements. For the data of Fig's. 5a and 5b, we show in Fig's. 5c and 5d the anticipated single peak (or dip) in the force vs velocity curve, with no zero crossing and a width $\sim \gamma_p/k$. Such model calculations can not be used for the data of Fig. 3 because the VSR arise from coherences that are not included. We plan to

extend the semiclassical methods we have developed, that include the multiple magnetic sublevels [22,23], to two frequencies to model these experiments.

Cooling atoms with two frequencies is a fundamentally new SDLC scheme that requires neither polarization gradients nor magnetic fields. Its damping, maximum force, capture range, and diffusion are comparable to those of many previously studied SDLC schemes such as polarization gradients [1,2] and magnetically induced laser cooling [3]. However there are additional free parameters that provide flexibility for further study of SDLC processes. These are the detunings δ_1 and δ_2 , saturation parameters s_1 and s_2 , and the phase between the standing waves ϕ . It also provides a better insight into particular interpretations of SDLC such as the Sisyphus picture. We plan to extend our study of this system to include polarization differences between the two beams, polarization gradients of each beam, and the effect of magnetic fields.

Supported by NSF, ONR, AFOSR, and CAPES (Brazil).

REFERENCES

1. J. Dalibard and C. Cohen-Tannoudji, J. Opt. Soc. Am. B6, 2023 (1989).
2. P. Ungar et al., J. Opt. Soc. Am. B6, 2058 (1989).
3. B. Sheehy et al., Phys. Rev. Lett. 64, 858 (1990).
4. N. Lu et al., Phys. Rev. A35, 5088 (1986)
5. J. Javanainen, Phys. Rev. Lett. 64, 519 (1990).
6. S. Chang et al., Opt. Commun. 77, 19 (1990).
7. M. Prentiss et al., Opt. Lett. 16, 1695 (1991).
8. Y. Rozhdestvenskii and N. Jakobsen, Sov. Phys. JETP 72, 936, (1991).
9. D. Kosachiov et al., Opt. Commun. 85, 209 (1991).
10. Y. Ovchinnikov et al., J. Phys. B 24, L539 (1991).
11. A. Sidorov et al., J. Phys. B 24, 3733 (1991).
12. K. Moler et al., Phys. Rev. A45, 342 (1992).
13. R. Grimm et al., Phys. Rev. Lett. 65, 1415 (1990).
14. P. Hemmer et al., Phys. Rev. Lett. 68, 3148 (1992).
15. M. Kasevich and S. Chu, Phys. Rev. Lett. 69, 1741 (1992).
16. C. Cohen-Tannoudji and W. Phillips, Phys. Tod. 43, 33 (1990).
17. R. Gupta, S. Padua, C. Xie, H. Batelaan, and H. Metcalf, submitted to Opt. Lett., June, 1993.
18. S. Padua et al., Phys. Rev. Lett. 70, 3217 (1993).
19. We thank New Focus Corp. for the loan of an EOM.
20. S-Q. Shang et al., Phys. Rev. Lett. 67, 1094 (1991).
21. S-Q. Shang et al., Phys. Rev. Lett. 65, 317 (1990).
22. G. Nienhuis et al., Phys. Rev. A44, 462 (1991).
23. P. van der Straten et al., Phys. Rev. A47, 4160 (1993).

FIGURE CAPTIONS

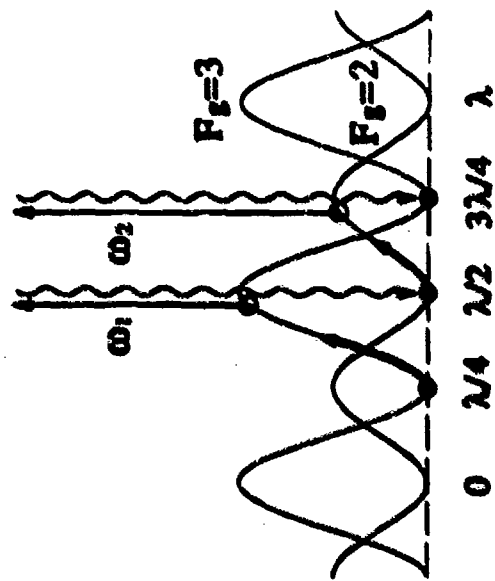
Figure 1. (a) shows the spatial dependence of the unequal light shifts (caused by either different transition strengths or different light intensities) near the two frequencies ω_1 and ω_2 . (b) shows the atomic levels and definitions of the δ 's.

Figure 2. (a) shows the measured atomic beam profile for $\phi = 0$ and π . Here $\delta_1 = \delta_2 \approx +6$ MHz ($\delta = 0$) and the intensity $I_1 \approx 3.2$ mW/cm² and $I_2 \approx 1.6$ mW/cm² ($\approx I_{\text{sat}} = hc/\lambda^3\tau$). A change of 1.0 on the vertical axis corresponds to a 100% change of the signal. (b) shows how the measured central peak height at large δ varies with ϕ . The solid line is a fit of a sine wave to the data.

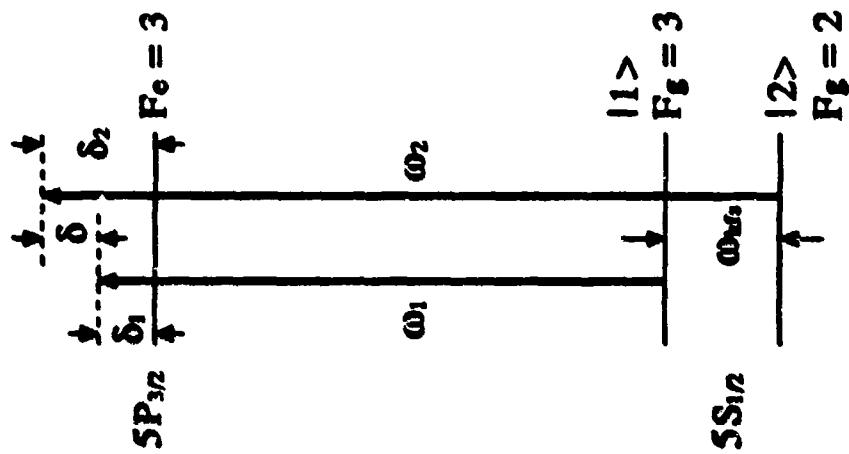
Figure 3. (a) shows the measured atomic beam profile for various values of δ that produce VSR at velocities $\pm\delta/2k$. A change of 1.0 on the vertical axis corresponds to a 100% change of the signal. (b) shows the measured resonant velocities the peaks vs δ . The straight line is a plot of $v = \delta/2k$. The laser intensity is $(0.6)I_{\text{sat}} \approx 1$ mW/cm² for each beam and $\delta_1 \approx 10$ MHz.

Figure 4. The spatial dependence of the light shifts for δ_1 and δ_2 with opposite signs and ϕ different from 0 or π . The arrows show the position and the direction of optical pumping between states $|1\rangle$ and $|2\rangle$. Atoms travel along the thickened lines to the right, and for the case shown, the average force is clearly to the right. For motion to the left, the force is still to the right.

Figure 5. (a) and (b) show the measured spatial profile of the deflected atomic beam for two different signs of the δ_i 's. A change of 1.0 on the vertical axis corresponds to a 100% change of the signal. Similar results are obtained by moving the retroreflecting mirror. The limit of velocity capture range is evident in the data. (c) and (d) show the calculated force curves. The laser intensity is ≈ 1.6 mW/cm² for all parts, $\delta_1 = +6$ MHz and $\delta_2 = -3$ MHz for (a) and (c), and $\delta_1 = -3$ MHz and $\delta_2 = +6$ MHz for (b) and (d).

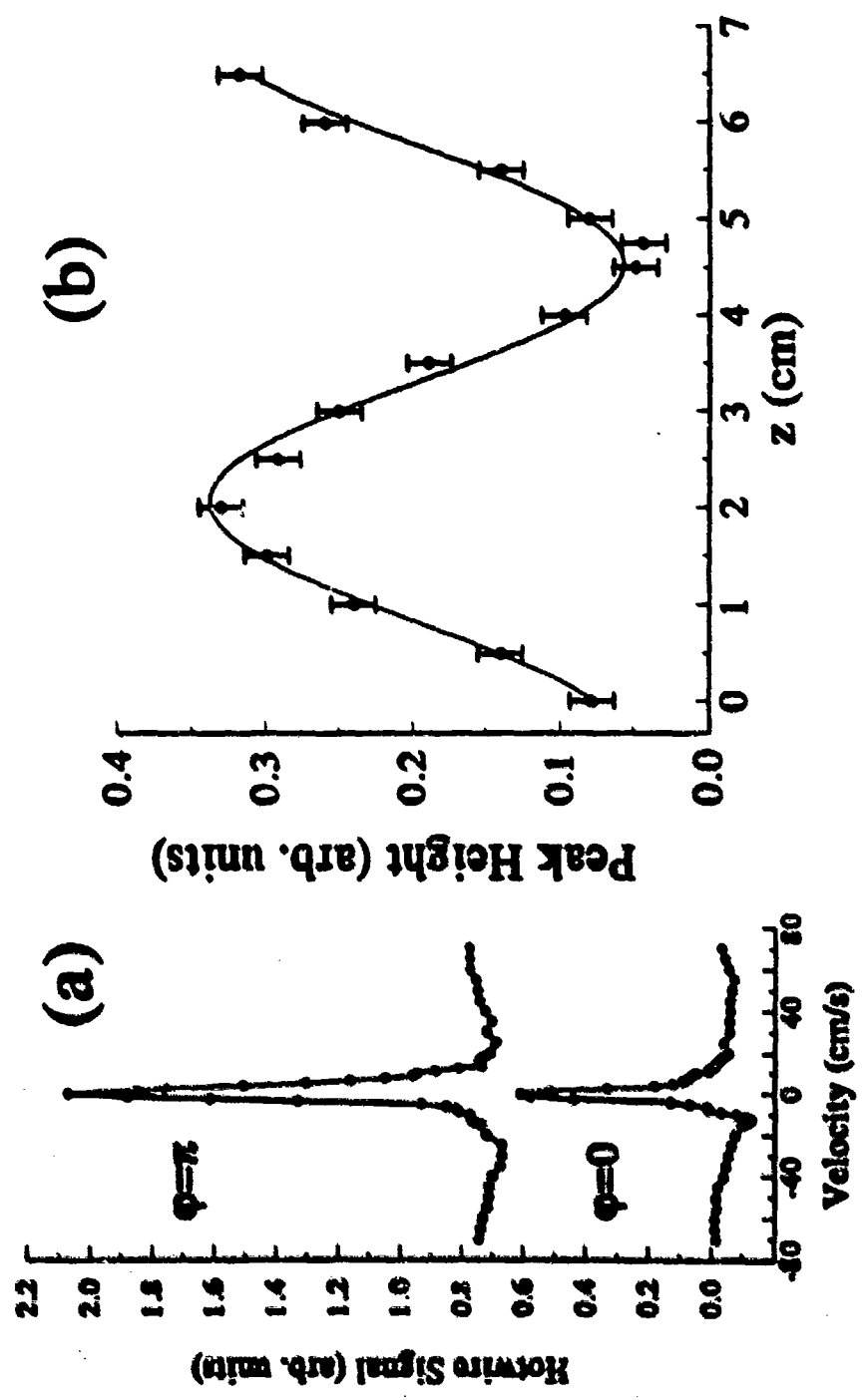


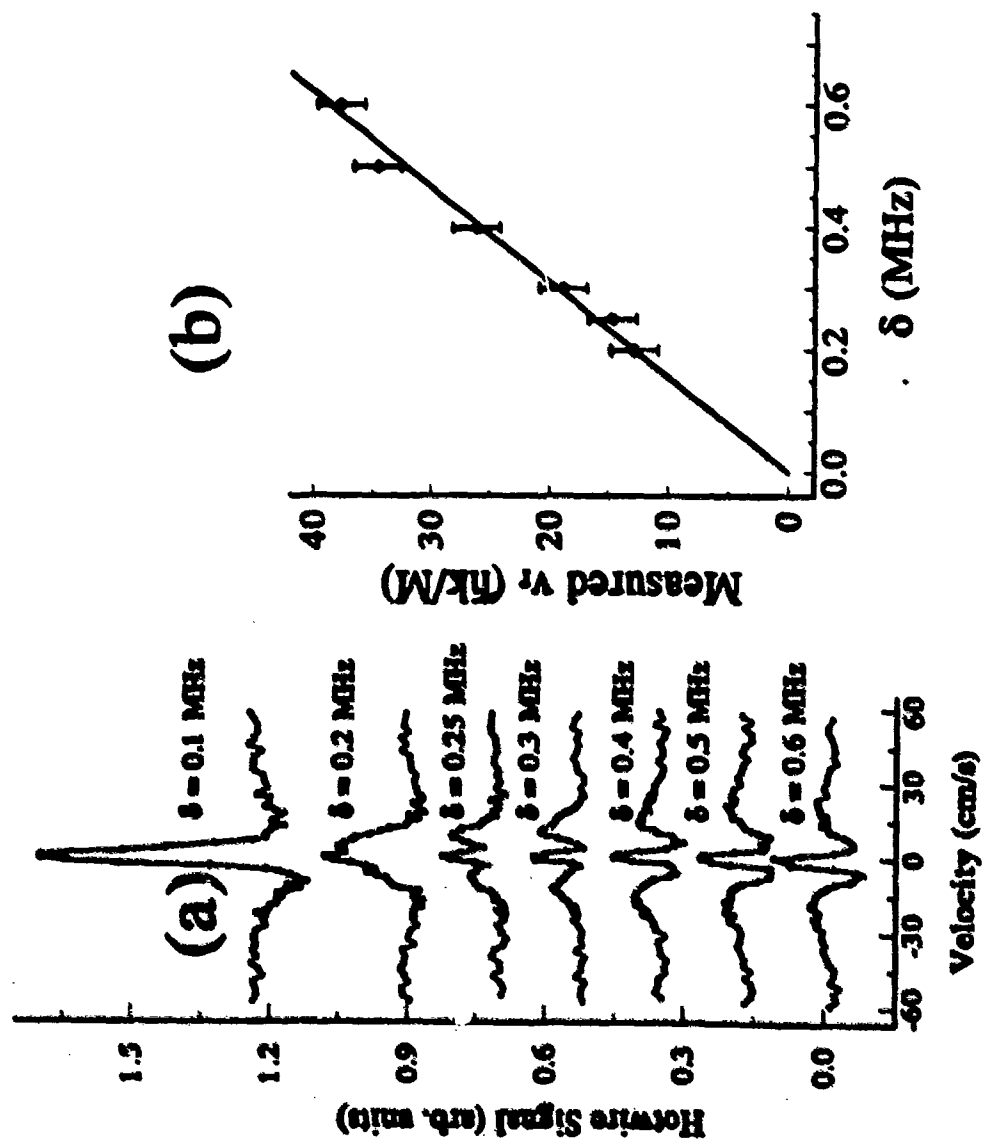
(a)



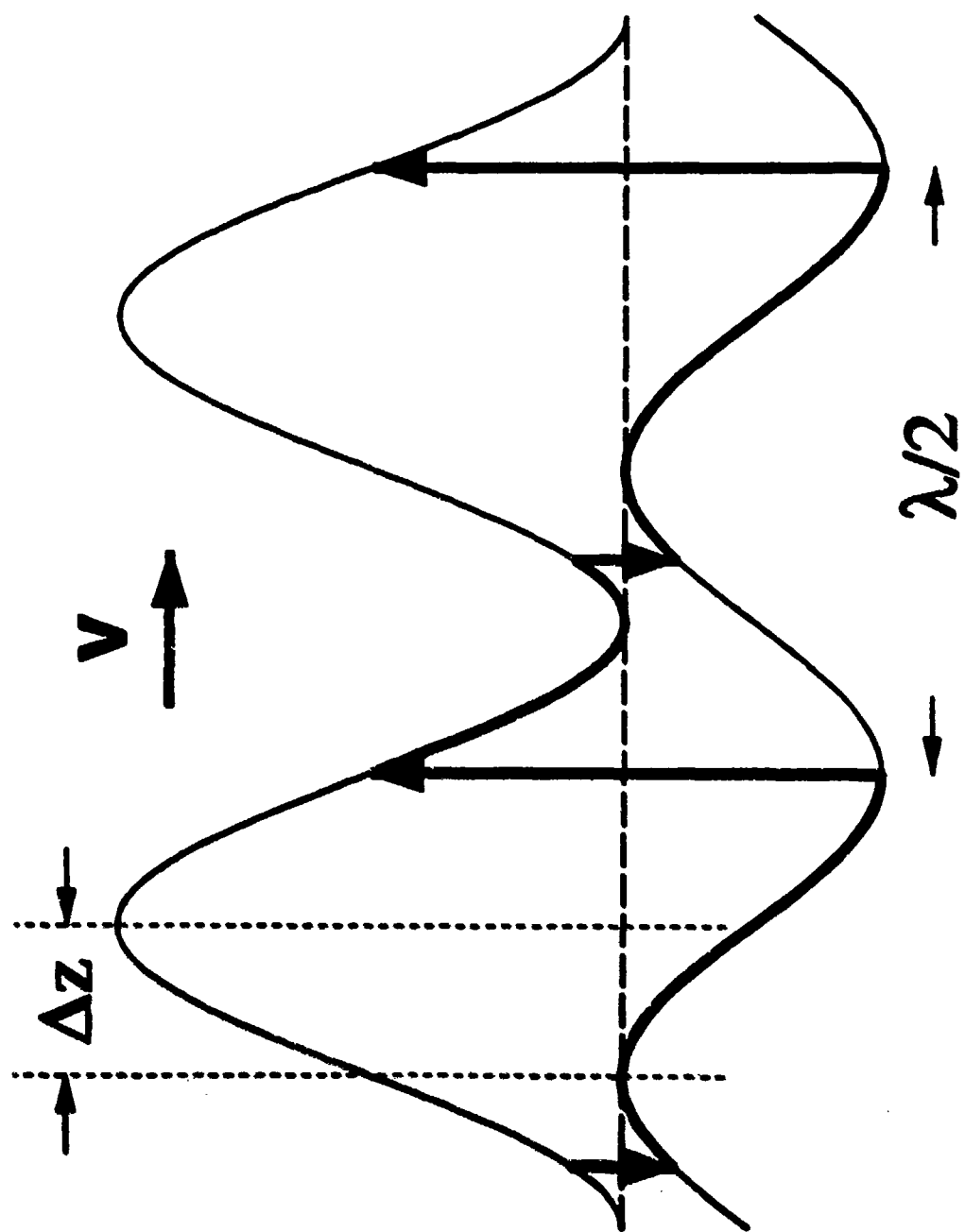
(b)

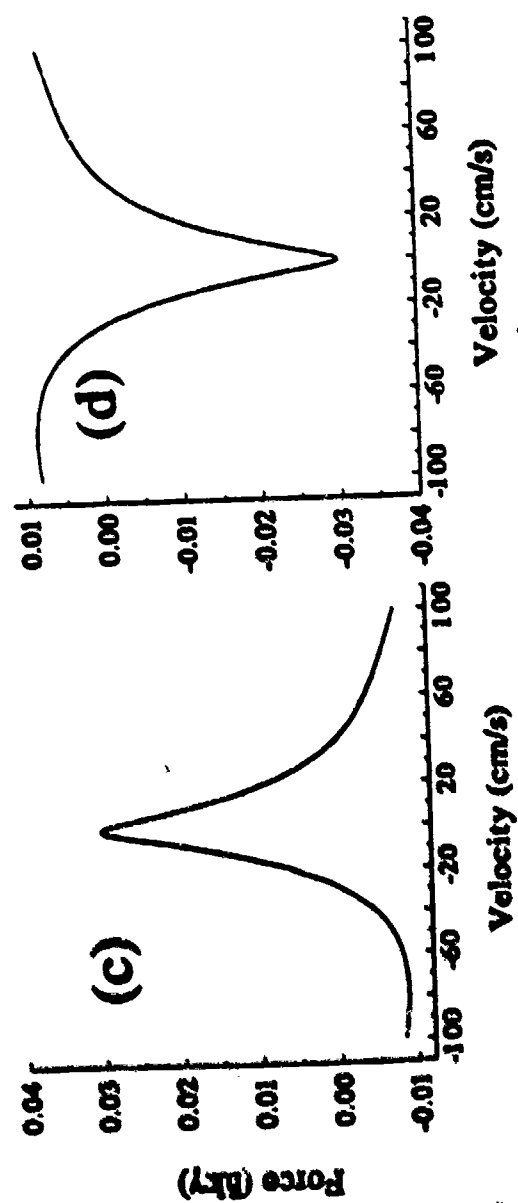
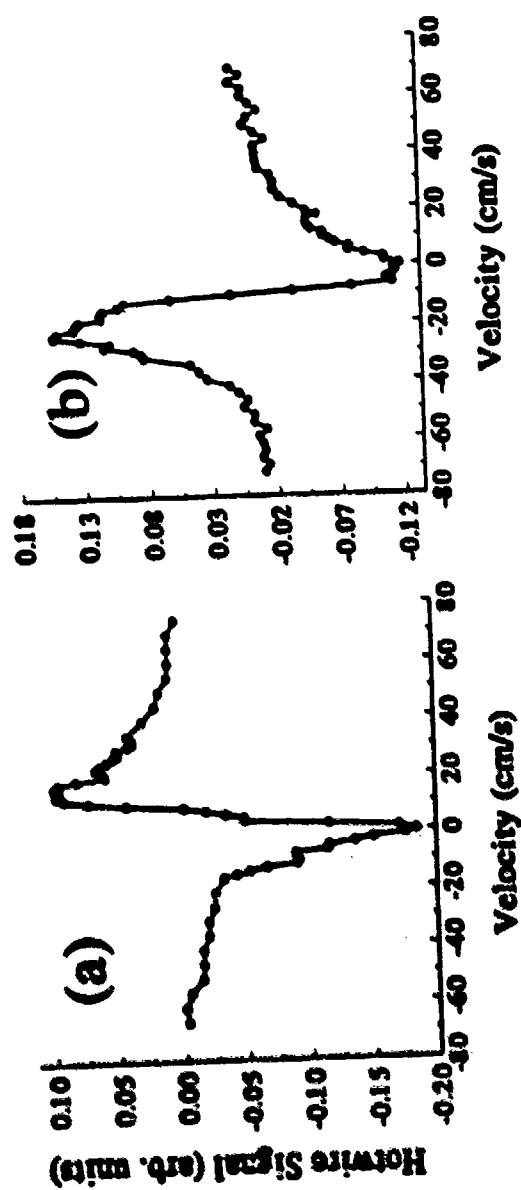
Fig 2





504





*Submitted to Phys Rev
Lett*

Energy Bands and Bloch States in 1D Laser Cooling

M. Doery, M. Widmer, J. Bellanca, E. Vredenburg, T. Bergeman and H. Metcalf

Physics Department, SUNY, Stony Brook, NY 11794-3800

(August 27, 1993)

Abstract

We describe calculations that predict and analyze distinctive quantum features in the velocity distribution in 1D laser cooling for light shift potential well depths only a few times the recoil energy. These features arise from transitions between energy bands, or even between Bloch states, in the periodic potential. They occur with a σ^+ standing wave, both with and without a small B field, and for $\text{lin} \perp \text{lin}$ laser cooling. We have observed these features experimentally in a beam of metastable helium atoms cooled on the $2^3S_1 \rightarrow 2^3P_2$ transition, with velocity resolution ~ 0.3 recoil.

PACS numbers: 32.80.Pj, 42.50.Vk

Typeset using REVTeX

Recent progress in laser cooling has produced atoms with mechanical energies less than the light shifts induced by the laser light [1,2]. This means atoms may be confined in the periodic array of potential wells between the nodes (or antinodes) of optical standing waves. At such low energies, the deBroglie wavelength of the atoms is comparable to the optical wavelength. Motion in these wells is thus quantized: the eigenstates of atomic motion show a band structure analogous to that of electrons moving in the periodic potential of a crystal. Since a theory of this band structure in laser cooling was developed [3], there has been a keen interest in studying its effects experimentally. Recently, the frequency intervals between energy bands have been investigated with a probe laser using four-wave mixing [4], through sidebands in the atomic fluorescence [5], and through rf spectroscopy [6]. Up to now, however, there have been no observations of quantum effects in the velocity distribution, which is arguably closer to the focus of laser cooling.

Here we report measurements and calculations that, for the first time, do reveal quantum effects in the velocity distribution of cooled atoms. We find not only effects of transitions between the bands, but also effects of transfer of population between Bloch states within these bands. Effectively, we are probing the velocity substructure of bands in the periodic light shift potential. Observation of these features requires that the velocity resolution be smaller than the recoil velocity V_R . Furthermore, the laser-atom interaction time must be at least a few times longer than the optical pumping time, and the light shift potential wells must be shallow enough for only a few bands to occur below the tops of the potential hills. These last two conditions are met by choice of laser intensity and detuning, while the first one is facilitated by cooling metastable He 2^3S atoms (He^*) on the $2^3S_1 \leftrightarrow 2^3P_2$ transition. He^* has a large recoil velocity $V_R \equiv \hbar k/M = 9.2 \text{ cm/s}$ due

to its small mass M ($\lambda \equiv 2\pi/k = 1.083 \mu\text{m}$ is the laser wavelength).

We discuss three cooling configurations where we have observed energy band or Bloch state transition effects. The first is a pure σ^+ laser standing wave driving the $\text{He}^* J = 1 \rightarrow 2$ transition, which produces a dip in the velocity distribution near $V = 0$. The dip is caused by differences in the zero-point velocity distributions in light shift potential wells of different depths. The second configuration is Magnetically Induced Laser Cooling (MILC) where a σ^+ standing wave and a magnetic field produce sub-Doppler cooling [7]. Transitions between Bloch states *within* the lowest energy band in the standing wave cause a peak in the velocity distribution near $V = 0$ whose width is about equal to V_R . The third case occurs in polarization gradient laser cooling with counter-propagating laser beams of orthogonal linear polarizations ($\text{lin} \perp \text{lin}$) [8]. Here we find dispersion-like features in the velocity distribution near $V = \pm V_R$, caused by net transfer of population from states just above the lowest band gap to states just below it.

The experimental apparatus used in our studies is shown schematically in Fig. 1. He^* atoms come from a discharge-excited nozzle source, cooled by liquid N_2 . Through time-of-flight measurements we established that the supersonic longitudinal velocity distribution has an average velocity $v = 1400 \text{ m/s}$ and a velocity spread $\Delta v_{\text{RMS}} = 240 \text{ m/s}$ at our standard operating conditions. The on-axis source output is $\sim 5 \times 10^{13} \text{ He}^* \text{ atoms s}^{-1}$ sr^{-1} , while the ratio of singlet to triplet metastables in the beam is < 0.02 . About 1 cm downstream of the nozzle there is a conical skimmer, followed 25 cm further by a $30 \mu\text{m}$ wide \times 7 mm high slit that reduces the flux to $2 \times 10^8 \text{ He}^* \text{ atoms s}^{-1}$.

Directly after this slit, the atoms interact with two counter-propagating laser beams of equal intensity. The beams have a nearly Gaussian intensity profile with a waist radius

$w = 16$ mm (e^{-2} intensity point) and are apertured to a diameter of 32 mm. They originate from a home-built, laser diode-pumped CW LNA-laser [9]. The laser's frequency is locked to a cavity that in turn is locked to a Zeeman-tuned [10], weak RF discharge in helium. The interaction region is surrounded by three orthogonal pairs of Helmholtz coils to create a well-defined magnetic field B . The Earth's magnetic field was cancelled to ± 5 mG using the Mechanical Hanle Effect on the $2^3S_1 \rightarrow 2^3P_1$ transition [11].

The transverse velocity distribution of the He^* beam, modified by the interaction with the laser light, is measured with a detector 1.9 m downstream of the interaction region. This detector consists of a stainless steel plate placed behind a $30\text{ }\mu\text{m}$ wide slit in a moveable, metal cage. The two $30\text{ }\mu\text{m}$ slits separated by 1.9 m provide velocity resolution of 2.7 cm/s or $0.3 V_R$. The internal energy of the He^* atoms can free an electron from the plate on impact, and the resulting current (~ 10 fA) is amplified, collected and recorded. The detector's transverse position in the atomic beam is scanned with a computer controlled stepper motor.

We have used two types of density matrix quantum cooling calculations [3,12-14] to interpret the measurements. The density matrix ρ obeys the Liouville equation $\dot{\rho} = -(i/\hbar)[H, \rho] + \dot{\rho}_{sc}$, where H includes internal energies, kinetic energies, atom-laser interactions, and magnetic field interactions if present, and $\dot{\rho}_{sc}$ expresses the spontaneous radiative decay and repopulation of ground state sublevels. The calculations that best model the experiments use basis states that are products of internal atomic states and free particle momentum eigenfunctions [3,13]: $\Psi = |J, m, p\rangle$. Excited states are explicitly included so Doppler cooling effects occur in the results, and one can also include the spatially varying laser intensity profile. These calculations match the measured velocity

distributions very well, but do not offer a clear picture of the cooling process.

More insight is provided by our second method because it explicitly uses eigenstates of the periodic light shift potential obtained by adiabatically eliminating the excited state [12,14,15]. It simulates the experiment less accurately because there is no Doppler cooling and the laser profile is assumed constant. Nevertheless, it shows the key features found both in the experiments and in the free particle calculations. The effective Hamiltonian for the ground state is $H_{eff} = (2S\delta/L)V_{ge}V_{eg}$, where $S \equiv 2\Omega^2/\Gamma^2$ ($= 1$ for intensity $I = \pi\hbar c/3\lambda^3\tau$), Ω is the single beam Rabi frequency, $\Gamma \equiv 1/\tau$ is the decay rate, $\delta \equiv \omega_{laser} - \omega_{atom}$ is the laser detuning from the atomic frequency, and $L \equiv 1 + 4\delta^2/\Gamma^2$. The matrix V_{ge} includes Clebsch-Gordan coefficients for the atom-laser interaction ($|V_{gi,ej}| \leq 1$). H_{eff} is diagonal in the magnetic quantum number m for σ^+ light or for lin \perp lin cooling on a $J_g = \frac{1}{2}$ transition. The well depth $U_0 = fS\delta/L$, where $f = 2$ for a σ^+ standing wave, and $f = 5/6$ for $J = 1 \rightarrow 2$ for lin \perp lin.

To help understand the following effects, some background on Bloch states is useful. When the light shift potential is diagonal, the eigenfunctions satisfy a Mathieu equation. Solutions may be written as an expansion in momentum eigenstates [15,16,3] $\Psi_{n,\nu}(x) = \sum_j a_{n,j,\nu} \exp[i(\nu+2j)kx]$ where n is the band number and ν is the Bloch index: $-1 < \nu \leq 1$. Thus $\Psi(x)$ obeys Floquet's theorem. In Table I we present the low order wavefunctions for $H_{eff} \sim U_0 \sin^2(kx)$, when U_0 is less than the recoil energy $E_R = MV_R^2/2 = \hbar^2 k^2/2M$. In general, $\Psi(x)$ represents a travelling wave, except when $\nu = 0$ or ± 1 , where energy gaps occur. For the few bands below the tops of the potential hills when the potential is shallow, states just below a gap are more strongly localized in the deep part of the wells than states just above it. Going from the bottom to the top of a band, the wave functions

go from being localized away from the deep part of the wells to being most localized in the deep part of the wells. In a shallow potential, the lowest ($n = 0$) band is an exception in that its $\nu = 0$ state is only slightly localized.

To explain our observations in the clearest way, we use a simple $J = \frac{1}{2} \rightarrow \frac{3}{2}$ model. We use a basis of eigenstates of the periodic light shift potential and neglect off-diagonal density matrix elements [12] (except for MILC, where they are always needed), and assume that the atomic recoil from spontaneous emission of a π (σ) photon is always directed perpendicular (parallel) to the laser axis (x -axis). In σ^+ excitation from $m = -\frac{1}{2}$ Bloch states, followed by π decay to $m = \frac{1}{2}$ states, the net change in the Bloch index is then $\Delta\nu = \pm 1$. Calculations based on this simplified model preserve the features found in more exact calculations.

We first discuss the quantum feature in a σ^+ standing wave (no polarization gradients or magnetic field). The data in Fig. 2a show an overall bell shape that arises from Doppler cooling, while the dip near $V = 0$ arises from purely quantum effects. Fig. 2a also shows computational results from the free particle basis (with Gaussian laser spatial profile), and from the periodic potential basis for a $J = \frac{1}{2} \rightarrow \frac{3}{2}$ transition.

The dip at $V = 0$ is a quantum feature that can be explained even with the simple model. Fig. 3a shows the excitation and decay branches, and Fig. 3b shows the two $m = \pm\frac{1}{2}$ potential wells. Because atoms in the shallower well have a smaller zero point vibrational energy than those in the deeper well, the velocity distribution in the lowest band of the shallower well is narrower. $\Delta m = 1$ excitation followed by $\Delta m = 0$ decay transfers atoms from the lowest band in the shallower $m = -\frac{1}{2}$ potential well to the lowest band in the deeper $m = +\frac{1}{2}$ well. This process replaces the narrow velocity distribution

in the shallow well with a broader one. Fig. 3c shows calculated velocity distributions $P(m, n, V) = P(-\frac{1}{2}, 0, V)$ and $P(\frac{1}{2}, 0, V)$ ($n = 0, 1, \dots$ is the band number), and their difference $\Delta P(V)$ (enlarged by a factor of 4), for typical laser parameters. $\Delta P(V)$ has a dip at $V = 0$ and two peaks at $V \sim \pm 1.3V_R$. Thus this quantum effect is caused by differences in the velocity distributions of the lowest states of the potential wells [17]. This same description holds for the $J = 1 \rightarrow 2$ transition in He^* , and causes the dip shown in Fig. 2a.

This non-Gaussian population distribution is relatively short lived. For the $J = 1 \rightarrow 2$ transition in He^* in a σ^+ polarized standing wave, the populations of the $m = -1$ and 0 states are depleted at the optical pumping rate $\Gamma_p = 2S\Gamma/L$. For the conditions of Fig. 2a, the dip appears after $\sim 1\mu\text{s}$, which is a few times $1/\Gamma_p \sim 0.3\mu\text{s}$. However, Doppler cooling of $m = 1$ atoms continues at the rate $\Gamma_{\text{Dopp}} = 16S\delta E_R/\hbar\Gamma L^2$. Since our interaction time is only $\sim 20\mu\text{s}$, we do not see the dip vanish, but our calculations indicate that it disappears after about $100\mu\text{s}$, which is a few times $1/\Gamma_{\text{Dopp}} \sim 20\mu\text{s}$.

The next quantum feature we discuss occurs when a transverse magnetic field is added to the σ^+ standing wave (MILC [7]). At low intensities the two peaks discussed above appear at approximately $\sim V = \pm 1.3V_R$, but there is also a central peak of width $\sim V_R$, as shown in Fig. 2b. The population distributions in the lowest bands are shown in Fig. 4a vs. energy. Fig. 4a shows that the population decreases sharply with energy in the lowest $m = -\frac{1}{2}$ band. No central peak occurs when the populations of the Bloch states in this band are uniform, as they nearly are for the pure σ^+ case. We conclude that the variation in the population over the band is responsible for the peak in $P(V)$ at $V = 0$ in Fig. 2b.

As discussed in Ref. [13], MILC is a cyclic process of $\Delta m = +1$ optical pumping and $\Delta m = \pm 1$ magnetic field mixing. (Hence in MILC, the peaks at $V = \pm 1.3V_R$ are continually regenerated.) In Fig. 4b, transitions between Bloch states (labeled A through D) in the lowest bands ($n = 0$) of the $m = \pm \frac{1}{2}$ potentials are shown by straight and curved (single) arrows, respectively. The numbers (0.87, etc.) give the relative pumping transition rates between states $|m, n, \nu\rangle$ as $T_{AD} = |\langle -\frac{1}{2}, 0, 0 | \sin(kz) | \frac{1}{2}, 0, 1 \rangle|^2 = 0.80$ and $T_{BC} = |\langle -\frac{1}{2}, 0, 1 | \sin(kz) | \frac{1}{2}, 0, 0 \rangle|^2 = 0.87$. In the deeper, $m = +\frac{1}{2}$ well, all states are comparably localized near the high intensity region, but in the shallow $m = -\frac{1}{2}$ well, the $n = 0$ wave functions become more strongly localized in the high-intensity part of the well as ν goes from 0 to 1. Therefore T_{BC} is greater than T_{AD} . The pumping rate from $m = -\frac{1}{2}$ to $m = \frac{1}{2}$ for $\nu = 0$ (point A) to $\nu = 1$ (D) is weaker than the pumping rate from $\nu = 1$ (B) to $\nu = 0$ (C) because atoms at B experience a higher average intensity than those at A. By contrast, the magnetic field mixing rate between the two $\nu = 1$ states (BD) is very nearly equal to that for $\nu = 0$ (AC). The net result of this cyclic process is an accumulation of atoms in the state with the lowest pumping rate, i.e., state A, (double arrow in Fig. 4b). As seen from Table I and Fig. 4c, atoms with $\nu = 0$ have a large probability to be at $V = 0$. Thus, a central peak occurs because of a two-step transfer of atoms *within* the lowest $m = -\frac{1}{2}$ energy band, and is a purely quantum feature. For deeper potentials with more bands below the tops of the potential hills, this quantum feature evolves into the usual MILC cooling peak.

The third quantum feature we discuss in 1D laser cooling occurs in lin \perp lin polarization gradient cooling at low intensities. For $U_0 \sim E_R$, we find that the velocity distribution has strong dispersion shapes centered at $V = \pm V_R$, which can also be understood in

terms of transitions between Bloch states within the low-lying energy bands. Calculations and experimental data on this effect are shown in Fig. 2c. To obtain the best match between experiment and theory in Fig. 2c, the optimum laser intensity parameter for the calculations was found to be $S = 1.2$ as compared with the nominal experimental value of 2.7. This discrepancy is unexplained at present.

In lin \perp lin cooling, each optical pumping step of the cyclic transfer from $m = -\frac{1}{2}$ to $m = \frac{1}{2}$ and back results in some energy loss. With shallow potentials, the lowest quantum states produce anomalies in the cooling process. We focus on the optical pumping/radiative decay transition from the $m = -\frac{1}{2}, n = 1$ band to the $m = \frac{1}{2}, n = 0$ band. Atoms in Bloch states $|m, n, \nu\rangle = |-\frac{1}{2}, 1, \lesssim 1\rangle$ are pumped to $|\frac{1}{2}, 0, \sim 0\rangle$ by σ^+ photons, then to $|-\frac{1}{2}, 0, \lesssim 1\rangle$ by σ^- photons (Fig. 5). From $|-\frac{1}{2}, 0, \lesssim 1\rangle$, atoms are pumped to higher states at rates smaller than for these processes, so there is a net loss of $|-\frac{1}{2}, 1, \lesssim 1\rangle$ atoms and a net accumulation of $|-\frac{1}{2}, 0, \lesssim 1\rangle$ atoms. For $|-\frac{1}{2}, 1, \lesssim 1\rangle$, the most probable $|V|$ is slightly $> V_R$, while for $|-\frac{1}{2}, 0, \lesssim 1\rangle$, the most probable $|V|$ is slightly $< V_R$, as seen from the velocity distributions in Fig. 5b or the (1,0.8) and (0,0.8) functions in Table I. This two-step transition accounts for the dip at $V > V_R$ and the peak at $V \lesssim V_R$, and reflects the differing character of Bloch states just above and just below the lowest band gap.

In summary, the experiments and calculations reported here show that in order to understand laser cooling on the level of one recoil velocity, one must understand the redistribution of population among Bloch states in the periodic light shift potential.

This work was supported by NSF, ONR, AFOSR, the US Dept of Education, and by a grant of computer time from the Cornell National Supercomputer Facility.

REFERENCES

- [1] P. Lett et al., Phys. Rev. Lett. **61**, 169 (1988).
- [2] C. Salomon et al., Europhys. Lett. **12**, 683 (1990).
- [3] Y. Castin and J. Dalibard, Europhys. Lett. **14**, 761 (1991).
- [4] P. Verkerk et al., Phys. Rev. Lett. **68**, 3861 (1991).
- [5] P. Jessen, Phys. Rev. Lett. **69**, 49 (1992).
- [6] R. Gupta et al., Proceedings of Fermi School CXVIII, ed. by E. Arimondo and W. Phillips, North Holland, 1992, p 345.
- [7] B. Sheehy et al., Phys. Rev. Lett. **64**, 858 (1990).
- [8] J. Dalibard and C. Cohen-Tannoudji, J.O.S.A. B **6**, 2023 (1989).
- [9] T. Chuang and H. Metcalf, Appl. Optics **30**, 2495 (1991).
- [10] T. Dineen et al., Opt. Commun. **92**, 277 (1992).
- [11] R. Kaiser et al., Z. Phys. D **18**, 17 (1991).
- [12] Y. Castin, J. Dalibard, and C. Cohen-Tannoudji, in Moi et al, Eds. *Light Induced Kinetic Effects on Atoms, Ions and Molecules*, (Pisa, 1991).
- [13] T. Bergeman, submitted for publication.
- [14] M. Doery, E. Vredenburg, T. Bergeman, in preparation.
- [15] M. Wilkens et al., Phys. Rev. A **44**, 3130 (1991).

[16] N. MacLachlan, *Theory and Application of Mathieu Functions* (Dover, New York, 1964).

[17] At higher intensity a broader dip occurs in the Doppler cooled velocity distribution because the force curve reverses its slope near $V = 0$. This high-intensity feature is not a quantum effect.

TABLES

TABLE I. Low order expressions for some unnormalized Mathieu functions, labeled by (n, ν) (adapted from Ref. [16]). Here $u = U_0/E_R$ and $z = kz$. Energies (third column) are relative to the potential mean.

(n, ν)	Ψ	E/E_R
0,0	$1 - (u/8) \cos(2z) \dots$	$-u^2/32 \dots$
0,0.8	$\exp(0.8iz) - (5u/16) \exp(-1.2iz) \dots$	$0.64 - 0.09u^2 \dots$
0,1	$\sin(z) - (u/32) \sin(3z) \dots$	$1 - u/4 \dots$
1,1	$\cos(z) - (u/32) \cos(3z) \dots$	$1 + u/4 \dots$
1,0.8	$\exp(-1.2iz) + (5u/16) \exp(0.8iz) \dots$	$1.44 + 0.07u^2 \dots$

FIGURES

FIG. 1. Schematic of the experimental apparatus.

FIG. 2. Experimental data (dots) and free particle basis computational results (solid lines) for the velocity distribution of He^+ atoms with (a) a σ^+ standing wave, $S_{\text{max}} = 1.65, \delta = -2\Gamma$; (b) a σ^+ standing wave plus 50 mG B field, $S_{\text{max}} = 4.5, \delta = -4\Gamma$; (c) lin \perp lin cooling, $S_{\text{max}} = 2.7, \delta = -8\Gamma$. For (c), calculations were performed with $S_{\text{max}} = 1.2$. The laser intensity has a Gaussian spatial distribution. Dashed lines give results of periodic potential basis calculations for the simpler case of $J = 1/2 \rightarrow 3/2$, with adjusted uniform laser intensity.

FIG. 3. Analysis of the quantum feature in Fig. 2a, using a $J = 1/2 \rightarrow 3/2$ transition. (a) Excitation and decay scheme, with Clebsch-Gordan factors and m values as shown; (b) One period of the light shift potential for $m = \pm 1/2$, with the lowest energy bands indicated; (c) Velocity distributions for the lowest energy bands, and their difference.

FIG. 4. Analysis of the quantum feature in Fig. 2b (MILC). (a) Calculated populations in Bloch states (discretized to a mesh of $\Delta\nu = 0.1$) for the lowest energy bands for $m = \pm 1/2$. (b) Low-lying energy bands for $m = \pm 1/2$, with optical pumping (straight arrows) and magnetic field coupling (curved single arrows) transition elements. ν is the Bloch index. The double arrow shows the net population transfer. (c) Velocity distribution functions, $P(V)$, for the $m = -1/2, n = 0, \nu = 0$ and 1 Bloch states, initial and final states of the two-step transfer process.

FIG. 5. Analysis of the quantum feature in lin \perp lin cooling in Fig 2c, in terms of a $J = 1/2 \rightarrow 3/2$ transition. (a) Low lying energy bands for $m = \pm 1/2$, with arrow showing important transitions between Bloch states. (b) $P(V)$ functions for the initial and final Bloch states in the two-step transfer shown in (a).

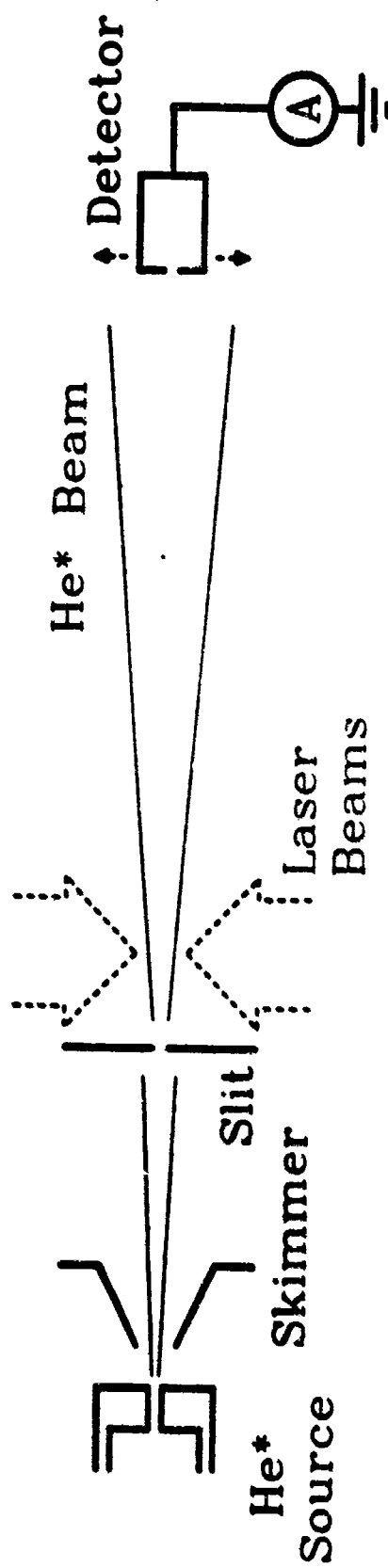


Fig. 1

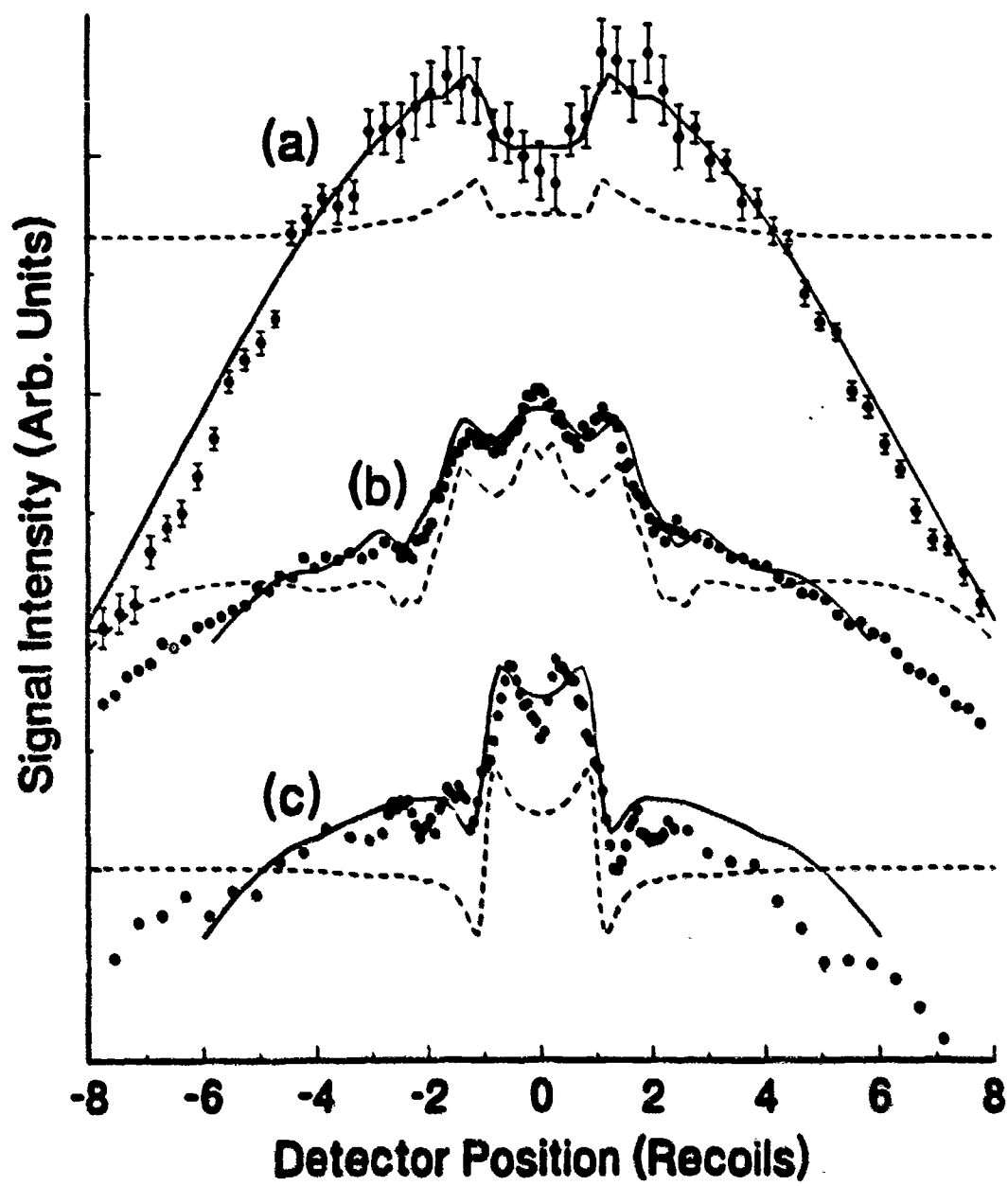


Fig. 2

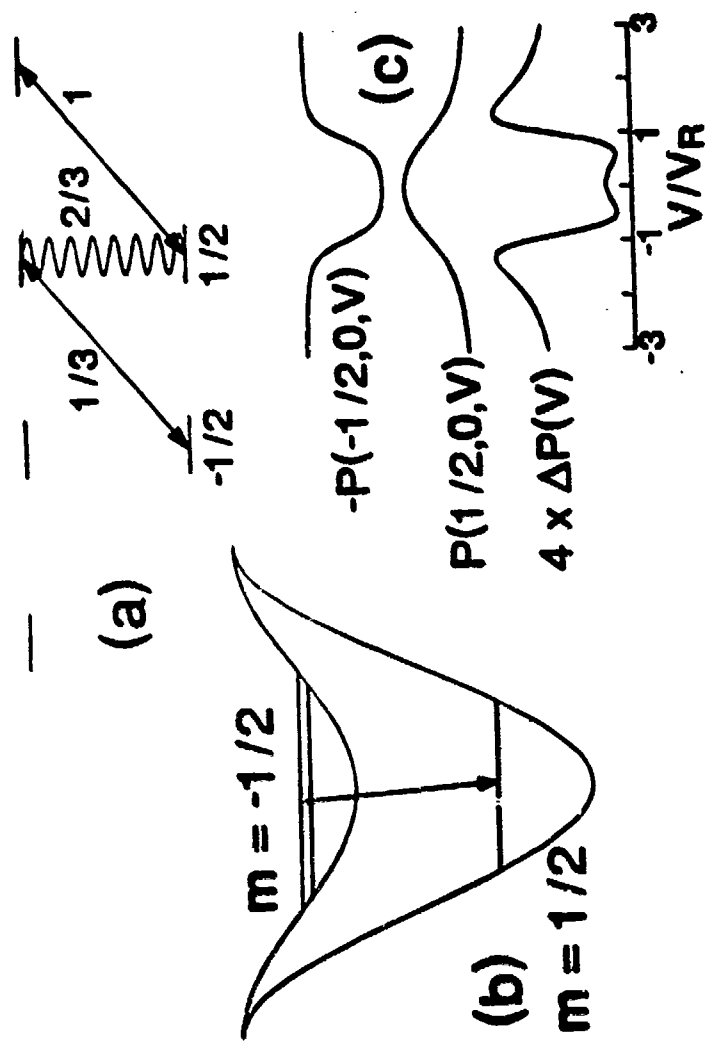


Fig 3

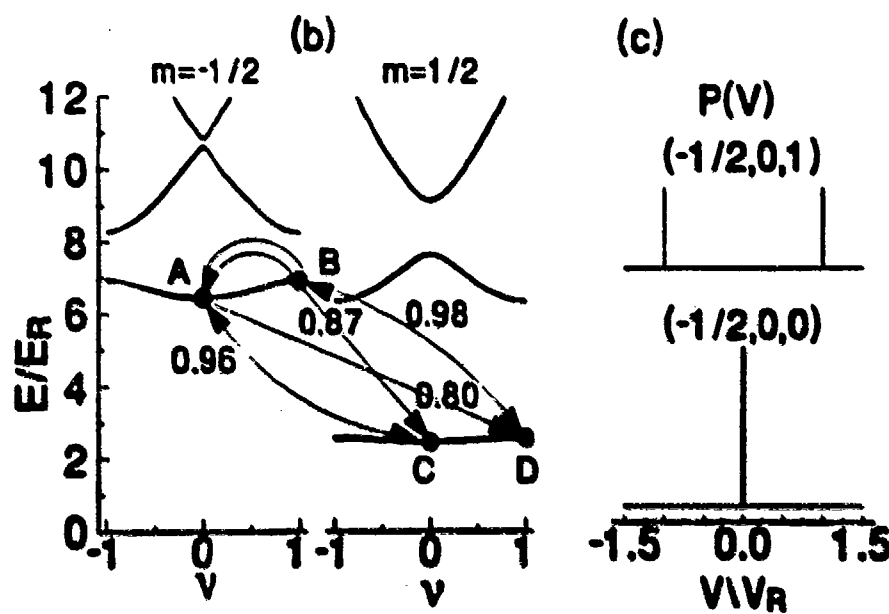
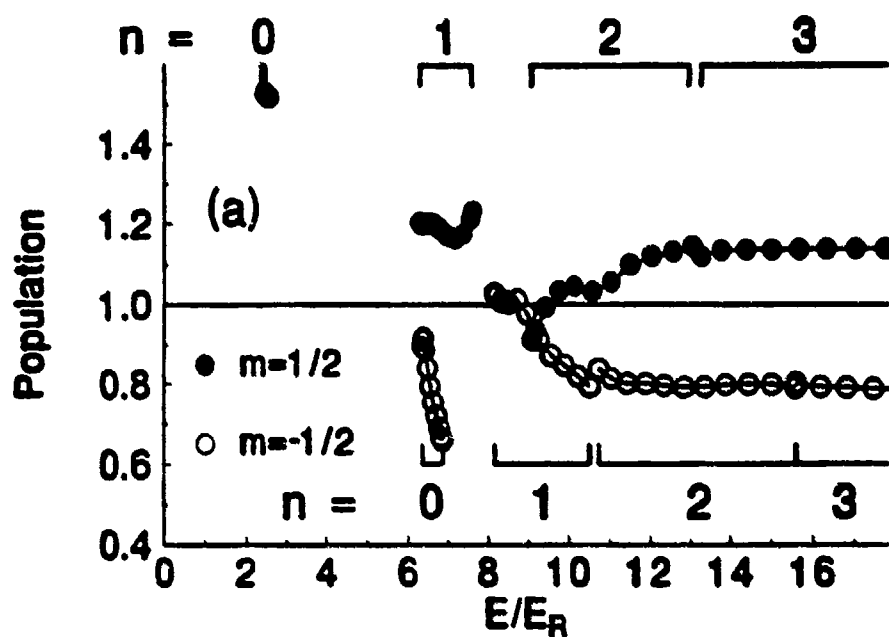


Fig 4

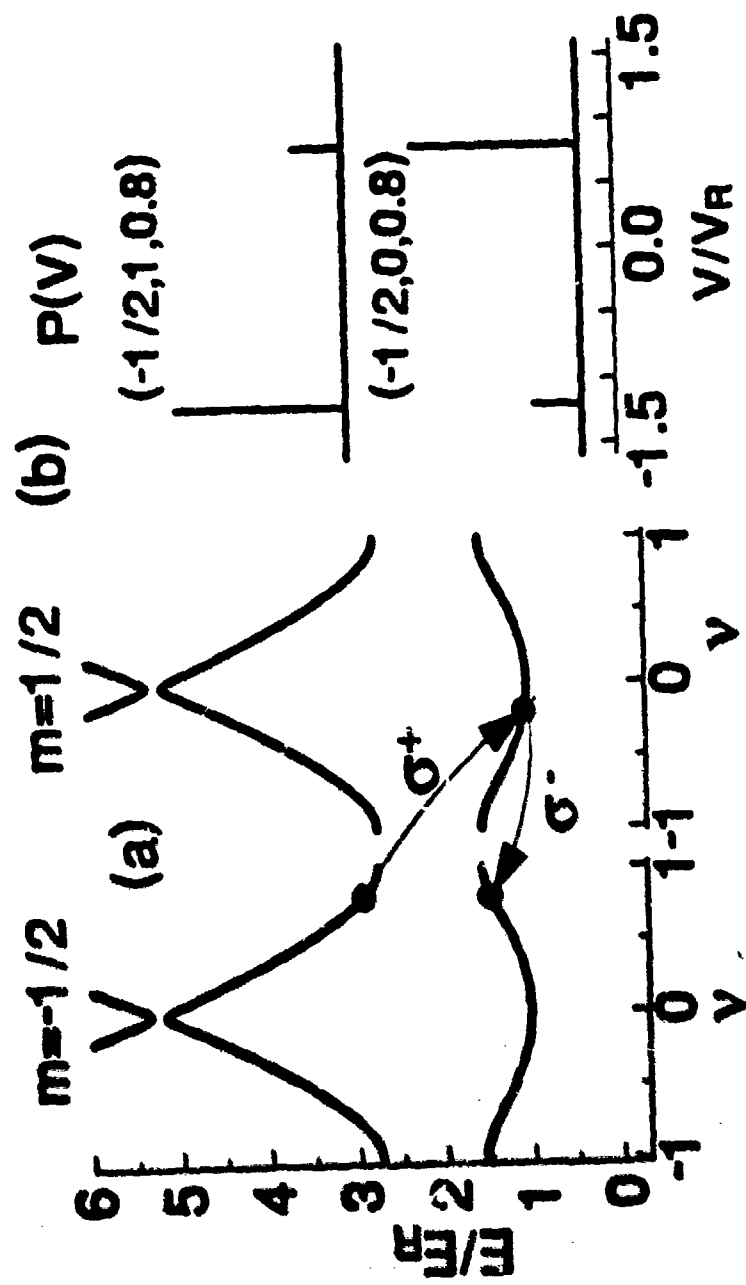


Fig. 5

8/24/93

Slowing of ^{85}Rb Atoms with Isotropic Light

H. Batelaan, S. Padua, D.H. Yang*, C. Xie, R. Gupta and H. Metcalf

Physics Dept., S.U.N.Y., Stony Brook, NY 11790

Abstract

We have demonstrated slowing of a rubidium atomic beam by isotropic monochromatic light. The results agree with a model calculation, thus allowing its use for designing an isotropic light slower. The large hyperfine splittings of rubidium lead to natural multi-frequency slowing, which is also included in our model.

PACS nr. 32.80.Pj, 42.50.Vk

I. INTRODUCTION

The ultimate goal for atomic beam slowing and cooling is the compression of the entire velocity distribution of atoms in a beam as they emanate from a source to one narrow peak at a desired low velocity. Although this goal is far from being reached at present, atomic beam slowers are commonly used for atomic clocks and for loading of magneto-optical traps and optical molasses. Improvements to atomic beam slowers are therefore of current interest. Recently slowing and cooling by white light [1] and isotropic monochromatic light [2] have been demonstrated to be promising new techniques.

In isotropic laser light, the resonance frequency ω_f of an atom moving at a velocity v will be matched by the Doppler-shifted laser frequency when the wavevector \vec{k} of the light makes an angle θ with the atomic velocity \vec{v} :

$$\omega_f = \omega_l - k v \cos \theta, \quad (1)$$

where ω_i is the laser frequency and $i(f)$ indicates the initial (final) state. For red detuned light ($\omega_i - \omega_{if} < 0$) this resonance condition requires $\theta > \pi/2$, meaning that the recoil due to the absorbed photons opposes the atomic motion and slows the atoms. Subsequent spontaneous emission does not exert a force on the atoms on average. As the atoms are decelerated, they absorb light from a increasing angle θ (angle tuned), until the maximum value of $\theta (= \pi)$ is reached. Because the light is isotropic, the atomic motion is directly opposed irrespective of its direction, while for Zeeman (magnetically tuned) [3] and chirped (frequency tuned) [4] slowing, only the longitudinal velocity component of the atomic motion is opposed. This major advantage prevents the atomic beam from being transversely expanded (apart from spontaneous emissions), in contrast to Zeeman tuned and chirped slowing.

In this article, we describe the application of the isotropic slowing technique to a rubidium beam in order to test experimental techniques and a numerical model for the slowing process. The resulting slowed beam of cold atoms is enhanced by natural multi-frequency slowing [2], for which the rubidium atom has an appropriate hyperfine splitting of the excited state. The carefully tested model is then used to calculate isotropic slowing over an extended length.

II. EXPERIMENT

A schematic view of our apparatus is shown in Fig. 1. A thermal beam of Rb is collimated to ~ 10 mrad by an aperture (A1) suspended from a cold trap, and travels through a slower made from the diffusely reflective material Spectralon [5]. The 20 cm long cylindrical slower has an inner diameter of 3 mm and outer diameter of 2 cm. The reflectivity r of the material is specified

by the manufacturer to be 99.1%. A beam from a Ti:sapphire laser, split into two branches by a beam splitter (BS), enters the tube via two 1 mm diameter holes situated 5 cm from each cylinder end. The laser light has a line width of ≤ 1 MHz and is side-locked to the Doppler broadened $5S_{1/2} \rightarrow 5P_{3/2}$ transition of Rb near $\lambda = 780$ nm with an accuracy of ± 50 MHz using absorption in a vapor cell. Saturated absorption is used to calibrate the Doppler broadened absorption spectrum frequency scale. An electro-optical modulator (EOM) [6] divides the laser power between the main laser frequency $\omega_1 = 2\pi \times \nu_1$ (Fig. 2) and two side bands at $\omega_1 \pm 2\pi \times 2.91$ GHz. One sideband (ν_2) counteracts optical pumping into a single ground state hyperfine sublevel, while the other is not used. Alternatively, we use the Ti:sapphire laser and a Sharp model LTO25 diode laser (DL1) to provide two frequencies, instead of the EOM.

The laser beam from another Sharp model LTO24 diode laser (DL3) is directed at an angle of 30° with the atomic beam to determine the longitudinal velocity distribution by measuring the intensity of the emitted fluorescence as a function of the laser frequency. The saturated absorption signal from this laser also serves as a calibration of its frequency. A beam from a frequency locked laser (DL2) perpendicular to the atomic beam cancels velocity selective optical pumping effects.

Two concave spherical mirrors (CM) collect the fluorescence [7,8] and focus it on a hybrid photodiode-amplifier detector [9] (PD). Stray laser light emanating from the Spectralon tube is shielded from the detector (aperture A2). We chop the side bands of the EOM at 500 Hz and subtract the gated signal from the gated background to reduce the noise markedly.

III. A MODEL CALCULATION

We assume that the initial longitudinal velocity distribution of the atomic beam is thermal and given by [10]

$$f(v) \propto v^3 e^{-mv^2/2k_B T}, \quad (2)$$

where k_B is the Boltzman constant and T is the oven temperature. The force on the atoms can be written as

$$F(z) = \int \sum_{g,e} (\Pi_g R_{ge} c_{ge} p - \Pi_e R_{eg} c_{eg} p) d\Omega, \quad (3)$$

where the subscript g (e) indicates the ground (excited) hyperfine levels, Π indicates the steady state population and Ω ($=(\theta, \phi)$) indicates the direction from which an atom absorbs light. The angle θ is defined relative to the direction of the atomic motion. The projection of the recoil momentum of the atom p along its direction of motion is given by

$$p = \hbar k \cos \theta \quad (4)$$

The transition rate [11] from an initial (i) state to a final (f) state is given by

$$c_{if} = (2J_i + 1)(2F_f + 1) \left\{ \begin{matrix} F_f & 1 & F_i \\ J_i & 1 & J_f \end{matrix} \right\}^2 \frac{1}{\tau}. \quad (5)$$

Here, the initial (final) state can be either the ground or excited state. The lifetime τ of the excited J_e state (for the $5^2P_{3/2}$ state of ^{85}Rb) is 27 ns [12], $I = 5/2, J_g = 1/2, J_e = 3/2, F_g = 2, 3, F_e = 1, 2, 3, 4$ and $\{ \}$ are the usual 6-j symbols [13]. The photon scattering rate $R_{if}(z, v)$ is proportional to the convolution of the laser frequency distribution I inside the tube and the atomic line shape $S_{if}(\omega)$ associated with the transition from the initial to the final state [14]

$$R_{if}(z, v) = \frac{\Gamma c \lambda^2}{8\pi} \rho(z) \int \int_0^\infty \frac{S_{if}(\omega) I_{if}(v, \omega, \theta)}{\hbar \omega} d\omega d\Omega, \quad (6)$$

where $\Gamma (= 2\pi \times 6 \text{ MHz})$ is the atomic line width for ^{85}Rb and $\rho(z)$ is the light energy density at position z . In the atomic line shape

$$S_{if}(\omega) = \frac{\Gamma/\pi}{(\omega - \omega_{if})^2 + \Gamma^2} \quad (7)$$

$\omega_{if} = \omega_f - \omega_i$ denotes the frequency difference between the hyperfine levels F_f and F_i . Here, I is the normalized laser frequency distribution in the atomic rest frame

$$I_{if}(v, \omega, \theta) = \frac{1}{4\pi^2} \frac{\Gamma_l}{(\omega - \omega_l + kv \cos \theta)^2 + \Gamma_l^2} d\Omega, \quad (8)$$

where Γ_l is the laser line width. The energy density $\rho(z)$ is derived by an iterative procedure [15].

For a Lambertian reflector, which obeys

$$J(\alpha) = J_0 \cos \alpha, \quad (9)$$

where J_0 is the incident laser power and $J(\alpha)$ the reflected power at an angle α with respect to the normal of the reflector surface, a straightforward derivation for a cylindrical geometry yields

$$P_n(z) = r^n \int_0^L \int_0^{2\pi} \left(\frac{r(1 - \cos \phi)}{z^2 + 2r^2(1 - \cos \phi)} \right)^2 P_{n-1}(z') r d\phi dz', n = 1, 2, \dots \quad (10)$$

for the power distribution P_n of the n -th reflection of the laser light in the cylinder. The initial power distribution is given by P_0 . For example, with one entrance hole at $z = 0$ the total laser power $P = P_0(0)$ and $P_0(z \neq 0) = 0$. The length of the cylinder is L and the reflectivity r . We have assumed that the power distribution is symmetric in ϕ . The total power distribution may be obtained by summing over all reflections, $P(z) = \sum_{n=0}^{\infty} P_n(z)$. We can immediately calculate the energy density from [10],

$$\rho(z) = 4P(z)/c \quad (11)$$

by assuming that the power distribution is isotropic. We have verified analytically that for an infinite cylinder, for which the surface is a homogeneous,

Lambertian source the power distribution is isotropic. These approximations are motivated by the small radius over length ratio for the cylinder.

In the force expression the steady state populations Π_e, Π_g of the hyperfine levels as a function of the position z are calculated by substituting $R_{if}(z, v)$ in the rate equations [11,16]. Obtaining from the calculated force the final velocity of the atom v_f for each initial velocity v_i , we obtain the final velocity distribution,

$$f(v_f) = \frac{dv_i}{dv_f} f(v_i), \quad (12)$$

expressing the conservation of atoms.

IV. RESULTS

To test the effective laser power in the tube we measured and calculated the fraction of atoms optically pumped from the $F_g=3$ into the $F_g=2$ state as a function of laser power injected into the Spectralon tube. We chose this fraction to be the ratio of the maxima of the atomic velocity distribution with and without laser power, and plotted the result in Fig. 3. The calculation is the result of the time dependent rate equations [16] with the isotropic photon scattering rate (Eq. 6) for $r=99\%$. For an oven temperature of $T=130^\circ\text{C}$ the density of rubidium results in an estimated mean free path of the photon of 6 cm, while for an oven temperature of $T=170^\circ\text{C}$ the mean free path is only 0.6 cm. On the other hand a photon travels on average 2.5 cm before being absorbed by a tube with a 92% reflectivity (see below) and 3 mm diameter. Therefore we attribute the decrease in the optical pumping efficiency with increasing temperature both to the optical thickness of the atomic beam and to the strongly Doppler-shifted fluorescence from all these atoms that is prevented from escaping by multiple reflections in the Spectralon. All velocity distributions presented below were taken with an oven temperature of

$T = 130^\circ\text{C}$ where the atomic beam is not optically thick. The optical pumping efficiency test is thus used as an atomic calibration of the energy density inside the Spectralon tube.

Still, roughly a factor of 4 discrepancy exists between the measured and the calculated optical pumping efficiency. An additional experimental test revealed the source of the problem. Fig. 4 shows the result of a measurement of the relative light power that has diffused to the outside of the tube as a function of position along it. The experimental result for a Rb-exposed Spectralon tube before and after cleaning were compared with the result calculated from equation 10. The results for the relative light power were scaled appropriately. The drop in reflectivity of the exposed tube corresponds to a factor of 4 drop in intensity. In accordance with the atomic calibration of the energy density, we used a factor 4 to correct the laser power in all subsequent calculations for the velocity distributions.

The measured fluorescence spectrum was used to determine the velocity distribution, which has contributions from each of the three accessible excited hyperfine states. A given frequency of the detection laser corresponds to three different detunings, which in their turn via $\delta_{ij} = kv_{ij}\cos\theta$ correspond to atoms with three different longitudinal velocities. In our case, the repumping detection laser (DL2) was strongly saturating, while the frequency ramped detection laser (DL3) was operated in the linear range, causing the relative strengths of the different contributions to be proportional to c_{ij} . Taking these three corrections into account in our calculated distributions gives excellent agreement with the experimental result for the initial velocity distribution (Fig. 5).

In Fig. 6 the difference between the final and initial velocity distribution is shown. A negative value of this difference indicates that atoms have been removed, while a positive value shows an increase in the number of atoms. Fig.

6a shows that atoms around 400 m/s have been slowed to velocities around 150 m/s. The experimental detuning δ_1 (Fig. 2) is -190 ± 50 MHz relative to the $F_g=3$ to $F_e=4$ transition and the detuning used in the calculation is -210 MHz. The EOM is driven at 2.91 ± 0.01 GHz, which means that the detuning δ_2 relative to the $F_g=2$ to $F_e=3$ transition is also -190 MHz. The total laser power $P = 100$ mW, and the ratio β of each EOM sideband over carrier is $\beta = 1$. The vertical scale is normalized to the height of the maximum of the initial atomic velocity distribution, so that the peak of slowed atoms (Fig. 6a) contains $\sim 2\%$ of all the incident atoms.

The acceleration in the velocity distribution shown in Fig. 6b has been measured under the same experimental conditions as in Fig. 6a, except for a positive 190 MHz detuning. The presence of the double dip structure can be mostly attributed to the $F_g=3$ to $F_e=4$ and to the $F_g=3$ to $F_e=3$ transitions. The Doppler resonance condition (Eq. 1) is met for the $F_g=3$ to $F_e=4$ transition at 170 m/s and for the $F_g=3$ to $F_e=3$ transition at 280 m/s, which agree with the positions of the dips.

For negative detuning the Doppler resonance condition (Eq. 1) is met for the $F_g=3$ to $F_e=4$ transition at 170 m/s and for the $F_g=3$ to $F_e=3$ transition at 60 m/s. Since the interaction time is longer at low velocities, the slowing process is more efficient than the acceleration process, and the two peaks merge into one. This is natural multi-frequency slowing and is especially effective because of the appropriate hyperfine splitting of Rb. It can not be exploited in sodium [2], where the hyperfine splitting is too small. Instead one must assist the angle-tuned slowing with a stepwise change in laser frequency (multi-frequency slowing). The large excited state hyperfine splitting of rubidium provides this effect naturally.

The results in Fig. 6c and 6d have been measured for a ratio of EOM sideband over carrier $\beta = 0.02$. For positive detuning the resonance condition (at

170 m/s) can only be met by the cyclic $F_g=3$ to $F_e=4$ transition. Therefore a weak repumping sideband is sufficient to maintain the acceleration process. However, for negative detuning the $F_g=3$ to $F_e=3$ (and $F_g=3$ to $F_e=2$) transition can excite atoms at 170 m/s due to angle-tuning. This means that a weak repumping sideband is not sufficient to maintain the slowing process.

Finally, having established confidence in the numerical model by the agreement with the measurements, we show the result of calculations for a 20, 60 and 100 cm long slowers with a 500 mW input power (Fig. 7). Note that the fraction of atoms around 50 m/s has increased by a factor of 100 over the initial distribution. Because this strong increase shows promise for important applications of this technique, we are currently building an extended length slower.

V. ACKNOWLEDGEMENTS

We thank Alex Martin, Wolfgang Ketterle and Edgar Vredenbrecht for helpful discussions. This work was supported by NSF, ONR, AFOSR and CAPES (Brazil).

* Permanent address: Peking University, Beijing, China.

REFERENCES

- [1] M. Zhu, C. W. Oates and J. L. Hall, *Phys. Rev. Lett.* **67**, 46 (1991)
- [2] W. Ketterle, A. Martin, M. A. Joffe and D. E. Pritchard, *Phys. Rev. Lett.* **69**, 2483 (1992)
- [3] W. D. Phillips, J. V. Prodan, and H. J. Metcalf, *J. Opt. Soc. Am. B* **2**, 1755 (1985)
- [4] W. Ertmer, R. Blatt, J. L. Hall, and M. Zhu, *Phys. Rev. Lett.* **54**, 996 (1985)
- [5] Labsphere Inc., P. O. Box 70, North Sutton, NH 03260
- [6] We thank New Focus Corp. (340 Pioneer Way Mountain View, CA 94041) for loaning us the electro-optic modulator.
- [7] K. Shimizu and F. Shimizu, *J. Chem. Phys.* **78**, 1126 (1983)
- [8] U. Hefter and K. Bergmann, *Atomic and Molecular Beam Methods* (edited by Giacinto Scoles, Oxford University Press, NY 1988)
- [9] United Detector Technology, 12525 Chadron Avenue, Hawthorne, CA 90250
- [10] F. Reif, *Fundamentals of Statistical and Thermal Physics* (McGraw-Hill, NY 1965)
- [11] E. de Clercq, M. de Labacherrie, G. Avila, and M. Tetu, *J. Physique* **45**, 239 (1984)
- [12] C.E.Theodosiou, *Phys.Rev.A* **30**, 2899 (1984)
- [13] Rotenberg M, Bivins R, Metropolis N and Wooten J K *The 3J and 6J Symbols* (Crosby Lockwood, London 1959)
- [14] P. W. Milonni and J. H. Eberly *Lasers* (John Wiley & Sons, NY 1988) pp. 220-227
- [15] For the case of a sphere, see: D. G. Goebel, *Appl. Opt.* **6**, 125 (1967)
- [16] G. Avila, V. Giordano, V. Candelier, E. de Clercq, G. Theobald, and P. Cerez, *Phys. Rev A* **36**, 3719 (1987)

Figure captions

Fig. 1. A schematic view of the apparatus. An explanation of its components is given in the text.

Fig. 2. A scheme of the relevant energy levels of ^{85}Rb .

Fig. 3. Fraction of atoms in the $F_0=3$ state after the atoms pass through the slower for oven temperatures of 170° (Δ) and 130° (\square) are given. The line is the calculated result from the rate equations.

Fig. 4. Laser power measured as a function of position along the external wall of the Rb-exposed Spectralon tube of 10 cm length before (\circ) and after (Δ) cleaning. The calculated power is given for $r=99\%$ (\cdots), 98% ($-$), 96% ($- - -$) and 92% ($- \cdot - \cdot -$). The results are scaled appropriately. The laser beam enters the tube at the zero position.

Fig. 5. The measured and calculated initial velocity distribution.

Fig. 6. The difference between the slowed and initial atomic velocity distribution. The experimental and calculated results show agreement. The total laser power is $P = 100$ mW. (a) Natural multi-frequency slowing.

$\delta = -190 \pm 50$ MHz, $\beta = 1$. (b) Acceleration showing two dips, $\delta = 190 \pm 50$ MHz, $\beta = 1$. (c) Slowing disappears, $\delta = -190 \pm 50$ MHz, $\beta = 0.02$. (d) Acceleration remains, $\delta = 190 \pm 50$ MHz, $\beta = 0.02$.

Fig. 7. Calculated initial (solid line) and final atomic velocity distributions for $\delta = -75$ MHz, $P = 500$ mW, $r=92\%$, $\beta = 0.5$ and the EOM is driven at 2.97 GHz. The lengths of the slower are 20 cm (\cdots), 60 cm ($---$) and 100 cm ($-\cdot-\cdot-\cdot-$). The largest slowed peak at 50 m/s contains $\sim 25\%$ of all incident atoms.

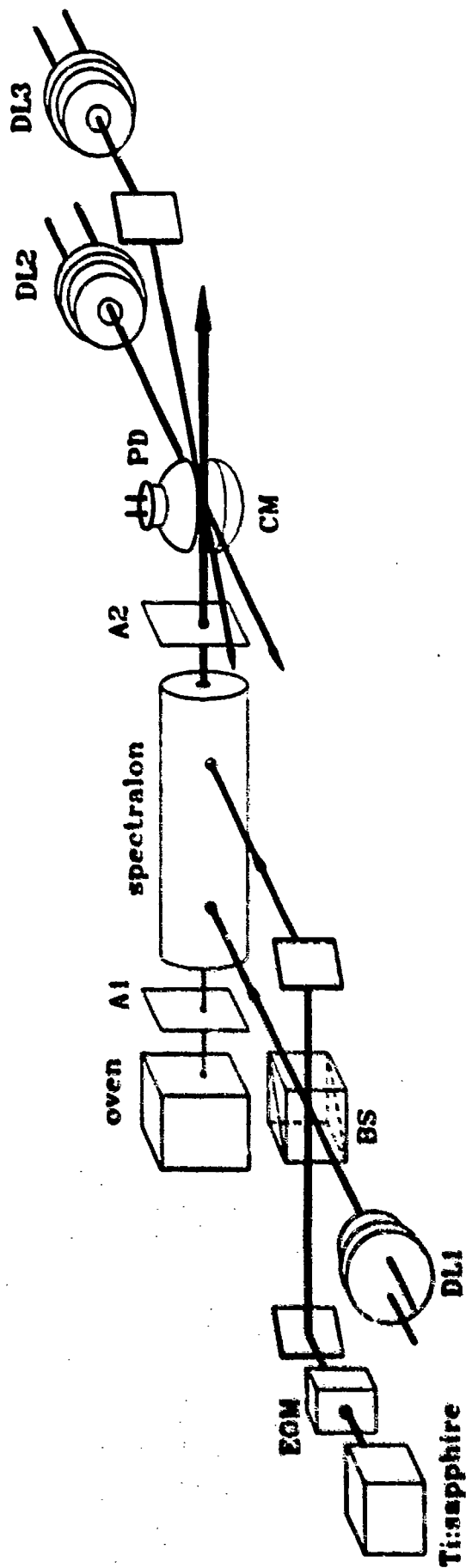


Fig 1

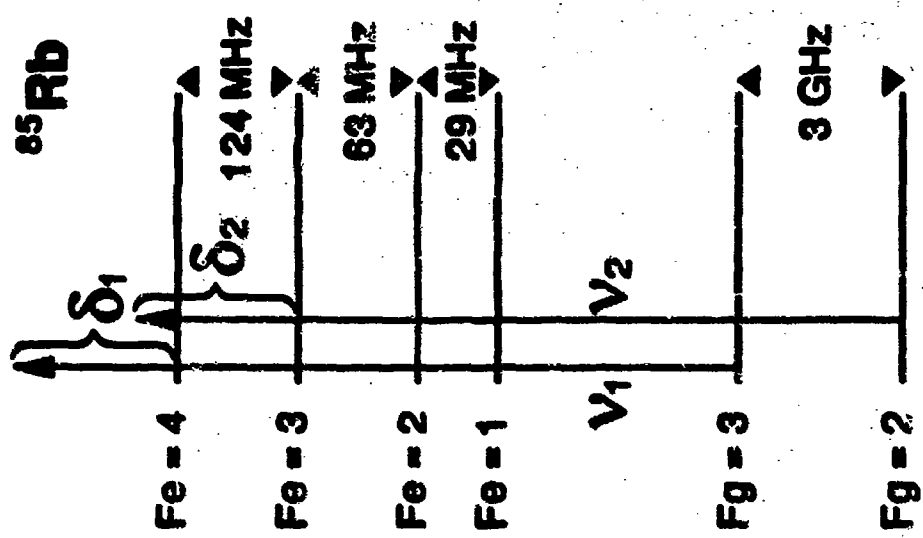


Fig 2

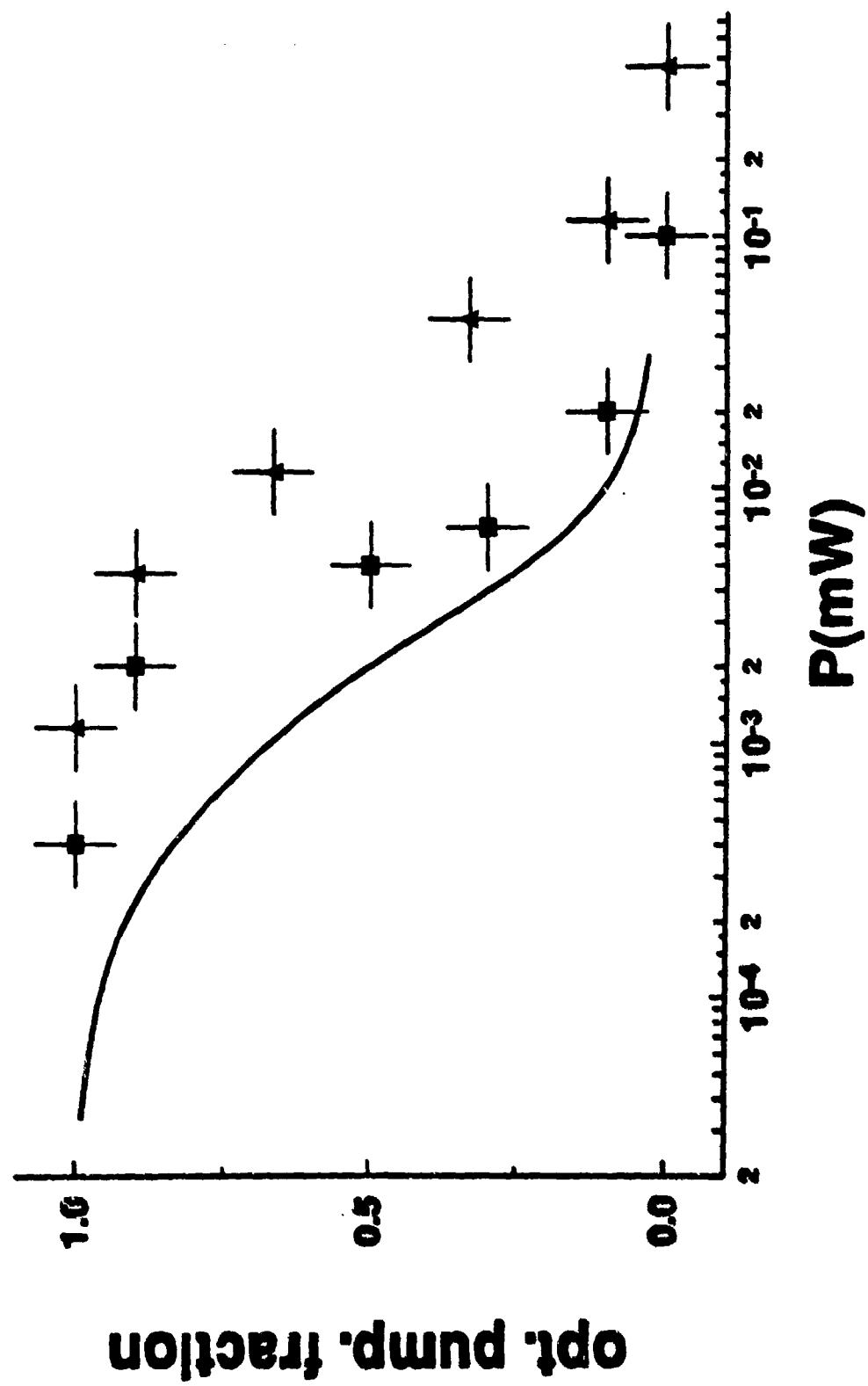


Fig 3

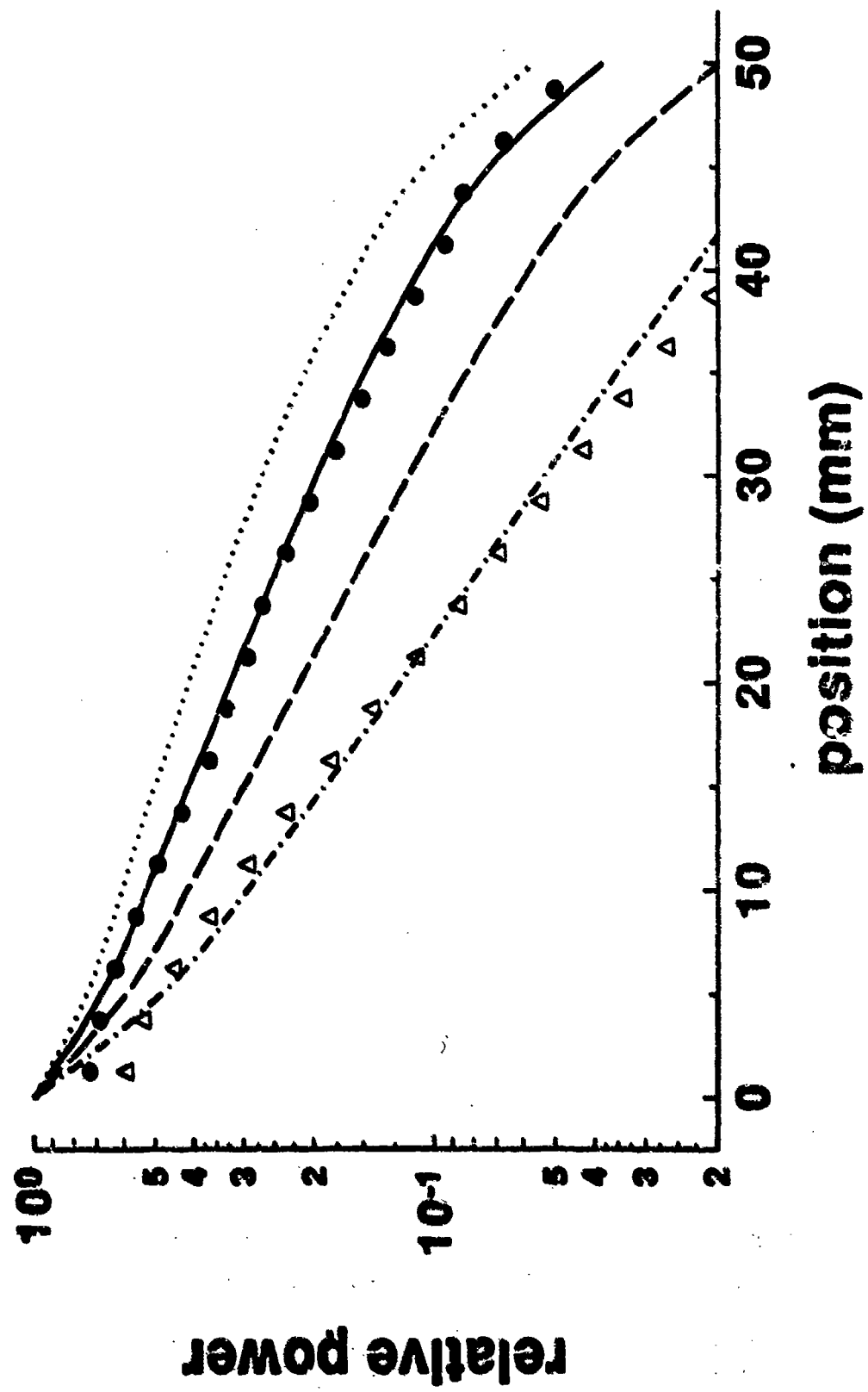


Fig 4

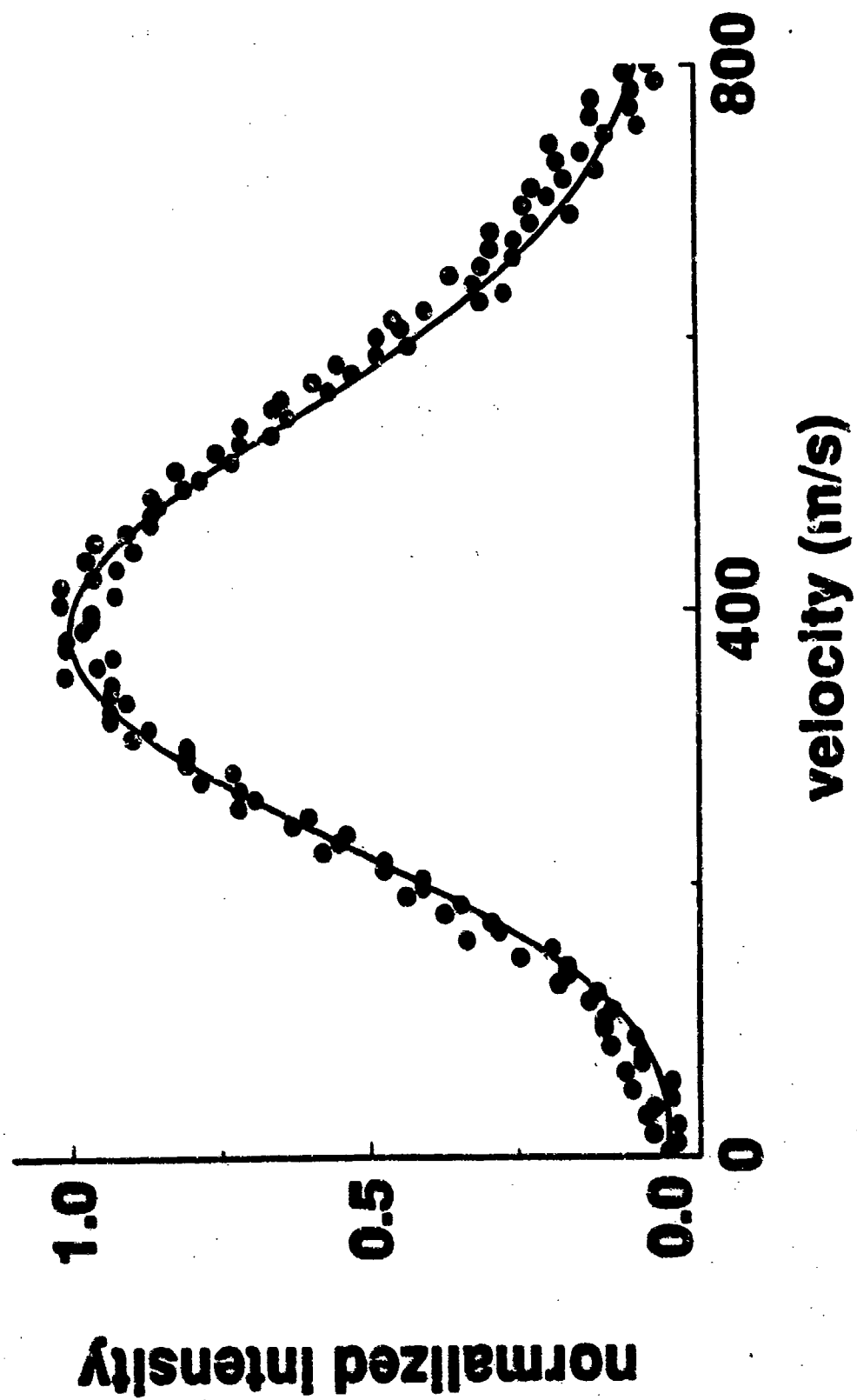


Fig 5

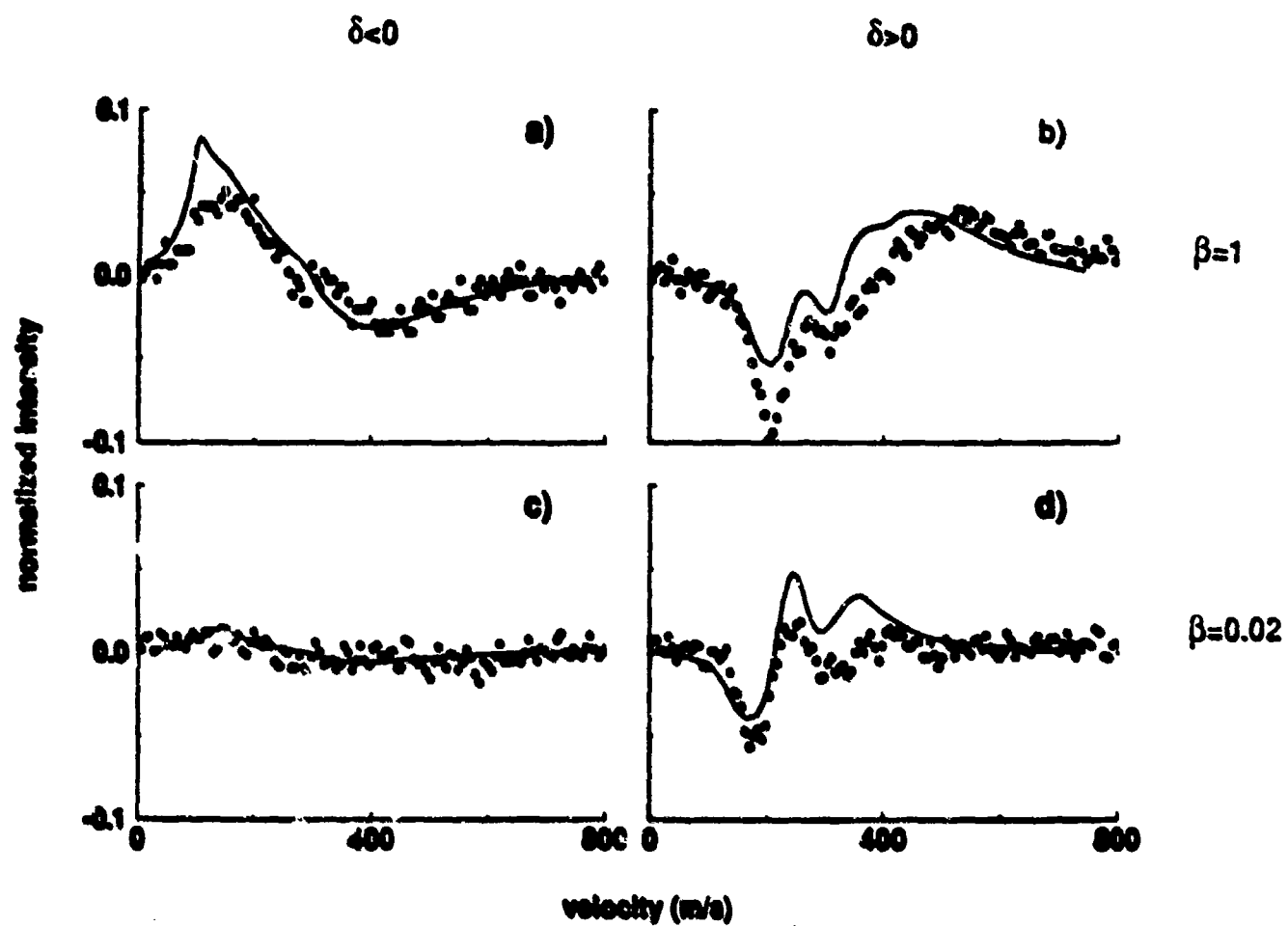


Fig 6

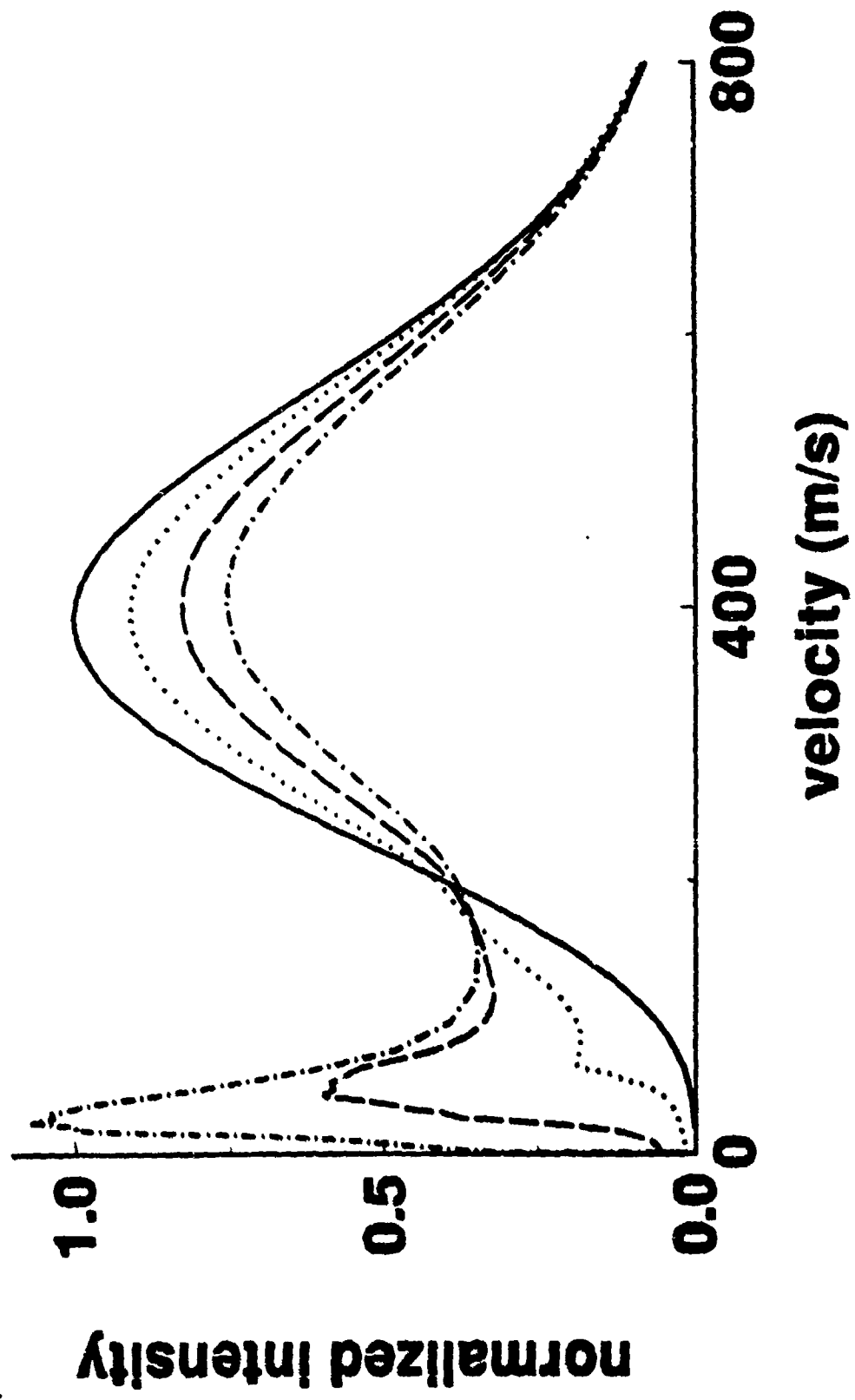


Fig 7